UNIVERSITY OF CALIFORNIA
RIVERSIDE

Variations in California Climate and Lake Productivity During the Holocene

A Thesis submitted in partial satisfaction
of the requirements for the degree of

Master of Science

in

Environmental Sciences

by

Jacob Emerson Ashford

September 2017

Thesis Committee:
Dr. James O. Sickman, Chairperson
Dr. Michael A. Anderson
Dr. Andrew B. Gray

The Thesis of Jacob Emerson Ashford is approved:

_____

_____

_____

Committee Chairperson

University of California, Riverside

ACKOWLEDGEMENTS

I want to thank my advisor, Dr. Sickman, for his guidance, support, and for sharing his passion for the Sierra Nevada. I would also like to thank Dr. Gray and Dr. Anderson for their help with my research and thesis. I would like to thank Dee Lucero for running endless samples for this project and the Gray Lab for the use of their instrumentation. I would like to thank Dr. Matt Kirby for his direction, advice, and help with the analysis and interpretation of the core data. Finally, I would like to thank my friends and family for their love and support throughout my time at UC Riverside and sharing the good and bad times with me to keep me level.

ABSTRACT OF THESIS

Variations in California Climate and Lake Productivity During the Holocene

by

Jacob Emerson Ashford

Master of Science, Graduate Program in Environmental Sciences
University of California, September 2017
Dr. James O. Sickman, Chairperson

Understanding century to millennial-scale variation in snowfall and extreme hydrologic events in the Sierra Nevada of California is hampered by short instrumental records (<120 years) and uncertainty caused by extrapolating paleoclimate data from lower elevation to the alpine, snow deposition zone. We investigated Holocene hydrologic variability and lake productivity in the alpine Sierra Nevada using a ca. 12,000 year record of sediments collected from Pear Lake (36°35'49"N, 118°40'29"W, 2904 m asl, maximum depth 24 m). High-resolution scanning revealed alternating, fine grained, light-dark bands (1 mm to 5 mm thick) for most of the core length. This pattern was interrupted at intervals by visually homogenous layers (up to 75 mm thick) containing coarse grain particles up to 10 mm in diameter. Bulk elemental and stable isotope measurements were used to investigate sources of organic matter in lake sediments and used as a proxy for aquatic productivity. Laser diffraction particle analysis was used to obtain particle size distributions of the core at 1 cm increments to quantify the frequency of periods of relative wetness (rain-on-snow flooding, large avalanches, atmospheric rivers) and dryness (decadal to centennial-scale droughts).

At Pear Lake, the frequency of pluvial episodes declined during the Holocene from 37 in the early Holocene (11250 to 7250 cal yr BP) to 22 episodes during the middle Holocene (7250 to 3000 cal yr BP) to 15 episodes during the late Holocene (3000 cal yr BP to present). High percent silt and silt unimodal distributions, which indicate drier conditions, were more frequent in the middle and late Holocene relative to the early Holocene. The highest concentration of dry periods occurred within the last 1500 years. The $\delta^{13}C$ and $\delta^{15}N$ of terrestrial and aquatic organic matter overlaps substantially in the Sierra Nevada, thus they do not indicate organic matter sources in Pear Lake sediments. However, correlations between elemental and stable isotope data in the middle and late Holocene may indicate the influence of climate change on lake productivity. Overall, the data suggest a wetter, more dynamic, early Holocene followed by a drier, more drought-proned middle Holocene, and a variable early Holocene with intense climate extremes.

TABLE OF CONTENTS

LIST OF FIGURES

LIST OF TABLES

Chapter 1: Introduction

Background

Water is a valuable resource to society. Although having too little water can be harmful and detrimental to municipalities and agriculture, having too much water can be catastrophic. Historically, extreme floods and droughts have caused destruction and stress in communities across the United States (e.g. Great Flood of 1862, western United States). As the population of California grew, threats of water scarcity and the expense of rebuilding after destructive floods became serious socioeconomic issues (Gumprecht, 2001). These climate extremes and the rapid expansion of the United States westward lead to the widespread damming of natural waterways, water diversions, and mitigation plans such as the channelization of the Los Angeles River in the 1900's (Desfor & Keil, 2004).

California, particularly southern California, is sensitive to issues regarding water scarcity due to an uneven distribution of precipitation in the state and juxtaposed water demand and water supply. The majority of precipitation falls during the winter months as snow in the mountain ranges of California, mainly in the Sierra Nevada, which spans more than half of the state. The largest winter storms are often influenced by atmospheric rivers, large plumes of atmospheric moisture from the tropical Pacific that intersect the West Coast with a narrow band of high intensity precipitation (Guan et al., 2010). Atmospheric rivers can generate as much as four times daily snow water equivalent

(SWE) of non-atmospheric rivers and have recorded frequencies of as many as 14 in a month (Guan et al., 2010, 2013).

Snowpack accumulates over winter and thaws in spring providing a natural water storage system for lower elevation regions of California. An extensive network of dams, reservoirs, and aqueducts have been built over the last century in an attempt to meet the municipal and agricultural water demands of the State. Even with these extensive water conveyance systems California was severely stressed by the recent 2012-2015 drought. State mandates on water use and conservation were necessary to ensure water availability for municipal and agricultural needs and to mitigate groundwater overdrafting (Brown, 2015).

Following the extreme drought of 2012-2015, the winter of 2016-2017 had one of the largest snowpacks in the Sierra Nevada in the past 120 years (California Cooperative Snow Survey) (CDEC)Although the state benefitted from much needed groundwater and reservoir recharge, there was flooding across California and some reservoirs overflowed and/or were in danger of failing due to the massive influxes of water (e.g. Oroville Dam; (Bee). These large shifts in weather cannot be predicted easily and the historic instrumental record is not sufficiently long to provide robust parameters for climate modeling. The use of paleoclimate records derived from analysis of lake sediments can provide scientists a longer temporal record to understand decadal- to centennial-scale climate trends.

Fluctuations in precipitation are not the only relevant effects of a changing climate. Nutrient loading and acid deposition have impacted terrestrial and aquatic ecosystems

throughout California (Routh et al., 2004; Sickman et al., 2003; Wolfe et al., 2001). Observational records of Sierra Nevada lake productivity and community structure are short and it is likely that few of these records lack signs of human influence. Changes in the nutrient balance and environmental conditions of mountain lake systems during the 20th Century can be seen in diatom community assemblages, pollen reconstructions, and geochemical analysis of modern sediments. Paleoreconstructions based on these proxies have been used as reference points for detecting modern changes in lakes and to investigate the effects of past climate shifts on lake ecology and productivity (Ahmad & Davies, 2017; Sickman et al., 2013; Smol, 2010). Understanding the response of lake systems to past climate shifts, and particularly long lasting climate extremes (e.g. drought), can help us to understand the potential ecological and water quality effects of ongoing climate change. Paleo records can also help us identify environmental conditions of the pre-industrial era and help build a framework for restoration projects of impaired waterways. The European Commission is striving to return water bodies to "good ecological status" and is using paleolimnological methods to discover a reference point for "undisturbed conditions" (Smol, 2010).

Evidence for human caused climate change is compelling and includes depletion of stratospheric ozone (Varotsos, 2002), melting ice caps (Kaser et al., 2006), coral reef decline (Baker et al., 2008), and biogeochemical changes in aquatic ecosystems (Jambrina-Enriquez et al., 2017; Sickman et al., 2013; Sickman et al., 2003; Wolfe et al., 2001). High elevation lakes in the Sierra Nevada, are more susceptible to changing climate than lower elevation systems and show the effects of climate change earlier

(Elser et al., 2009; Psenner, 2003; Smol, 2010). Oligotrophic lakes are sensitive to small changes in nutrient loading and atmospheric deposition due to air pollution. The inherent sensitivity of high elevation systems combined with projections that climate variability and amplitude will increase (Dettinger, 2011; Parry, 2007) create a compelling need for better understanding of linkages between lake productivity and climate variations.

Lacustrine and marine sediments record information about the environmental conditions during the period they were deposited. Sediments can record centennial- to millennial-scale changes in climate (Kirby et al., 2015; Kirby et al., 2012; MacDonald et al., 2016; Moy et al., 2002; Noren et al., 2002), annual- to decadal-scale shifts in aquatic productivity (Brenner et al., 1999; Jambrina-Enriquez et al., 2017; Lamb et al., 2006; Routh et al., 2004; Vaalgamaa et al., 2013), nutrient loading (Homyak et al., 2014; Routh et al., 2004; Sickman et al., 2013; Sickman et al., 2003; Vaalgamaa et al., 2013), and precipitation (Cayan, 1996; Kirby et al., 2010; Menking & Anderson, 2003), and single events such as floods (Brown et al., 1999; Thorndycraft et al., 1998). However, intense seasonal mixing and biological activity are common causes of increased sediment disturbance and unrefined sediment records. Temporal resolution in cores can range from varved sediments which record data on an annual to biannual time scale to sediments where unsupported ^{210}Pb is reached in the first centimeter of accumulation (> 200 years old) (Sickman, unpublished).

Studies have used lake sediments to identify the effects of anthropogenic effects on pristine ecosystems and the extent of climate change on lake trophic state (Jambrina-Enriquez et al., 2017). Increased deposition of atmospheric nitrogen and phosphorus has

caused some oligotrophic systems to progress towards a more mesotrophic state (Elser et al., 2009). Sickman et al. (2013) investigated changes in acid neutralizing capacity (ANC) of high elevation lakes using reconstructions of diatom community structure. The authors noted a recovery of ANC from 1980-2000 after a severe decrease in the early- to mid-1900's due to increased fossil fuel usage. Sediments can also describe environmental conditions in a system and describe organic matter sources and diagenetic properties of sediments (Brenner et al., 1999; Diefendorf et al., 2008; Meyers, 1997, 2003; Meyers & Ishiwatari, 1993).

Climate shifts are recorded in sediment biogeochemistry and physical characteristics. Studies have tracked changes in climate trends such as the shifting range of the North American Monsoon through the Holocene (Bird & Kirby, 2006), the influences of Pacific Decadal Oscillation on precipitation variability (Kirby et al., 2010) and fluctuation of El Nino Southern Oscillation patterns (Kirby et al., 2005; Menking & Anderson, 2003). Lake level changes and sediment characteristics have been used to identify periods of extended drought on the West Coast (Benson et al., 2002; MacDonald et al., 2016; Menking & Anderson, 2003; Mensing et al., 2004).

The overall climate trends of the Holocene in western North America can be divided into three somewhat distinct periods: early, middle, and late Holocene. The early Holocene is generally considered to be a wet and stormy transition out of the last glacial (Barron et al., 2003; Bird & Kirby, 2006; Kirby et al., 2015). The middle Holocene was exceptionally arid in most records but was interrupted by intermittent pluvial periods (Barron et al., 2003; Benson et al., 2002; Kirby et al., 2015; MacDonald et al., 2016;

Mensing et al., 2004) and the late Holocene is commonly described as a period of extreme wetness and dryness (Barron et al., 2003; Benson et al., 2002; Kirby et al., 2015; Kirby et al., 2010; Stine, 1990). The high variability of the late Holocene is expected to continue as anthropogenic forcing continues to influence climate extremes (Dettinger, 2011; Parry, 2007).

The research presented in the subsequent chapters describes geochemical and physical analyses conducted on a sediment core collected during October 2013 from Pear Lake in the alpine zone of the southern Sierra Nevada of California (Figure 1-1). The core provides a 580 cm record of Holocene biogeochemical and physical variability in the Sierra Nevada starting about 10,000 years before present. In Chapter 2 we describes the general biogeochemical and physical properties of the core and introduce the sediment proxies that will be examined later on in Chapter 3. In Chapter 3 we provide an in-depth investigation of a grain size proxy for climate variability and discuss factors that may be impacting lake ecology and productivity on centennial to millennial timescales. A description of general Holocene climate variability at Pear Lake is presented and compared to other paleoclimate records derived from lake cores spanning the west coast. In Chapter 4, we provide a summary of our findings and propose additional analyses of the sediment core.

Study Site

The Sierra Nevada is a 70,000 square kilometer, 700 km long mountain range in California. It is predominantly composed of granitic rock gradually sloping upward on

the western face with a steep eastern escarpment. Elevations above 4,000 m are present in the southern end of the range with lower peaks to the north (3,300 to 1,800 m). Amid the polished bedrock are poorly developed soils, generally Entisols and Inceptisols. The Sierra Nevada climate is Mediterranean with most of the precipitation falling as snow in the winter, although non-winter precipitation is not uncommon (Homyak et al., 2014; Sadro & Melack, 2012; Zavaleta, 2016).

Pear Lake (36º36'02"N, 118º40'00"W) is an oligotrophic lake, whose watershed lies predominantly in the alpine (treeless) zone of the Sierra Nevada (2,904 m a.s.l.). The average depth of Pear Lake is 7.4 m, a maximum depth of 24 m, and a lake volume of 591,000 m^3 (Figure 1-2). Even in drought years, annual catchment runoff exceeds lake volume producing a maximum lake residence time of < 1 year. During wet years, the volume of runoff can 5-times greater than lake volume resulting in the lake being flushed multiple times during snowmelt.

Pear Lake has an area of 8 ha and lies within a 142 ha watershed comprised of mostly bedrock, talus, and boulders. The highest elevation in the watershed, Alta Peak, is 3,415 meters. Less than 20% of the watershed is vegetated (Figure 1-3) with a few pines near the lake outlet and shrubs and grasses scattered throughout the remainder of the watershed.

Pear Lake is typically ice covered from November through May and experiences autumn and spring turnover. Suboxic conditions are commonly observed in the hypolimnion when the lake is stratified during summer and winter (Figure 1-4). Evidence for low redox in the lake's hypolimnion includes the precipitation of iron in hypolimnetic

waters when they are brought to the surface and oxygenated. Time-depth plots of temperature and oxygen show strong summer and winter stratification with oxygen depletion in bottom waters (Figure 1-4). In a multiyear record of temperature and oxygen (based on approximately bimonthly lake visits) we observed persistent anoxia in bottom waters suggesting that the lake did not undergo full mixing during the spring and autumn. However, finer-resolution data collected using *in situ* dissolved oxygen sensors over the course of a year, clearly shows that the lake mixes fully during spring and autumn, but low oxygen conditions develop rapidly once the lake re-stratifies (Figure 1-5).

The morphology of Pear Lake, with a single deep depression, coupled with the persistent low oxygen state of these deep waters make it an ideal subject for sediment analysis. Pear Lake sediment supply is event driven and the majority of the sediment is washed in during large precipitation events and snowmelt. Sedimentation rates at Pear Lake are among the highest we have measured in the Sierra Nevada. We hypothesize that the depression (Figure 1-2) mitigates the mixing of sediments settling out in that area and once sediments have passed below the lip of the depression, physical and biological disturbance is unlikely. Low oxygen levels minimize organic matter decomposition and reduce post-deposition diagenesis. Other high elevation lakes that our lab has cored do not show the lithological complexity that Pear Lake has and sedimentation rates are very low (< 1 mm/yr). For example, Emerald Lake lies in the next basin over from Pear Lake and has similar watershed characteristics, yet its sediment show minimal lamination and sedimentation rates are less than 1/3 of those at Pear Lake. The complex morphology, specifically the deep depression, and persistent anoxia in the hypolimnion of Pear Lake

are major contributors to the quality of the sediment record and the resolution of the chronology.

References

Ahmad, K., & Davies, C. (2017). Stable isotope (delta C-13 and delta N-15) based interpretation of organic matter source and paleoenvironmental conditions in Al-Azraq basin, Jordan. *Applied Geochemistry, 78*, 49-60. doi:10.1016/j.apgeochem.2016.12.004

Baker, A. C., Glynn, P. W., & Riegl, B. (2008). Climate change and coral reef bleaching: An ecological assessment of long-term impacts, recovery trends and future outlook. *Estuarine, Coastal and Shelf Science, 80*(4), 435-471.

Barron, J. A., Heusser, L., Herbert, T., & Lyle, M. (2003). High-resolution climatic evolution of coastal northern California during the past 16,000 years. *Paleoceanography, 18*(1). doi:10.1029/2002pa000768

Bee, S. Retrieved from http://www.sacbee.com/opinion/editorials/article132360764.html

Benson, L., Kashgarian, M., Rye, R., Lund, S., Paillet, F., Smoot, J., . . . Lindstrom, S. (2002). Holocene multidecadal and multicentennial droughts affecting Northern California and Nevada. *Quaternary Science Reviews, 21*(4-6), 659-682. doi:10.1016/s0277-3791(01)00048-8

Bird, B. W., & Kirby, M. E. (2006). An Alpine Lacustrine Record of Early Holocene North American Monsoon Dynamics from Dry Lake, Southern California (USA). *Journal of Paleolimnology, 35*(1), 179-192. doi:10.1007/s10933-005-8514-3

Brenner, M., Whitmore, T. J., Curtis, J. H., Hodell, D. A., & Schelske, C. L. (1999). Stable isotope (delta C-13 and delta N-15) signatures of sedimented organic matter as indicators of historic lake trophic state. *Journal of Paleolimnology, 22*(2), 205-221. doi:10.1023/a:1008078222806

Brown, J. (2015). *Executive Order B-29-15* Retrieved from https://www.gov.ca.gov/docs/4.1.15_Executive_Order.pdf.

Brown, P., Kennett, J. P., & Ingram, B. L. (1999). Marine evidence for episodic Holocene megafloods in North America and the northern Gulf of Mexico. *Paleoceanography, 14*(4), 498-510. doi:10.1029/1999pa900017

Cayan, D. R. (1996). Interannual climate variability and snowpack in the western United States. *Journal of Climate, 9*(5), 928-948. doi:10.1175/1520-0442(1996)009<0928:icvasi>2.0.co;2

CDEC. California Cooperative Snow Surveys. Retrieved from https://cdec.water.ca.gov/snow/index.html

Desfor, G., & Keil, R. (2004). *Nature and the City: Making Environmental Policy in Toronto and Los Angeles*: University of Arizona Press.

Dettinger, M. (2011). Climate Change, Atmospheric Rivers, and Floods in California - A Multimodel Analysis of Storm Frequency and Magnitude Changes. *Journal of the American Water Resources Association, 47*(3), 514-523. doi:10.1111/j.1752-1688.2011.00546.x

Diefendorf, A. F., Patterson, W. P., Holmden, C., & Mullins, H. T. (2008). Carbon isotopes of marl and lake sediment organic matter reflect terrestrial landscape change during the late Glacial and early Holocene (16,800 to 5,540 cal yr B.P.): a multiproxy study of lacustrine sediments at Lough Inchiquin, western Ireland. *Journal of Paleolimnology, 39*(1), 101-115. doi:10.1007/s10933-007-9099-9

Elser, J. J., Andersen, T., Baron, J. S., Bergström, A.-K., Jansson, M., Kyle, M., . . . Hessen, D. O. (2009). Shifts in lake N: P stoichiometry and nutrient limitation driven by atmospheric nitrogen deposition. *Science, 326*(5954), 835-837.

Guan, B., Molotch, N. P., Waliser, D. E., Fetzer, E. J., & Neiman, P. J. (2010). Extreme snowfall events linked to atmospheric rivers and surface air temperature via satellite measurements. *Geophysical Research Letters, 37*(20).

Guan, B., Molotch, N. P., Waliser, D. E., Fetzer, E. J., & Neiman, P. J. (2013). The 2010/2011 snow season in California's Sierra Nevada: Role of atmospheric rivers and modes of large-scale variability. *Water Resources Research, 49*(10), 6731-6743.

Gumprecht, B. (2001). *The Los Angeles River: Its Life, Death, and Possible Rebirth*: Johns Hopkins University Press.

Homyak, P. M., Sickman, J. O., & Melack, J. M. (2014). Phosphorus in sediments of high-elevation lakes in the Sierra Nevada (California): implications for internal phosphorus loading. *Aquatic Sciences, 76*(4), 511-525. doi:10.1007/s00027-014-0350-y

Jambrina-Enriquez, M., Recio, C., Vega, J. C., & Valero-Garces, B. (2017). Tracking climate change in oligotrophic mountain lakes: Recent hydrology and productivity synergies in Lago de Sanabria (NW Iberian Peninsula). *Science of the Total Environment, 590*, 579-591. doi:10.1016/j.scitotenv.2017.02.231

Kaser, G., Cogley, J., Dyurgerov, M., Meier, M., & Ohmura, A. (2006). Mass balance of glaciers and ice caps: consensus estimates for 1961–2004. *Geophysical Research Letters, 33*(19).

Kirby, M. E., Knell, E. J., Anderson, W. T., Lachniet, M. S., Palermo, J., Eeg, H., . . . Hiner, C. A. (2015). Evidence for insolation and Pacific forcing of late glacial through Holocene climate in the Central Mojave Desert (Silver Lake, CA). *Quaternary Research, 84*(2), 174-186. doi:10.1016/j.yqres.2015.07.003

Kirby, M. E., Lund, S. P., Patterson, W. P., Anderson, M. A., Bird, B. W., Ivanovici, L., . . . Nielsen, S. (2010). A Holocene record of Pacific Decadal Oscillation (PDO)-related hydrologic variability in Southern California (Lake Elsinore, CA). *Journal of Paleolimnology, 44*(3), 819-839. doi:10.1007/s10933-010-9454-0

Kirby, M. E., Lund, S. P., & Poulsen, C. J. (2005). Hydrologic variability and the onset of modern El Nino Southern Oscillation: a 19,250-year record from Lake Elsinore, southern California. *Journal of Quaternary Science, 20*(3), 239-254. doi:10.1002/jqs.906

Kirby, M. E., Zimmerman, S. R. H., Patterson, W. P., & Rivera, J. J. (2012). A 9170-year record of decadal-to-multi-centennial scale pluvial episodes from the coastal Southwest United States: a role for atmospheric rivers? *Quaternary Science Reviews, 46*, 57-65. doi:10.1016/j.quascirev.2012.05.008

Lamb, A. L., Wilson, G. P., & Leng, M. J. (2006). A review of coastal palaeoclimate and relative sea-level reconstructions using δ13C and C/N ratios in organic material. *Earth-Science Reviews, 75*(1), 29-57. doi:http://dx.doi.org/10.1016/j.earscirev.2005.10.003

MacDonald, G. M., Moser, K. A., Bloom, A. M., Potito, A. P., Porinchu, D. F., Holmquist, J. R., . . . Kremenetski, K. V. (2016). Prolonged California aridity linked to climate warming and Pacific sea surface temperature. *Scientific Reports, 6*.

Menking, K. M., & Anderson, R. Y. (2003). Contributions of La Nina and El Nino to middle holocene drought and late Holocene moisture in the American Southwest. *Geology, 31*(11), 937-940. doi:10.1130/g19807.1

Mensing, S. A., Benson, L. V., Kashgarian, M., & Lund, S. (2004). A Holocene pollen record of persistent droughts from Pyramid Lake, Nevada, USA. *Quaternary Research, 62*(1), 29-38. doi:10.1016/j.yqres.2004.04.002

Meyers, P. A. (1997). Organic geochemical proxies of paleoceanographic, paleolimnologic, and paleoclimatic processes. *Organic Geochemistry, 27*(5), 213-250. doi:http://dx.doi.org/10.1016/S0146-6380(97)00049-1

Meyers, P. A. (2003). Applications of organic geochemistry to paleolimnological reconstructions: a summary of examples from the Laurentian Great Lakes. *Organic Geochemistry, 34*(2), 261-289. doi:http://dx.doi.org/10.1016/S0146-6380(02)00168-7

Meyers, P. A., & Ishiwatari, R. (1993). Lacustrine Organic Geochemistry - An Overview of Organic-Matter Sources and Diagenesis in Lake-Sediments. *Organic Geochemistry, 20*(7), 867-900. doi:10.1016/0146-6380(93)90100-p

Moy, C. M., Seltzer, G. O., Rodbell, D. T., & Anderson, D. M. (2002). Variability of El Nino/Southern Oscillation activity at millennial timescales during the Holocene epoch. *Nature, 420*(6912), 162-165. doi:10.1038/nature01194

Noren, A. J., Bierman, P. R., Steig, E. J., Lini, A., & Southon, J. (2002). Millennial-scale storminess variability in the northeastern United States during the Holocene epoch. *Nature, 419*(6909), 821-824. doi:10.1038/nature01132

Parry, M. L. (2007). *Climate change 2007-impacts, adaptation and vulnerability: Working group II contribution to the fourth assessment report of the IPCC* (Vol. 4): Cambridge University Press.

Psenner, R. (2003). Alpine lakes: Extreme ecosystems under the pressure of global change. *EAWAG news, 55*, 12-14.

Routh, J., Meyers, P. A., Gustafsson, Ö., Baskaran, M., Hallberg, R., & Schöldström, A. (2004). Sedimentary geochemical record of human–induced environmental changes in the Lake Brunnsviken watershed, Sweden. *Limnology and Oceanography, 49*(5), 1560-1569. doi:10.4319/lo.2004.49.5.1560

Sadro, S., & Melack, J. M. (2012). The effect of an extreme rain event on the biogeochemistry and ecosystem metabolism of an oligotrophic high-elevation lake. *Arctic, Antarctic, and Alpine Research, 44*(2), 222-231.

Sickman, J. O., Bennett, D. M., Lucero, D. M., Whitmore, T. J., & Kenney, W. F. (2013). Diatom-inference models for acid neutralizing capacity and nitrate based on 41 calibration lakes in the Sierra Nevada, California, USA. *Journal of Paleolimnology, 50*(2), 159-174. doi:10.1007/s10933-013-9711-0

Sickman, J. O., Melack, J. M., & Clow, D. W. (2003). Evidence for nutrient enrichment of high-elevation lakes in the Sierra Nevada, California. *Limnology and Oceanography, 48*(5), 1885-1892.

Smol, J. (2010). The power of the past: using sediments to track

the effects of multiple stressors on lake ecosystems. *Freshwater Biology, 55*, 43-59.

Stine, S. (1990). Late holocene fluctuations of Mono Lake, eastern California. *Palaeogeography, Palaeoclimatology, Palaeoecology, 78*(3-4), 333-381.

Thorndycraft, V., Hu, Y., Oldfield, F., Crooks, P. R. J., & Appleby, P. G. (1998). Individual flood events detected in the recent sediments of the Petit Lac d'Annecy, eastern France. *Holocene, 8*(6), 741-746. doi:10.1191/095968398668590504

Vaalgamaa, S., Sonninen, E., Korhola, A., & Weckström, K. (2013). Identifying recent sources of organic matter enrichment and eutrophication trends at coastal sites using stable nitrogen and carbon isotope ratios in sediment cores. *Journal of Paleolimnology, 50*(2), 191-206. doi:10.1007/s10933-013-9713-y

Varotsos, C. (2002). The southern hemisphere ozone hole split in 2002. *Environmental Science and Pollution Research, 9*(6), 375-376.

Wolfe, A. P., Baron, J. S., & Cornett, R. J. (2001). Anthropogenic nitrogen deposition induces rapid ecological changes in alpine lakes of the Colorado Front Range (USA). *Journal of Paleolimnology, 25*(1), 1-7. doi:10.1023/a:1008129509322

Zavaleta, H. M. a. E. (2016). *Ecosystems of California*: University of California Press.

Chapter 2: Productivity Proxies in Pear Lake Sediments

Introduction

Lake and marine sediments are rich archives that can record environmental conditions over thousands to hundreds of thousands of years. The data archived in these records can range from climatological and ecological shifts of African rift lakes over millennia (Livingstone, 1975), to reconstructing environmental conditions with diatom and chironomid cyst assemblages (Lotter et al., 1997), to identifying the cause of the fall of the Mayan civilization (Hodell et al., 1995). Sediment cores have been used as paleo records to monitor climate patterns through grain size analysis (Brown et al., 2002; Kirby et al., 2012; MacDonald et al., 2000), to investigate aquatic and terrestrial ecology from pollen and diatom assemblages (Engel et al., 2010; Routh et al., 2004; Vaalgamaa et al., 2013), and to reconstruct temperature using chironomid proxies (Bloom et al., 2003; MacDonald et al., 2008; Porinchu et al., 2009). Sediment records have also been used to look at the more recent past. Sickman et al., (2013) used shallow lake sediments to reconstruct acid neutralizing capacity in montane lakes and to document their recovery from acid deposition. Routh (2004), Wolfe (2001), and Vaalgamaa (2013) used sediment geochemical records to monitor external nutrient loading and eutrophication in lacustrine and marine systems since the mid-19th century.

The goal of this chapter is to provide a preliminary description of the high resolution sediment cores collected from Pear Lake during October 2013. Magnetic susceptibility, density, stable isotope, elemental, and grain size analyses as well as a general core

lithological categorization and imagery will be presented. We will also provide a description of the general trends in these core features over the Holocene and discuss their potential utility as environmental proxies.

Methods

Core Collection and Characterization

In October 2013, the National Lacustrine Core Facility (LacCore) assisted in collecting two sediment cores, using Livingstone and Bolivia corers, from the deepest part of the Pear Lake basin (z_{max} = 24 m). SQNP-PEAR13-1A (Core A) and SQNP-PEAR13-1B (Core B) were collected 10 m apart and were visually determined to have high lithological correlation. Due to Core B being slightly compressed by raised bedrock, the majority of our analyses were done on Core A, however, Core B was used to replace portions where the lithology of Core A was disturbed during collection. Core A, is 6.7 m long and was collected in eight sections approximately 90 cm in length. The core was split and characterized for sediment density using a gamma ray attenuation porosity evaluator and magnetic susceptibility using a Bartington point sensor (Geotek). Magnetic susceptibility is reported in SI units ($x10^{-5}$ m^3 kg^{-1}). Macrofossils and bulk sediments were collected for radiocarbon dating, and high resolution photographic images were captured before the core was wrapped in film and placed in refrigerated storage for later sub-sampling. The core images were later analyzed visually and each lamination was cataloged and characterized for the majority of the core. In the data presented below, we

will describe the basic features of the cores as a function of sediment depth rather than age.

Stable Isotope and Elemental Analyses

The core was subsampled contiguously at 1 cm increments and prepared for nitrogen and carbon stable isotope and elemental analysis. Approximately one cubic centimeter of sediment was extracted, weighed, and dried at 60 ºC overnight. The sample was then ground with mortar and pestle and homogenized before a subsample was taken for analysis in an isotope ratio mass spectrometer interfaced with an elemental analyzer. All runs included National Institutes for Standards and Technology (NIST) glutamic acid standards (RM 8573 and 8574) and were reported in per mil units (‰) relative to known atmospheric N_2 ($\delta^{15}N$) and Pee Dee Belemnite ($\delta^{13}C$). For elemental analysis NIST peach (RM 1547) was used as the standard for %C and %N.

Grain Size Preparation and Analysis

Samples were taken from the top 580 cm of the core for grain size analysis. Approximately one cubic centimeter of sediment was collected every centimeter and prepared according to Kirby (2010). Organic matter was removed using ≥ 40 ml 30% H_2O_2, carbonates were removed with 10 ml of 1 N HCl, and biogenic silica was removed using 10 ml of 1 N NaOH. All samples were sieved at 1 mm after chemical treatment to remove gravel and extra coarse sands. In lieu of sonication, 0.1 g of sodium hexametaphosphate was added as a dispersing agent and the samples were shaken for ≥ 8 hours the night before grain size analysis. Samples were analyzed on a Beckman-Coulter

LS 13-320 laser particle size analyzer (LS 13-320). When necessary, samples were split or combined to reach optimal parameters for the analysis established by the LS 13-320 calibration. The sieved coarse sand and gravel was quantified (counted and weighed) and presence and absence of gravel (diameter $\geq$ 2 mm) was recorded for each sample. The LS 13-320 integrated software was used to convert the raw count data into binned groups for further analysis. The freeware program GRADISTAT (Blott & Pye, 2001) was then used to calculate statistics on the output data from the LS 13-320 including the percent sand, silt, and clay fractions.

Results

Core Lithology

The deepest portion of the core (630 – 690 cm) was composed of glacial flour and regolith. As the watershed developed, fine banding began to occur at ~630 cm and the process of landscape response and recovery from glaciation reached its final stages at approximately 580 cm. Here, banding became more regular and carbon levels in the sediment reached normal range of the data (core means: %C = 3; C:N = 11; $\delta^{13}C$ = -26 ‰). The focus of this study will be on the top 580 cm of the core. Core lithology was estimated graphically (Figure 2-1) from the core images that are provided in Supplemental Materials. The majority of the core consists of light and dark banding of variable thickness (1 mm to 5 mm) that is interrupted by several large clasts (up to 75 mm) of visually homogenous material. The banding is also interrupted by a few clasts that consist of coarse grains ranging from coarse sand (1 mm to 2 mm) to gravel (2 mm to

10 mm). There are several tephra layers, the most notable at approximately 58, 248, and 252 cm.

Magnetic Susceptibility and Density

Magnetic susceptibility was variable throughout the core with a range of 6.1 (z_{min} = 155 cm) to 132.1 (z_{max} = 318 cm) and an average of 35.6 (Figure 2-2). The majority of the variation was between 15 and 50 with 9 predominant peaks above 60. There was a significant downward trend in magnetic susceptibility as depth decreased (slope = 3.5 $x10^{-5}$ m^3 kg^{-1}/cm, $p < 0.0001$). Sediment density fluctuated between 0.46 g/cm^3 (z_{min} = 154 cm) and 2.09 g/cm^3 (z_{max} = 319 cm) with an average of 1.15 g/cm^3 (Figure 2-2). There were ten prominent peaks above 1.5 g/cm^3 that corresponded with the peaks in magnetic susceptibility. The density of the sediment decreased with decreasing depth (slope = 0.021g cm^{-3}/cm, $p < 0.0001$) and was significantly correlated with magnetic susceptibility ($r = 0.73$; $p < 0.0001$).

Stable Isotope and Elemental Analyses

We used percent carbon by dry weight (%C) as a proxy for organic matter content in the sediment. It is important to note that past studies of Pear Lake have shown virtually no carbonate in modern lake sediments (Sickman, unpublished). The percent carbon values oscillated with a wavelength of approximately 100 cm (~2,000 years) and increased with decreasing depth (slope = -0.362%C/cm, $p < 0.0001$; Figure 2-3). The values ranged between 0.02% and 14.7% with an average of 6.9% carbon. Percent

nitrogen (%N) had a regular oscillation pattern as well (x_{min} = 0.01%, x_{max} = 1.2%, $\bar{x}$ = 0.58%; Figure 2-3) and was strongly correlated with carbon (r = 0.963; p < 0.0001). Percent nitrogen increased with decreasing depth (slope = -0.039%N/cm; p < 0.0001). Starting at approximately 150 cm, both carbon and nitrogen percent began larger scale fluctuations with less local variation. The carbon to nitrogen ratio (C:N) fluctuated regularly for the majority of the record (x_{min} = 9.8, x_{max} = 28.9, $\bar{x}$ = 14.2; Figure 2-3) with exception of a 40 cm section in the early portion of the record (510 – 550 cm) which exhibited approximately double the amplitude of variation. C:N declined with decreasing depth (slope = 0.14/cm, p < 0.0001). Carbon isotope composition ranged from -30.2‰ to -22.5‰ with an average of -26.4‰ (Figure 2-3). There was a decrease in $\delta^{13}C$ with a slope significantly different from zero toward the core surface (slope = 0.002 $\delta^{13}C$/cm, p < 0.0001). Nitrogen isotope composition showed a more variable trend through the core. The range was -1.7‰ to +3.8‰ with an average of +1.7‰, and displayed several conspicuous monotonic trends including a $\delta^{15}N$ decline from 570 – 550 cm, an increase from 550 – 450 cm, flat response from 450 – 100 cm, and then a decline from 100 – 1 cm (Figure 2-3). Overall, $\delta^{15}N$ showed an increase toward the surface of the core (slope = 0.24 $\delta^{15}N$/cm, p < 0.0001).

Grain Size Analysis

Grain size parameters (sand, silt, clay) were measured in percent by volume. Clay variability was relatively small (x_{min} = 1.0%, x_{max} = 11.5%, $\bar{x}$ = 7.2%; Figure 2-4) and strongly correlated with silt (r = 0.90, p < 0.0001). The Pear Lake watershed is dominated

by sand and silt dynamics and for the purposes of this analysis, clay will be ignored and assumed to follow patterns described in the silt fraction. Silt was variable throughout the core (x_{min} = 10.5%, x_{max} = 87.4%, $\bar{x}$ = 54.3%; Figure 2-4) and showed an increase with decreasing depth (slope = -0.016%/cm, $p < 0.0001$). Sand percent had a strong negative correlation to silt percent ($r = -0.998$, $p < 0.0001$). The sand percent was also variable throughout the core (x_{min} = 13%, x_{max} = 88.5%, $\bar{x}$ = 38.5%; Figure 2-4) and decreased with decreasing depth (slope = 0.016%/cm, $p < 0.0001$). Silt and sand percent had similar minima (10%, 1%) and maxima (87%, 88%), respectively but, on average, silt was more dominant in the lake sediment record ($\bar{x}_{silt}$ = 54.3% vs. $\bar{x}_{sand}$ = 38.5%). Gravel particles ($\geq$ 2 m diameter) were present throughout the core with variable frequency and often correlated with high percent sand. The frequency of gravel decreased toward the present.

Discussion

Principal Component Analysis

A principal component analysis of the multiple proxies measured in Pear Lake sediments revealed several notable correlations. There is a negative correlation between %C and %sand ($r = -0.193$, $\alpha = 0.05$; Table 2-1), and %N and %sand ($r = -0.204$, $\alpha = 0.05$, Table 2-1). Carbon and nitrogen percent by weight are used as a proxy for organic matter in the sediments. The introduction of sand sized particles into the sediments act as a simple dilution of organic matter by adding relatively heavy, inorganic material which explains the inverse correlation.

There is an inverse correlation between the organic matter proxies (%C and %N) and $\delta^{13}C$ ($r = -0.505$, $r = -0.555$; $\alpha = 0.05$; respectively; Table 2-1). Inferences about lake organic matter source and lake productivity can potentially be inferred from these correlations. There is a significant positive correlation between C:N and $\delta^{15}N$ ($r = 0.284$, $\alpha = 0.05$; Table 2-1). Based on the paleolimnology literature, $\delta^{15}N$ can be used to infer sources of N in the sediments. Magnetic susceptibility and density have an inverse relationship with %C and %N (%C: $r = -0.465$, $r = -0.385$, $\alpha = 0.05$; %N: $r = -0.447$, $r = -0.359$, $\alpha = 0.05$; respectively; Table 2-1). There is also a strong correlation between magnetic susceptibility and density ($r = 0.730$, $\alpha = 0.05$; Table 2-1). The correlation between density, and therefore magnetic susceptibility, and organic matter (%C and %N) shows that sediments with higher density have less organic matter. It is also notable that density is not significantly correlated to sand or silt ($r = 0.079$, $r = -0.076$, $\alpha = 0.05$; respectively; Table 2-1). Density has a weak correlation with clay ($r = -0.088$, $\alpha = 0.05$; Table 2-1) that is likely connected to the tendency of the clay fraction to hold organic matter (Hedges & Keil, 1995; Lützow et al., 2006).

Magnetic Susceptibility and Density

Magnetic susceptibility provides an estimate of magnetic minerals in a sediment sample based on the response to an induced magnetic field (Oldfield et al., 1979; Thompson et al., 1975). Increased magnetic susceptibility in sediments is often connected with increased terrestrial input and has been used as a proxy for relative hydrologic changes in lake sediment records. Benson (2002) used magnetic susceptibility to

reconstruct past lake levels of Pyramid Lake, Nevada. The increase in magnetic susceptibility was attributed to an increase in ferromagnetic magnetite from the lakeshore being moved to the deeper portion of the lake where the core was taken. Baker (2001) and Brown (2002) used magnetic susceptibility to determine increases in erosion and external inputs into lake systems caused by precipitation. Using a similar assumption, Kirby (2004) developed a proxy for lake level and described lake level changes in Lake Elsinore, California with variations magnetic susceptibility. Intense precipitation and floods were identified by Thorndycraft (1998) as peaks in magnetic susceptibility caused by increased terrestrial-sourced, coarse grain size material in the sediment.

The Pear Lake magnetic susceptibility and density records show a series of large peaks throughout the core (Figure 2-2), but the PCA analysis showed that MS is not significantly correlated with sand and silt. Instead, a large portion of the magnetic susceptibility peaks are coincident with coarse grain size material in the sediment and could be connected to large scale precipitation events which will be discussed more with the grain size analysis. The deepest portion of the core has increased magnetic susceptibility likely due to glacial flour remnants and low levels of organic matter in the sediment.

We hypothesize that the bathymetry of Pear Lake and watershed:lake area ratio (17.8:1) (Chapter 1, Figure 1-2) is not conducive to the use of magnetic susceptibility as a lake level proxy. Firstly, the lake margins are steep and the lake is deep with a lack of extended sandy shores that could move sediments into the lake center with gradual lake shrinkage. Secondly, the watershed area is sufficient that even very dry years such as

water year 2015, provide enough runoff to turn over the lake volume at least once, thus it would take many exceedingly dry years in series to effect a lake level drop and this drop could be erased by a single “normal” snowpack.

Magnetic susceptibility can also be used to identify the presence of tephra layers. Ash layers in sediment cores are generally visibly distinct, but spikes in magnetic susceptibility can be used to support visual identification (Baker et al., 2001; Geiss et al., 2003; Lees et al., 1998). Based on visual and MS analysis, we detected conspicuous tephra layers in the Pear Lake sediment core at: z = 59, 100, 136, 248, 252 cm. Some of these layers (z = 59, 248, 252 cm) may be associated with the Mono-Inyo complex eruptions of 600 to 625 cal yr BP and 5039 to 5297 cal yr BP (Anderson, 1990; Wood, 1977).

Elemental and Isotope Analysis

Carbon and Nitrogen (C:N)

Elemental analysis of sediment cores has been used a proxy for multiple ecological and hydrologic parameters in lakes (Ahmad & Davies, 2017; Brenner et al., 1999; Brown et al., 2002; Vaalgamaa et al., 2013). The carbon to nitrogen ratio (C:N) of plants varies among primary producers with vascular plants having a C:N of approximately 15 or greater and aquatic plants/plankton (nonvascular plants) having a C:N of approximately 4 to 10 (Kendall et al., 2001; Lamb et al., 2006; Meyers & Ishiwatari, 1993; Peterson, 1999). The lack of cellulose in nonvascular plants sometimes allows for the use of C:N values to distinguish the difference between terrestrial and aquatic organic matter in

sediments. It is well established that C:N can be used as a proxy for terrestrial input into lake systems (Ahmad & Davies, 2017; Brenner et al., 1999; Kirby et al., 2012; Lamb et al., 2006; Meyers, 1997) and, although diagenesis can alter the original C:N of organic matter, some researchers (Meyers, 1997; Meyers & Ishiwatari, 1993) argue that the alteration due to diagenesis is not enough to erase the original source signal. Matsumoto (2012) created an index for the contribution of terrestrial and aquatic organic matter to Lake Hovsgol, Mongolia. The relative contribution of terrestrial and aquatic organic matter to the system allowed the authors to make inferences about the regional climate, particularly in regards to relative temperature variations. Lake productivity shifts have also been identified using C:N proxies (Routh et al., 2004). A decrease in C:N values was identified as an increase in aquatic productivity. Engel (2010) used C:N values to describe local environmental conditions and decompositional environments in a cirque basin in the Czech Republic. The authors were able to identify periods of variable peat accumulation and decomposition, which were related to environmental and climatological conditions present at the time of deposition. Brown (2002; 2000) used total organic carbon measurements and other sediment characteristics to identify hydrologic events on varying scales in Ritterbush Pond, Vermont. The authors suggest that increased C:N indicated extreme precipitation events.

The C:N ratio in Pear Lake sediment is relatively constant throughout the core length. The samples vary primarily between 13 and 15, suggesting a mixture of aquatic and terrestrial sources of organic matter, but one likely dominated by aquatic organic matter (Ahmad & Davies, 2017; Kendall et al., 2001; Meyers & Ishiwatari, 1993). The

lowest values of C:N may also be influenced by fluctuations in aquatic productivity and algal/phytoplankton species composition (Ahmad & Davies, 2017; Kendall et al., 2001; Lamb et al., 2006; Meyers & Ishiwatari, 1993; Peterson, 1999). Only the two largest C:N correlate to peaks in magnetic susceptibility and may indicate increased terrestrial input. Thus, the C:N ratio does not appear to be a viable proxy for organic matter provenance in Pear Lake.

Percent carbon and percent nitrogen follow the same general patterns throughout the core. Low levels below z = 580 cm suggest a lake and watershed undergoing primary succession following glacial retreat. The two large dips at 59 – 47 cm and 83 – 81 cm were likely tephra layers according to magnetic susceptibility and visual confirmation. Percent carbon and nitrogen do not correlate strongly with other sediment parameters and are seemingly in and out of phase with other proxies (Figure 2-3). We therefore cannot interpret the variations in %C, %N, or C:N as proxies for organic matter sources. Instead these parameters are possibly responding to complicated processes internal to the lake such as lake mixing, phytoplankton succession, nutrient regeneration from sediments and even zooplankton grazing (Routh et al., 2004; Wolfe et al., 2001)

$\delta^{13}C$, $\delta^{15}N$ Stable Isotope Analysis

Organic matter sources, lake productivity, and climate trends can be recorded in the distribution of stable isotopes in lake sediments. Baker (2001) used $\delta^{13}C$ to reconstruct lake level and discuss interactions of regional climate forcing. Engel (2010) used $\delta^{13}C$ to infer relative temperature and shifting environmental conditions during the growing

season in a cirque lake in the Czech Republic. The authors also used $\delta^{15}N$ in tandem with $\delta^{13}C$ and C:N to determine the status of decomposition in the lake and organic matter sources. Climate change can also be inferred from the $\delta^{15}N$ of lake sediments (Wolfe et al., 2001). Recent evidence suggests that increasingly depleted $\delta^{15}N$ in modern sediments indicates shifts in trophic state brought on by elevated atmospheric N deposition (Holtgrieve et al., 2011). Relative increases in sediment $\delta^{13}C$ have been used as a proxy for aquatic productivity in lakes around the world (Brenner et al., 1999; Diefendorf et al., 2008; Engel et al., 2010; Meyers, 2003; Vaalgamaa et al., 2013). The carbon isotope enrichment of the organic matter is attributed to increased primary productivity and decreased fractionation of $\delta^{13}C$. Vascular plants have a $\delta^{13}C$ that ranges from -30 to -14‰ and aquatic algae and freshwater plankton have a $\delta^{13}C$ of -45 to -28‰ (Ahmad & Davies, 2017; Kendall et al., 2001; Lamb et al., 2006; Meyers & Ishiwatari, 1993; Peterson, 1999; Thornton & McManus, 1994). However, in many lake systems the overlap among terrestrial C3 plants, aquatic algae, and freshwater plankton makes $\delta^{13}C$ difficult to use as a proxy on its own (Lamb et al., 2006; Meyers, 1997; Meyers & Ishiwatari, 1993).

Terrestrial vegetation has a $\delta^{15}N$ of approximately 0‰ and aquatic vegetation has a $\delta^{15}N$ of about 8‰ (Kendall et al., 2001; Meyers & Ishiwatari, 1993; Peterson, 1999; Thornton & McManus, 1994). This difference is due to the sources of nitrogen used by terrestrial vegetation and aquatic primary producers. Dissolved organic nitrogen in lakes is usually around 8‰ and nitrogen used by terrestrial plants is sourced from the atmosphere which has a $\delta^{15}N$ of 0‰ (Kendall et al., 2001; Meyers & Ishiwatari, 1993;

Peterson, 1999). The variability of the top 450 cm $\delta^{15}N$ (approximately 0‰ to 4‰) is indicative of a combination of terrestrial and aquatic organic matter in the sediment. The bottom 70 cm of the core show the most negative $\delta^{15}N$ values (down to -2‰) for the entire record. The low $\delta^{15}N$ values are likely due to the primary succession of the watershed and vegetation and ecosystem dynamics coming to equilibrium after glaciation.

Although potentially useful in some systems, stable isotopes values in lake sediments can be significantly affected by diagenesis. The fractionation associated with denitrification, decomposition, and other post-depositional processes can alter the isotope ratios in sediment organic matter. In systems with low carbon, such as Pear Lake, diagenesis of $\delta^{13}C$ may be minimal (Meyers & Lallier-Vergès, 1999). Pear Lake is also intensely nitrogen limited therefore there is likely no fractionation of $\delta^{15}N$ due during assimilation by phytoplankton and algae. Denitrification is likely an important factor in Pear Lake owing to the persistence of low redox conditions in the hypolimnion (Routh et al., 2004) (Chapter 1). Due to the nutrient limitation in Pear Lake, we believe that the stable isotopes are faithfully recording the source of the organic matter in the sediment.

Overall, the carbon and nitrogen isotope composition of bulk sediments in Pear Lake suggests a mixture of terrestrial and aquatic sourced organic matter. The inverse correlation between %C and %N and $\delta^{13}C$ in Pear Lake sediments could have productivity implications. In general, increasing organic matter content is accompanied by decreasing $\delta^{13}C$ suggesting that inputs from in-lake productivity, with generally lower $\delta^{13}C$, are the dominant source of sediment organic matter. The main issue with this

interpretation is that the $\delta^{13}C$ in aquatic and terrestrial primary producers has a large degree of overlap (Figure 2-6) and unless the C:N ratio is definitively terrestrial or aquatic, $\delta^{13}C$ is not an effective proxy for organic matter in Pear Lake. An alternative interpretation for the inverse correlation between %C and %N and $\delta^{13}C$ is that the relationship results from carbon isotope fractionation in the water column. Phytoplankton growth in Pear Lake is not carbon limited, but alkalinity is typically less than 40 µEq/L. There have been periods when lake bicarbonate levels have decreased due to a lack of available CO_2 for production (Sickman, unpublished). If dissolved inorganic carbon (DIC) in the lake is low, then primary producers will be less discriminating against ^{13}C during photosynthesis resulting in higher $\delta^{13}C$ of algal and phytoplankton tissues with organic matter deposited under these conditions having a higher $\delta^{13}C$ value. For this scenario to be valid the C:N ratio in this isotopically enriched organic matter must be lower to reflect the carbon limitation in the system, however at Pear Lake C:N and %C are positively correlated (Table 2-1), thus fractionation during DIC uptake does not explain patterns in sediment $\delta^{13}C$.

Another potential proxy for productivity and organic matter sources (terrestrial versus aquatic) is the $\delta^{15}N$ of the organic matter. In some systems $\delta^{15}N$ is significantly different and when paired with C:N can be used to identify autochthonous (aquatic) versus allochthonous (terrestrial) organic matter. Aquatic and terrestrial $\delta^{15}N$ in the Pear Lake Basin is not significantly different and when plotted with generalized ranges of $\delta^{15}N$ and C:N (Figure 2-6), we see that the majority of the sediment core data fall directly in the middle of both ranges. It is apparent that stable isotope and elemental analysis are not

sufficient to identify organic matter sources in Pear Lake likely due to low organic matter in the lake system and the low amounts of terrestrial productivity in the watershed.

Grain Size Analysis

Sediment cores record the various size classes of sediment that are deposited on a given time scale. Variations in the distribution of coarse and fine grain material can be used to infer changes in the hydrologic condition of lake systems. In many cases, increases in coarse grain size particles are linked to increased terrestrial input into a system due to higher energy hydrologic flux (Ambers, 2001; Brown et al., 2002; Brown et al., 2000; Noren et al., 2002; Parris et al., 2010). Drake (1999) used grain size analysis to identify flood-induced terrestrial deposition on the Eel shelf off the coast of northern California. Flood layers were also identified on a modern time scale in a western Oregon reservoir and used to infer basin hydrologic changes due to local land use changes (Ambers, 2001). Lake sediments cores can also show relative storminess, extreme hydrologic events, and flood occurrence over millennial time scales (Brown et al., 2000; Eden & Page, 1998; Noren et al., 2002; Parris et al., 2010). Kirby (2015; 2012) and Hiner (2016) used grain size and other sediment proxies to describe shifts in climate and climate forcing during the Holocene. Grain size has been used frequently to determine storminess and flood frequency, but can be equally useful to determine drought frequency and intensity. Grain size paired with isotope measurements and pollen analysis has been used to identify persistent droughts during the Holocene in California and Nevada Lakes (Benson et al., 2002; Kirby et al., 2012).

Pear Lake is a silt and sand dominated system (Figure 2-4). Clay shows minor fluctuations and is highly correlated with silt. Using high percent sand as a proxy for wetness and high percent silt (lack of sand) as a proxy for aridity the data show a series of climatic shifts throughout the record. The majority of the percent sand peaks are in the deepest portions of the core describing a stormy early lake history. Percent sand peaks are distributed throughout the record including three episodes of sustained high percent sand from 300 – 275, 212 – 192, and 140 – 80 cm. These periods are assumed to be large terrestrial inputs cause by extreme hydrologic events. The number of percent sand peaks decreases with decreasing depth, but the magnitude and width of the peaks increase. Silt percent increases with decreasing depth and from 278 – 248, 192 – 140, and 80 – 0 cm there is a notable lack of large percent sand peaks and notably high, sustained silt percent (Figure 2-4). These periods may have been drier than the rest of the record and encompassed major droughts. The grain size analysis is discussed more thoroughly in Chapter 3 in the context of Holocene climate variability.

References

Ahmad, K., & Davies, C. (2017). Stable isotope (delta C-13 and delta N-15) based interpretation of organic matter source and paleoenvironmental conditions in Al-Azraq basin, Jordan. *Applied Geochemistry, 78*, 49-60. doi:10.1016/j.apgeochem.2016.12.004

Ambers, R. K. R. (2001). Using the sediment record in a western Oregon flood-control reservoir to assess the influence of storm history and logging on sediment yield. *Journal of Hydrology, 244*(3-4), 181-200. doi:10.1016/s0022-1694(01)00331-6

Anderson, R. S. (1990). Holocene forest development and paleoclimates within the central Sierra Nevada, California. *The Journal of Ecology*, 470-489.

Baker, P. A., Seltzer, G. O., Fritz, S. C., Dunbar, R. B., Grove, M. J., Tapia, P. M., . . . Broda, J. P. (2001). The history of South American tropical precipitation for the past 25,000 years. *Science, 291*(5504), 640-643. doi:10.1126/science.291.5504.640

Benson, L., Kashgarian, M., Rye, R., Lund, S., Paillet, F., Smoot, J., . . . Lindstrom, S. (2002). Holocene multidecadal and multicentennial droughts affecting Northern California and Nevada. *Quaternary Science Reviews, 21*(4-6), 659-682. doi:10.1016/s0277-3791(01)00048-8

Bloom, A. M., Moser, K. A., Porinchu, D. F., & MacDonald, G. M. (2003). Diatom-inference models for surface-water temperature and salinity developed from a 57-lake calibration set from the Sierra Nevada, California, USA. *Journal of Paleolimnology, 29*(2), 235-255.

Blott, S. J., & Pye, K. (2001). GRADISTAT: a grain size distribution and statistics package for the analysis of unconsolidated sediments. *Earth surface processes and Landforms, 26*(11), 1237-1248.

Brenner, M., Whitmore, T. J., Curtis, J. H., Hodell, D. A., & Schelske, C. L. (1999). Stable isotope (delta C-13 and delta N-15) signatures of sedimented organic matter as indicators of historic lake trophic state. *Journal of Paleolimnology, 22*(2), 205-221. doi:10.1023/a:1008078222806

Brown, S., Bierman, P., Lini, A., Davis, P. T., & Southon, J. (2002). Reconstructing lake and drainage basin history using terrestrial sediment layers: analysis of cores from a post-glacial lake in New England, USA. *Journal of Paleolimnology, 28*(2), 219-236. doi:10.1023/a:1021623020656

Brown, S. L., Bierman, P. R., Lini, A., & Southon, J. (2000). 10 000 yr record of extreme hydrologic events. *Geology, 28*(4), 335-338. doi:10.1130/0091-7613(2000)028<0335:yroehe>2.3.co;2

Diefendorf, A. F., Patterson, W. P., Holmden, C., & Mullins, H. T. (2008). Carbon isotopes of marl and lake sediment organic matter reflect terrestrial landscape change during the late Glacial and early Holocene (16,800 to 5,540 cal yr B.P.): a multiproxy study of lacustrine sediments at Lough Inchiquin, western Ireland. *Journal of Paleolimnology, 39*(1), 101-115. doi:10.1007/s10933-007-9099-9

Drake, D. E. (1999). Temporal and spatial variability of the sediment grain-size distribution on the Eel shelf: the flood layer of 1995. *Marine Geology, 154*(1-4), 169-182. doi:10.1016/s0025-3227(98)00111-x

Eden, D. N., & Page, M. J. (1998). Palaeoclimatic implications of a storm erosion record from late Holocene lake sediments, North Island, New Zealand. *Palaeogeography Palaeoclimatology Palaeoecology, 139*(1-2), 37-58. doi:10.1016/s0031-0182(97)00136-3

Engel, Z., Skrzypek, G., Paul, D., Drzewicki, W., & Nývlt, D. (2010). Sediment lithology and stable isotope composition of organic matter in a core from a cirque in the Krkonoše Mountains, Czech Republic. *Journal of Paleolimnology, 43*(4), 609-624. doi:10.1007/s10933-009-9356-1

Geiss, C. E., Umbanhowar, C. E., Camill, P., & Banerjee, S. K. (2003). Sediment magnetic properties reveal holocene climate change along the Minnesota prairie-forest ecotone. *Journal of Paleolimnology, 30*(2), 151-166. doi:10.1023/a:1025574100319

Geotek. Magnetic Susceptibility. Retrieved from http://www.geotek.co.uk/products/magsusc/

Hedges, J. I., & Keil, R. G. (1995). Sedimentary organic matter preservation: an assessment and speculative synthesis. *Marine Chemistry, 49*(2), 81-115. doi:http://dx.doi.org/10.1016/0304-4203(95)00008-F

Hiner, C. A., Kirby, M. E., Bonuso, N., Patterson, W. P., Palermo, J., & Silveira, E. (2016). Late Holocene hydroclimatic variability linked to Pacific forcing: evidence from Abbott Lake, coastal central California. *Journal of Paleolimnology, 56*(4), 299-313. doi:10.1007/s10933-016-9912-4

Hodell, D. A., Curtis, J. H., & Brenner, M. (1995). Possible role of climate in the collapse of Classic Maya civilization.

Holtgrieve, G. W., Schindler, D. E., Hobbs, W. O., Leavitt, P. R., Ward, E. J., Bunting, L., . . . Holmgren, S. (2011). A coherent signature of anthropogenic nitrogen deposition to remote watersheds of the northern hemisphere. *Science, 334*(6062), 1545-1548.

Kendall, C., Silva, S. R., & Kelly, V. J. (2001). Carbon and nitrogen isotopic compositions of particulate organic matter in four large river systems across the United States. *Hydrological Processes, 15*(7), 1301-1346.

Kirby, M. E., Knell, E. J., Anderson, W. T., Lachniet, M. S., Palermo, J., Eeg, H., . . . Hiner, C. A. (2015). Evidence for insolation and Pacific forcing of late glacial through Holocene climate in the Central Mojave Desert (Silver Lake, CA). *Quaternary Research, 84*(2), 174-186. doi:10.1016/j.yqres.2015.07.003

Kirby, M. E., Lund, S. P., Patterson, W. P., Anderson, M. A., Bird, B. W., Ivanovici, L., . . . Nielsen, S. (2010). A Holocene record of Pacific Decadal Oscillation (PDO)-related hydrologic variability in Southern California (Lake Elsinore, CA). *Journal of Paleolimnology, 44*(3), 819-839. doi:10.1007/s10933-010-9454-0

Kirby, M. E., Poulsen, C. J., Lund, S. P., Patterson, W. P., Reidy, L., & Hammond, D. E. (2004). Late Holocene lake level dynamics inferred from magnetic susceptibility and stable oxygen isotope data: Lake Elsinore, southern California (USA). *Journal of Paleolimnology, 31*(3), 275-293. doi:10.1023/B:JOPL.0000021710.39800.f6

Kirby, M. E., Zimmerman, S. R. H., Patterson, W. P., & Rivera, J. J. (2012). A 9170-year record of decadal-to-multi-centennial scale pluvial episodes from the coastal Southwest United States: a role for atmospheric rivers? *Quaternary Science Reviews, 46*, 57-65. doi:10.1016/j.quascirev.2012.05.008

Lamb, A. L., Wilson, G. P., & Leng, M. J. (2006). A review of coastal palaeoclimate and relative sea-level reconstructions using δ13C and C/N ratios in organic material. *Earth-Science Reviews, 75*(1), 29-57. doi:http://dx.doi.org/10.1016/j.earscirev.2005.10.003

Lees, J. A., Flower, R. J., Ryves, D., Vologina, E., & Sturm, M. (1998). Identifying sedimentation patterns in Lake Baikal using whole core and surface scanning magnetic suceptibility. *Journal of Paleolimnology, 20*(2), 187-202. doi:10.1023/a:1008043230549

Livingstone, D. (1975). Late Quaternary climatic change in Africa. *Annual Review of Ecology and Systematics, 6*(1), 249-280.

Lotter, A. F., Birks, H. J. B., Hofmann, W., & Marchetto, A. (1997). Modern diatom, cladocera, chironomid, and chrysophyte cyst assemblages as quantitative

indicators for the reconstruction of past environmental conditions in the Alps. I. Climate. *Journal of Paleolimnology, 18*(4), 395-420.

Lützow, M. v., Kögel-Knabner, I., Ekschmitt, K., Matzner, E., Guggenberger, G., Marschner, B., & Flessa, H. (2006). Stabilization of organic matter in temperate soils: mechanisms and their relevance under different soil conditions–a review. *European Journal of Soil Science, 57*(4), 426-445.

MacDonald, G., Felzer, B., Finney, B., & Forman, S. (2000). Holocene lake sediment records of Arctic hydrology. *Journal of Paleolimnology, 24*(1), 1-13. doi:10.1023/a:1008100714795

MacDonald, G. M., Moser, K. A., Bloom, A. M., Porinchu, D. F., Potito, A. P., Wolfe, B. B., . . . Orme, A. J. (2008). Evidence of temperature depression and hydrological variations in the eastern Sierra Nevada during the Younger Dryas stade. *Quaternary Research, 70*(2), 131-140.

Matsumoto, G. I., Kanou, R., Sato, C., Horiuchi, K., & Kawai, T. (2012). Paleoenvironmental changes in northwest Mongolia during the last 27 kyr inferred from organic components in the Lake Hovsgol sediment core record. *Limnology, 13*(1), 55-63. doi:10.1007/s10201-011-0355-3

Meyers, P. A. (1997). Organic geochemical proxies of paleoceanographic, paleolimnologic, and paleoclimatic processes. *Organic Geochemistry, 27*(5), 213-250. doi:http://dx.doi.org/10.1016/S0146-6380(97)00049-1

Meyers, P. A. (2003). Applications of organic geochemistry to paleolimnological reconstructions: a summary of examples from the Laurentian Great Lakes. *Organic Geochemistry, 34*(2), 261-289. doi:http://dx.doi.org/10.1016/S0146-6380(02)00168-7

Meyers, P. A., & Ishiwatari, R. (1993). Lacustrine Organic Geochemistry - An Overview of Organic-Matter Sources and Diagenesis in Lake-Sediments. *Organic Geochemistry, 20*(7), 867-900. doi:10.1016/0146-6380(93)90100-p

Meyers, P. A., & Lallier-Vergès, E. (1999). Lacustrine sedimentary organic matter records of Late Quaternary paleoclimates. *Journal of Paleolimnology, 21*(3), 345-372.

Noren, A. J., Bierman, P. R., Steig, E. J., Lini, A., & Southon, J. (2002). Millennial-scale storminess variability in the northeastern United States during the Holocene epoch. *Nature, 419*(6909), 821-824. doi:10.1038/nature01132

Oldfield, F., Rummery, T., Thompson, R., & Walling, D. E. (1979). Identification of suspended sediment sources by means of magnetic measurements: some preliminary results. *Water Resources Research, 15*(2), 211-218.

Parris, A. S., Bierman, P. R., Noren, A. J., Prins, M. A., & Lini, A. (2010). Holocene paleostorms identified by particle size signatures in lake sediments from the northeastern United States. *Journal of Paleolimnology, 43*(1), 29-49. doi:10.1007/s10933-009-9311-1

Peterson, B. J. (1999). Stable isotopes as tracers of organic matter input and transfer in benthic food webs: A review. *Acta Oecologica, 20*(4), 479-487. doi:http://dx.doi.org/10.1016/S1146-609X(99)00120-4

Porinchu, D., Rolland, N., & Moser, K. (2009). Development of a chironomid-based air temperature inference model for the central Canadian Arctic. *Journal of Paleolimnology, 41*(2), 349-368.

Routh, J., Meyers, P. A., Gustafsson, Ö., Baskaran, M., Hallberg, R., & Schöldström, A. (2004). Sedimentary geochemical record of human–induced environmental changes in the Lake Brunnsviken watershed, Sweden. *Limnology and Oceanography, 49*(5), 1560-1569. doi:10.4319/lo.2004.49.5.1560

Sickman, J. O., Bennett, D. M., Lucero, D. M., Whitmore, T. J., & Kenney, W. F. (2013). Diatom-inference models for acid neutralizing capacity and nitrate based on 41 calibration lakes in the Sierra Nevada, California, USA. *Journal of Paleolimnology, 50*(2), 159-174. doi:10.1007/s10933-013-9711-0

Thompson, R., Battarbee, R. W., Osullivan, P. E., & Oldfield, F. (1975). Magnetic-Susceptibility of Lake Sediments. *Limnology and Oceanography, 20*(5), 687-698.

Thorndycraft, V., Hu, Y., Oldfield, F., Crooks, P. R. J., & Appleby, P. G. (1998). Individual flood events detected in the recent sediments of the Petit Lac d'Annecy, eastern France. *Holocene, 8*(6), 741-746. doi:10.1191/095968398668590504

Thornton, S. F., & McManus, J. (1994). Application of Organic Carbon and Nitrogen Stable Isotope and C/N Ratios as Source Indicators of Organic Matter Provenance in Estuarine Systems: Evidence from the Tay Estuary, Scotland. *Estuarine, Coastal and Shelf Science, 38*(3), 219-233. doi:http://dx.doi.org/10.1006/ecss.1994.1015

Vaalgamaa, S., Sonninen, E., Korhola, A., & Weckström, K. (2013). Identifying recent sources of organic matter enrichment and eutrophication trends at coastal sites using stable nitrogen and carbon isotope ratios in sediment cores. *Journal of Paleolimnology, 50*(2), 191-206. doi:10.1007/s10933-013-9713-y

Wolfe, A. P., Baron, J. S., & Cornett, R. J. (2001). Anthropogenic nitrogen deposition induces rapid ecological changes in alpine lakes of the Colorado Front Range (USA). *Journal of Paleolimnology, 25*(1), 1-7. doi:10.1023/a:1008129509322

Wood, S. H. (1977). Distribution, correlation, and radiocarbon dating of late Holocene tephra, Mono and Inyo craters, eastern California. *Geological Society of America Bulletin, 88*(1), 89-95.

Chapter 3: Climate Variations in the Sierra Nevada During the Holocene

Introduction

Lakes have been used as paleoclimate records on many time scales (event to millennial scale) through grain size analysis and the relative abundance of sands and silts (Brown et al., 1999; Campbell, 1998; Kirby et al., 2010; Parris et al., 2010; Rodbell et al., 1999). Seasonal to annual shifts in productivity and environmental conditions can produce varved sediments which can be used to discern annual variability in hydrologic dynamics from large floods to individual rain events (Amann et al., 2014; Ambers, 2001; Brown et al., 1999; Brown et al., 2000; Campbell, 1998). Sediment cores from short lived (annual to decadal) ephemeral lakes can provide records of regional climate based on their volatility and susceptibility to desiccation (Enzel et al., 1992; Kirby et al., 2015; Kirby et al., 2012). Lake level changes describing highstands and lowstands of decadal- to centennial-scale can identify periods of sustained extreme drought (Benson et al., 2002; Mensing et al., 2004; Negrini et al., 2006; Stine, 1994). Lakes have also been used to describe changes in insolation forcing since the last glacial and shifts in spatial patterns of multi-decadal scale climate forcing patterns (Bird & Kirby, 2006; Cayan et al., 1998; Kirby et al., 2007; Kirby et al., 2010; MacDonald et al., 2016; Menking & Anderson, 2003). Understanding variations in climate regimes, particularly climate extremes, is important for predicting future climate shifts. Modeling future climate is exceedingly complicated due to the large number of complex components that must be factored in, but

with a better understanding of our climate past there is potential for a more effective prediction of our climate future.

The climate of the Holocene on the west coast of North America has been described in three generalized periods: the early, middle and late Holocene. The early Holocene is generally considered to be a stormier, wetter time period coming out of the last glacial (Barron et al., 2003; Bird & Kirby, 2006; Kirby et al., 2015). The middle Holocene is often described as a period of increased aridity with intermittent phases of intense wetness (Barron et al., 2003; Benson et al., 2002; Kirby et al., 2015; MacDonald et al., 2016; Mensing et al., 2004). Finally, the late Holocene has been describe as both wet and dry and is generally considered to be a time of increased climate variability, particularly toward present day (Barron et al., 2003; Benson et al., 2002; Kirby et al., 2015; Kirby et al., 2010; Stine, 1990).

The objective of this chapter is to investigate multi-decadal to millennial scale climate trends of aridity and precipitation in a snow-fall dominated, alpine lake of the Sierra Nevada during the Holocene. The high elevation setting and geography surrounding Pear Lake provide a unique view into paleoclimate that is unlike the majority of the California paleoclimate literature based on lower elevation lacustrine systems. Because of granite bedrock and typically slow sedimentation rates, most high elevation lakes in the Sierra Nevada have sediment accumulations of 1 to 2 meters during the Holocene (Power, 1998) making high-resolution climate-reconstructions impossible. Owing to the favorable sediment-deposition environment in our study system, Pear Lake, we hypothesize we will be able to observe climate extremes including pluvial periods and

droughts on a decadal to millennial scale. Additionally, we hypothesize that sand dominated sediment layers in Pear Lake are the result of intense pluvial events such as winter rain-on-snow events (atmospheric rivers), avalanches following large snowfall events or intense summer or autumn rains caused by monsoonal moisture (North American Monsoon). To test these hypotheses we will use a grain size as a paleoclimate proxy to identify climate regimes and high energy deposition events in Pear Lake through the Holocene. This record will be compared to other paleo records across the West Coast to examine synchronicity and dissonance in the records and will be discussed in the framework of the proposed California climate dipole (Dettinger et al., 1998).

Methods

To test these hypotheses we use a grain size proxy to determine Holocene climate trends in Pear Lake. We assume that the event-driven sediment deposition in Pear Lake can record paleoclimate trends and collected a sediment core form the deepest portion of the lake. We created an age model for the sediment core to understand the chronology of the archive and the duration of the record and then used a grain size paleoclimate proxy to reconstruct the Holocene climate trends and compared our finding with various regional paleoreconstructions on decadal to millennial time scales.

Core Collection and Characterization

In 2013, the National Lacustrine Core Facility (LacCore) assisted in collecting two sediment cores, using Livingstone and Bolivia corers, from the deepest part of the Pear

Lake basin (z_{max} = 27 m). SQNP-PEAR13-1A (Core A) and SQNP-PEAR13-1B (Core B) were collected 10 m apart and were visually determined to have high lithological correlation. Due to Core B being compressed by raised bedrock, the majority of our analyses were done on Core A and Core B was only used to replace portions where the lithology of Core A was disturbed during collection. Core A, is 6.7 m long and was collected in eight sections approximately 90 cm in length. The core was split and characterized contiguously using magnetic susceptibility with a Bartington point sensor (Geotek) and reported in SI units ($x10^{-5}$ m^3 kg^{-1}). Macrofossils and bulk sediments were collected for radioisotope dating, and high resolution photographic images were captured before the core was wrapped in film and placed in refrigerated storage for later sub-sampling (Supplemental Materials). The stratigraphy of the core was visually characterized and due to the complexity of the core and the range in layer thickness (1 mm to 10 cm) an abbreviated lithological representation of the core was developed (Figure 3-1). The core was also characterized by particle size distribution using grain size analysis and biogeochemical properties were characterized using elemental analysis (%C, %N, C: ratio) and stable isotope analysis ($\delta^{15}N$ and $\delta^{13}C$).

Age Control

Radiocarbon and ^{210}Pb dates were used to create an age model. Thirteen macro-fossils and bulk sediment samples were collected from the core for radiocarbon dating (Table 3-1). All samples were prepared using the University of California, Irvine Keck Carbon Cycle AMS Laboratory Acid-Base-Acid sample pre-treatment protocol and were

analyzed by accelerator mass spectrometry by DirectAMS in Bothell, Washington. Radiocarbon concentrations are reported in $\Delta^{14}C$ units relative to the NIST Oxalic Acid I standard and corrected to a $\delta^{13}C$ value of -25‰ (Stuiver & Polach, 1977). A single inversion was omitted from the data leaving 12 radiocarbon dates for the age model. We created the age model (Figure 3-2) using BACON (v2.2), a program that uses Bayesian statistics and prior information to reconstruct depositional histories (Blaauw M, 2011). Dates were internally calibrated with IntCal13. Radiocarbon measurements were attempted on bulk samples collected from sections 7L and 8L however these sediments were predominantly composed of glacial flour with very little organic matter (0.05 to < 1% C by weight). The radiocarbon content of these samples was not significantly different from zero, therefore they were not included in the age model. We suspect that the carbon in the glacial flour was mainly derived from carbonate minerals present in trace inclusions of Sierra Nevada roof pendants dating to the Paleozoic and early Mesozoic periods (Brook, 1977; Kerrick et al., 1973).

The top 24 cm of the core was dated by ^{210}Pb at the Land Use and Environmental Change Institute (LUECI) on the campus of the University of Florida (Table 3-2). Radiometric measurements (^{210}Pb, ^{226}Ra and ^{137}Cs) were made using low-background gamma counting with well-type intrinsic germanium detectors (Appleby et al., 1986; Schelske et al., 1994). We used the constant rate of supply (CRS) model (Appleby & Oldfieldz, 1983; Oldfield & Appleby, 1984) to calculate sediment ages and propagated age errors using first-order approximations calculated according to Binford (1990).

Due to the thickness of some of the layers in the core, the age model was created using an adjusted dataset in which thicker sediment layers were consolidated into single points. These thick layers were generally deposited over a short time scale (hours to days) and the original age model described them to occur over tens to hundreds of years. Every homogeneous layer greater than or equal to 2 cm thick was grouped into a single data point for all sediment characteristics by averaging the characterization data (e.g. particle size distribution, stable isotope, elemental data) from the entire layer. The thick layers were considered short duration hydrologic input events and were visually detected as large homogenous layers. They were defined quantitatively as periods of elevated sand percent with at least one sample above a threshold of 59.5% sand (1.5 std. dev. above mean sand content for the entire core). The details of the %sand based proxy will be detailed below.

Grain Size Preparation and Analysis

Samples were taken from the top 580 cm of the core for grain size analysis. As previously stated, some samples were combined to account for hydrologic event based deposition (approximately 60 cm). The lower most 90 cm of the core were omitted because the base of the sediment core was primarily composed of glacial flour and regolith. Furthermore, the low presence of organic matter and unusual stable isotope values in the lower most 90 cm of sediment suggest that the watershed was undergoing a significant landscape response and recovery from glaciation. Approximately one cubic centimeter of sediment was collected every centimeter and prepared according to Kirby

(2010). Organic matter was removed using ≥ 40 ml 30% H_2O_2, carbonates were removed with 10 ml of 1 N HCl, and biogenic silica was removed using 10 ml of 1 N NaOH. All samples were sieved at 1 mm after chemical treatment to remove gravel and extra coarse sands. In lieu of sonication, 0.1 g of sodium hexametaphosphate was added as a dispersing agent and the samples were shaken for ≥ 8 hours the night before grain size analysis. Samples were analyzed on a Beckman-Coulter LS 13-320 laser particle size analyzer (LS 13-320). When necessary, samples were split or combined to reach optimal parameters for the analysis established by the LS 13-320 calibration. In this study, we will use SI units and the particle diameter size fraction distinctions (clay: < 2 µm, silt: 2 to < 62.5 µm, sand: 62.5 to < 2 mm) from the freeware program GRADISTAT (Blott & Pye, 2001) to describe the particle size distribution. The sieved coarse sand and gravel was quantified (counted and weighed) and presence and absence of gravel (diameter ≥ 2 mm) was recorded for each sample.

Stable Isotope and Elemental Analysis

The core was subsampled contiguously at 1 cm increments for its entire length and prepared for stable isotope and elemental analysis. One cubic centimeter of sediment was extracted, weighed, and dried at 60 ºC overnight. A subsample was then ground with mortar and pestle and homogenized before being weighed and analyzed on an isotope ratio mass spectrometer interfaced with an elemental analyzer at the Facility for Isotope Ratio Mass Spectrometry at UC Riverside. All runs included National Institutes for Standards and Technology (NIST) glutamic acid standards (RM 8573 and 8574) and

were reported in per mil units (‰) relative to atmospheric N_2 ($\delta^{15}N$) and Pee Dee Belemnite ($\delta^{13}C$). For elemental analysis, NIST peach (RM 1547) was used as the standard for %C and %N.

Data Analysis

The LS 13-320 software was used to convert the raw count data into binned groups for further analysis. The freeware program GRADISTAT (Blott & Pye, 2001) was then used to calculate statistics on the output data from the LS 13-320 including the percent sand, silt, and clay, and modal analysis. GRADISTAT provided primary, secondary, and tertiary modes in the data output (Figure 3-3). We used these modes and the particle size category that they fell under (sand or silt) to infer relative deposition intensity for each sample (Table 3-3). Each sample was categorized as sand- or silt-dominated depending on which particle size category the primary mode occupied and then the samples were categorized as unimodal (having one mode) or bimodal/trimodal (having two or three modes). Bimodal and trimodal samples could have modes in both sand and silt particle size categories. Samples with unimodal sand distributions were considered strong (high intensity) depositional environments and bimodal/trimodal sand distribution are considered moderate (lowest intensity) to extreme (highest intensity) depositional environments depending on the particle size distribution and amplitude of the modes (Figure 3-4). As explained in more depth in the Discussion, extreme sand-dominated samples were considered to represent wetter climate periods and extreme silt-dominated samples were considered to represent dryer periods (Brown et al., 2000; Campbell, 1998;

Kirby et al., 2012) (Table 3-3). We used regime shift detection (SRSD) software that used sequential t-test analysis to identify regime shifts in the data over centennial scales (Rodionov, 2004). This software allowed us to statistically quantify shifts from high-low and low-high precipitation regimes.

Results

Particle Size Distribution

This study will emphasize grain size analyses and focus on three Holocene periods described in the paleoclimate literature (early Holocene: 11250 – 7250; middle Holocene: 7250 – 3000; late Holocene: 3000 cal yr BP to modern). The Pear Lake basin is a sand-silt dominated catchment. Therefore, we hypothesize that hydrologic extremes, both wet and arid, can be best detected in sand and silt data and that clay data is supplementary. The presence of sand in the sediment had a relatively large range (x_{min} = 1.3%, x_{max} = 83.8%, $\bar{x}$ = 35.2%; slope = 0.001, $p < 0.0001$; Figure 3-7) and displayed peaks at variable times throughout the core length. The silt fraction of the sediment fluctuated similarly to sand, but with a distribution more skewed towards higher percent silt (x_{min} = 14.5%, x_{max} = 87.4%, $\bar{x}$ = 57.2%; slope = -0.001, $p < 0.0001$; Figure 3-7). The percent clay present in the sediment held within a relatively small range (x_{min} = 1.7%, x_{max} = 11.5%. $\bar{x}$ = 7.6%; Figure 3-7) and had a slope vs. time that was not different from zero. The sand and silt composition of the sediment was highly variable throughout the core and showed an expected strong inverse correlation as the clay portion remained relatively stable (r = -0.998, $p < 0.0001$).

Gravel particles (≥ 2 m diameter) were present throughout the core and often correlated with the peaks in percent sand and coarse sand modes (Figure 3-8). Evidence of gravel input was most prevalent in the early Holocene (65 occurrences, 34% of gravel-containing samples). The middle Holocene had approximately half as many gravel inputs as the early Holocene (35 occurrences, 20% of samples) and the late Holocene had only 15 occurrences (10% of samples).

Mode Analysis

Grain size distributions were categorized into two major groups; distributions with primary modes in the sand grain size category (sandy) or primary modes in the silt particle size category (silty) (Table 3-3). Overall, there were more sandy distributions in the early Holocene relative to the middle and late Holocene (early: 118, middle: 69, late: 56 occurrences) and more silty distributions in the middle Holocene than the early and late Holocene (early: 88, middle: 116, late: 73 occurrences). The silty distributions that we will focus on in this analysis are the silt unimodal distributions (Figure 3-9). Silt unimodal distributions in the middle and late Holocene (48 and 58 occurrences) were more than double the number observed in the early Holocene (19 occurrences). The sandy distributions that are significant to this analysis are the distributions with only sand modes (Figure 3-9). The early Holocene had double the number of distributions with only sand modes (71 occurrences) than the middle and late Holocene (35 and 37 occurrences).

Magnetic Susceptibility

Magnetic susceptibility was variable throughout the core with a range of 5.1 to 133 $x10^{-5}\,m^3\,kg^{-1}$ (SI) with an average of 33.3 (Figure 3-6). The majority of the variation was between 15 and 50 $x10^{-5}\,m^3\,kg^{-1}$ (SI) with 9 predominant peaks above 60 $x10^{-5}\,m^3\,kg^{-1}$ (SI). There was a significant downward trend toward present over the duration of the record (slope = 0.0018, $p < 0.0001$).

Elemental Analysis

Percent carbon by dry weight (%C) is used as a proxy for organic matter content in the sediment. It is important to note that past studies of Sierra Nevada lakes, including Pear Lake, have shown virtually no carbonate in the sediments (Sickman, unpublished). Organic matter content oscillated with a wavelength of approximately 2,000 years (Figure 3-5) and increased with decreasing age (slope = $-2.07x10^{-4}$, $p < 0.0001$; Table 3-4). The oscillations fluctuated between 0.02% and 14.7% with an average of 7.1% carbon. Total percent nitrogen had a regular oscillation pattern as well (x_{min} = 0.01%, x_{max} = 1.2%, $\bar{x}$ = 0.59%) and was strongly correlated with carbon ($r = 0.963$; $p < 0.0001$). There was also an increase in nitrogen with decreasing age (slope = $-2.2x10^{-5}$; $p < 0.0001$). Starting at approximately 3000 cal yr BP, both carbon and nitrogen percent began larger scale fluctuations with less local variation (Figure 3-5). The molar carbon to nitrogen ratio (C:N) fluctuated within a relatively small range for the majority of the record (x_{min} = 9.8, x_{max} = 28.9, $\bar{x}$ = 14.1; Table 3-4) with exception of a 40 cm section in the early portion of the record (9900 - 10500 cal

yr BP) which exhibited approximately double the amplitude of variation (Figure 3-5). C:N declined with decreasing age (slope = $7.3x10^{-5}$, $p < 0.0001$).

Isotope Analyses

Carbon isotope analysis ($\delta^{13}C$) revealed overall variation of -30.2‰ to -22.5‰ and an average of -26.4‰ (Table 3-4) and there was a decrease of $\delta^{13}C$ toward the core surface (slope = $9.9x10^{-5}$, $p < 0.0001$)(Figure 3-5). Nitrogen isotope composition ranged from -1.5‰ to 3.6‰ with an average of 1.7‰ (Table 3-4), and displayed several conspicuous monotonic trends including a $\delta^{15}N$ decline from 11000 – 10800 cal yr BP, an increase from 10800 – 9000 cal yr BP, flat response from 9000 – 1500 cal yr BP, and then a decline from 1500 to present (Figure 3-5). Through this variation, the $\delta^{15}N$ showed an increase toward the surface of the core (slope = $-1.2x10^{-4}$, $p < 0.0001$), but the overall significance of the recent monotonic trends are not well understood, i.e., do they represent changes in sources of nitrogen to the lake or are they a result of post-depositional changes caused by sediment diagenesis (Holtgrieve et al., 2011)?

Discussion

Proxy Interpretations

Grain Size

The distribution of grain sizes within sediment is a useful proxy for climatic shifts in lake systems. In general terms, it takes less energy to move silt and clay size particles than it does to move sand and gravel size particles. Parris et al. (2010) and Lamoureux

(2000) found that snowmelt does not move as much material into lakes as pluvial events and Bird and Kirby (2006) argued that snowmelt does not have sufficient energy to move thick sand layers present in their sediment core into Dry Lake's depocenter. Amann et al. (2014) observed that the highest sedimentation rates in an alpine environment occurred when peak snowmelt combined with large pluvial episodes. These studies support the idea that extreme pluvial events have higher energy than snowmelt alone and that pluvial events are recorded by grainsize in the sediment record of mountain lakes.

Sand and gravel size particles settle out of the lake and are deposited more quickly than silt and clay sized particles. Campbell (1998) found that when there is intense pluvial input into a lake, coarse materials (sand and gravel sized particles) are deposited while finer particles (silt and clay sized) are washed out of the lake due to increased flow and turbulence in the system. Grain size and sediment depositional characteristics have been used to identify distinct pluvial events and storminess (Eden & Page, 1998; Noren et al., 2002; Page et al., 1994; Thorndycraft et al., 1998) and flood events (Ambers, 2001; Drake, 1999; Nesje et al., 2001; Oliva et al., 2016; Parris et al., 2010) on a range of spatial and temporal scales. Signals of decadal-scale climate variability such as El Nino Southern Oscillation (ENSO) and Pacific Decadal Oscillation (PDO) have been identified using grain size distribution analysis (Kirby et al., 2010; Moy et al., 2002; Rodbell et al., 1999) in addition to larger millennial-scale climate shifts (Campbell, 1998; Kirby et al., 2007; Kirby et al., 2012; Moore et al., 2001).

Grain size has also been shown to record a range of precipitation intensities. Extreme events such as rain-on-snow events and potential atmospheric rivers have been identified

in lake sediments (Brown et al., 2000; Kirby et al., 2012) as well as small scale floods and annual shifts in hydrology (Brown et al., 1999; Last & Vance, 1997) and avalanche occurrence through intense coarse material and dropstone deposition (Luckman, 1975; Nesje et al., 2007; Seierstad et al., 2002) and the use of X-Ray Fluorescence (Vasskog et al., 2011). Aridity and droughts have also been identified through lake sediment grain size analysis and sediment characteristics (Benson et al., 2002; Campbell, 1998; Cook et al., 2004; Kirby et al., 2012; Mann et al., 2008; Mensing et al., 2004). In contrast, aridity may be inferred from the lack of coarse grain input, suggesting low energy fluxes into the lake which would increase lake residence time and allow for the smaller particles (silt and clay sized) to settle out more readily and build up in the record.

Grain size analysis of Pear Lake sediments reveal a highly variable record of sand and silt percent. In the following analysis, we will refer to time periods using operationally-defined terms regarding their general wetness and dryness (Table 3-5). The record shows many sand-dominated periods ranging from multi-decadal to centennial time scales. A quantitative threshold was applied to the percent sand data to quantify potentially extreme precipitation events. The threshold was set at 1 standard deviation above the mean (about 50% sand by volume) which is well outside the range of standard fluctuations in percent sand. The data show a decreasing frequency of extreme events from past to present (Figure 3-10). The early Holocene (11250 to 7250 cal yr BP) has more than twice as many extreme events (37 vs. 15 occurrences) as the late Holocene (3000 cal yr BP to modern). The middle Holocene (7250 to 3000 cal yr BP) shows an intermediate number of extreme events (22 occurrences), yet most of the middle

Holocene is comprised of some of the most storm-free periods on record (7250 to 5950, 5150 to 4250, and 3950 to 3000 cal yr BP).

We hypothesize that silt-dominated periods can be interpreted as relatively dry periods in the record and that percent silt is positively correlated with aridity. The percent silt data were standardized and grouped into 50-year bins (Figure 3-11) and a threshold for multi-decadal drought-like conditions was set at a silt percent above the 3rd quartile (approximately 63% silt or 0.49 standard deviations). The middle Holocene has 25 occurrences of multi-decadal drought-like conditions which is the most in the record. The late Holocene has twice as many multi-decadal drought-like occurrences as the early Holocene (22 vs. 9 occurrences). An additional threshold was set for extreme, centennial-scale droughts: Four uninterrupted periods (200 years) of above third quartile range standardized, binned silt. With this threshold, three centennial-scale extreme droughts were identified: 7500 – 6900, 5000 - 4750, and 700 - 350 cal yr BP. Having a centennial-scale threshold for sustained, extreme droughts ensures that only the most intensely arid periods gain the distinction and periods of mixed wetness and dryness cannot be aggregated to signify a drought-like period.

Mode Analysis

Modes in sediment distributions describe depositional environments in lacustrine and fluvial systems. Folk and Ward (1957) described the bimodal nature of the Bravos River bar and the story it told of the sediment sourcing and which conditions moved the different size classes of materials. They explained that the steady state flow of the river

moved the sands and silts downstream at a relatively constant rate and the gravels and boulders were moved in from the watershed during large hydrologic events. Amann (2014) used modes in lake sediments to help identify large floods. He showed that when the mode deviated from the silt-size particle range to a large peak in the sand-size particle range, there was a high correlation with paleo mega-floods.

It is important to note that throughout the entire Pear Lake record there were no clay modes and never more than one silt mode. The primary mode of a distribution describes which depositional intensity (sand = higher energy, silt = lower energy) was dominant for the time period of deposition. If the primary mode is in the sand fraction, that means that there was higher energy input into the system and large amounts of sand were deposited during that time (Campbell, 1998; Eden & Page, 1998; Noren et al., 2002; Page et al., 1994; Thorndycraft et al., 1998). A silt primary mode means that there is a lack of sand and by the same logic the time period is described as having low energy deposition. A unimodal distribution describes one dominant depositional condition. A bimodal or trimodal distribution describes a combination of depositional conditions. If one combines the information taken from the primary mode with the information gleaned from the number of modes, one can obtain a more descriptive analysis of hydrologic conditions (Table 3-3). A unimodal silt distribution explains a sustained, low energy depositional condition that is made up of mostly clay- and silt-size particles and has low levels of sand in the distribution. It describes a moderately undisturbed lake, with longer residence time, that allows for slow and steady deposition of silts and clays. A unimodal sand distribution generally describes either one or more high energy depositions over a short time scale,

such that some of the silt- and clay-size particles suspended at the time were either washed out or had a small relative volume next to the large coarse deposition. This type of distribution could have moderate to low silt contribution and minimal clay contribution.

A bi-/tri-modal distribution with a silt primary mode represents a silt dominated, low energy depositional environment interrupted by low- to moderate-intensity sand-size particle depositions. The sand depositions during this time period were not large enough to skew the distribution to the sand fraction and overwrite the silt mode. A bi-/tri-modal distribution with a sand primary mode could be a moderate or extreme depositional environment. If there is a silt mode present in the distribution, we cannot identify the relative intensity of the depositional conditions and we consider this a moderate deposition period. If the modes are all in the sand size category, then this describes extreme deposition and multiple high energy depositional environments.

Based on this interpretation of depositional modes, two "extreme" distribution categories are defined for Pear Lake: 1) distributions with modes only in the sand-size particle range (> 62.5 μm, henceforth referred to as "sand dominated") will be a proxy for high-energy depositional environments connected to extreme precipitation events and 2) unimodal silt distributions (referred to as "silt-dominated) will be a proxy for low-energy depositional environments connected to increased aridity. In the following analysis, we will refer to time periods using specific terms regarding their general wetness and dryness (Table 3-5).

The beginning of the early Holocene is replete with sand dominated distributions (Figure 3-9). The remainder of the early Holocene is a combination of sand and silt dominated distributions. The data describes an early Holocene that starts out extremely stormy with repeated high-energy inputs into the lake on a centennial scale and then leads into a less intense wet period with intermittent aridity on a multi-decadal scale.

The middle Holocene is a more arid period. The majority of the "extreme" distributions are silt dominated, but clumped sand-dominated distributions occurring on a multi-decadal scale are also present. These deviations from aridity coincide with the extreme-event-heavy periods identified in the percent sand/silt based grain size analysis. An intense, centennial-scale arid period is described by repeated silt dominated distributions from approximately 5000 to 4800 cal yr BP. This arid period was identified in the sand/silt distribution proxy as an extreme centennial-scale drought.

The late Holocene is relatively more variable than the early and middle Holocene. The beginning of the late Holocene shows mostly sand dominated distributions, but transitions into millennial-scale silt dominance with short sand dominated incursions. The most intense of the silt dominated periods coincides with the Medieval Climate Anomaly (MCA) and one of three previously described extreme centennial-scale droughts.

Presence of Gravel

The Pear Lake sediment core has gravel size particles (≥ 2 mm diameter) interspersed throughout core. The presence of gravel describes an intense depositional environment and an intense, high-energy flux into the lake. Strong atmospheric rivers,

avalanches and other intense pluvial events have been known to hit the Sierra Nevada and drop up to 8 inches of precipitation (snow water equivalent) over the course of three days (Guan et al., 2013). Our lab group has witnessed rain-on-snow and avalanche events that have moved large amounts of material (including trees!) on top of frozen lakes. When the lake thaws, this material is deposited and may account for some of the larger clasts (up to 10 cm) in the sediment core (Luckman, 1975; Nesje et al., 2007; Seierstad et al., 2002). A large majority of the gravel depositions occur during the event-heavy early Holocene, although the middle Holocene also has periods of gravel deposition (Figure 3-8).

Comparison of Pear Lake to Dendrohydrology Reconstructions

To see if our grain size record is responding to decadal-scale variations in in regional precipitation and hydrologic conditions, we compared a San Joaquin Basin discharge record with the most recent 1050 years from the Pear Lake record (Figure 3-12). Meko et al. (2014) used tree rings records from the Klamath, Sacramento, and San Joaquin River Basins to reconstruct regional hydroclimate for the past millennium. Each reconstruction was calibrated and compared to other reconstructions that geographically bounded the reconstruction regions. We temporally-aggregated the annual tree ring reconstruction to an approximately 15-year resolution so that it better matched the ca. decadal-scale resolution of the Pear Lake reconstructions. We next visually correlated wet and dry periods derived from the Pear Lake record to the temporally-aggregated tree ring record derived from trees at low to mid-elevations. The binned San Joaquin reconstruction and the Pear Lake record have remarkable correlation and are moderately synchronized in

peak and trough positioning, specifically from 900 to 550 and 475 to 175 cal yr BP when the peaks in discharge and percent sand are most in phase. The use of temporal aggregation to align the annual tree ring record to the sediment record likely produced lags in the peaks and troughs of the two records. Nevertheless, based on the comparison to dendroclimatology records, we conclude that the sediment grain size record in the Pear Lake core is a robust proxy for precipitation and runoff and is responding to decadal-scale variations in high elevation precipitation.

Pear Lake Regional Climate

Grain size analysis (%sand data) from Pear Lake reveals a variable regional climate that goes through a series of regime shifts from wet to dry throughout the Holocene (Figure 3-13). We have analyzed the modes of these distributions to support and build on our hypotheses regarding the climatic conditions and depositional environments present during the sedimentation process. To avoid making assumptions about timescales that are outside the confidence interval of our age model, we have adopted and adapted a version of bin criteria for "wet periods" from Kirby (2012). For this record we binned standardized sand data into 50-year bins and set criteria for both wet and dry periods: Four or more above zero occurrences with no more than two below zero occurrences separating them depicts a pluvial period. The same criterion was set for arid periods using below zero occurrences. Using this criterion we delineated 7 pluvial periods and 8 arid periods in the data that lasted ≥ 200 years (Figure 3-14).

The early Holocene (11250 to 7250 cal yr BP) in Pear Lake consists of four pluvial periods interrupted by two arid periods. From 11250 to 9550 cal yr BP, Pear Lake experienced high levels of precipitation and was marked by repeated peaks and general high standardized percent sand (Figure 3-10); there were a few small deviations into below zero binned percent sand, but the period was overwhelmingly sandy. The first phase of the early Holocene is also the portion of the record with the most repeated unimodal sand and distributions with only sand modes (Figure 3-9). We argue that the repeated high sand percent and high frequency of all-sand-mode distributions is indicative of an intensely stormy time period with high-energy fluxes going into the lake. The next two pluvials (9300 to 7950 and 7750 to 7250 cal yr BP) in the early Holocene were less intense. Significant sand peaks are present and the general sand percent is sufficiently high to maintain positive standardized sand bins, but the modal analysis describes a less extreme environment with few sand unimodal, or all-sand-mode distributions. We argue that these periods, although still stormy and wet, are part of the transition into the more arid middle Holocene seen in Menking (2003). There are two arid periods present in the early Holocene between 9550 to 9300 and 7950 to 7750 cal yr BP depicted by repeated below zero occurrences of binned sand percent and a section of sustained unimodal silt distributions (Figure 3-9).

Pear Lake transitioned into a period of increased aridity in the middle Holocene (7250 to 3000 cal yr BP). This interval consists of three arid periods (7250 to 5950, 5150 to 4250, and 3950 to 3000 cal yr BP) surrounding two pluvial excursions (5950 to 5150 and 4250 to 3600 cal yr BP) (Figure 3-14). The arid periods are characterized by

repeated below zero occurrences of binned sand percent and the second and third highest frequency of unimodal silt distributions in the record. We argue that the low percent sand, and therefore high percent silt, and the presence of many unimodal silt distributions is evidence of low-energy depositional environments and a lack of significant precipitation and hydrologic flux into the lake on a multi-decadal to centennial scale. The lack of high energy events lowers the amount of sand being deposited in the lake and reduces the amount of silt and clay being washed out of the lake. The low-energy state of the basin's hydrology allows for slow-settling silts and clays to deposit over long periods of time. The two pluvials present in the middle Holocene are accompanied by a series of standardized percent sand peaks and clusters of unimodal sand and distributions with only sand modes (Figures 3-9, 3-10).

The late Holocene record of Pear Lake (3000 cal yr BP to modern) is categorized by a variable climate that is skewed towards aridity. A pluvial from 3000 to 2600 cal yr BP starts the late Holocene which then trends back to a short-lived dry period from 2600 to 2350 cal yr BP (Figure 3-14). The basin then experienced an intense pluvial, which rivals the initial early Holocene pluvial (11250 to 9550 cal year BP, Figure 3-14) described above and includes the largest standardized percent sand peak in the record between 2350 and 1450 cal yr BP (Figure 3-14). The late Holocene pluvial is followed by intense aridity to present (1450 to 63 cal yr BP, Figure 3-14) including the Medieval Climate Anomaly (MCA, 1050 to 650 cal yr BP), although there is a small deviation from aridity during the Little Ice Age (LIA, 500 to 100 cal yr BP).

Holocene Climate

Early Holocene (11250 to 7250 cal yr BP)

The Pear Lake record is in congruence with paleolimnology records from across California. Repeated percent sand peaks and high overall percent sand for the majority of the early Holocene combined with a high frequency of all-sand modes to describe a storm-heavy, wet early Holocene with few short-lived arid periods intermixed. Based on lake grain size records in western North America, the early Holocene was considered to have a wet climate with increased storm intensity. Kirby et al. (2007) argued that a northern reaching, stronger magnitude North American Monsoon (NAM) during the early Holocene was the source of increased late-summer/early-fall precipitation in Southern California based on a sediment analysis from Lake Elsinore, California. The authors argued that increased silty “storm layers”, high magnetic susceptibility values, and signs of an increased lake level during this period support a wet early Holocene attributed to lower winter insolation forcing. Sediment records from Dry Lake, California also support a stormy, wet early Holocene (9000 to 7500 cal yr BP) (Bird & Kirby, 2006). Increased organic matter and charcoal macrofossils during this time period described a more productive basin and significant input of terrestrial organic matter into the lake associated with precipitation events in the form of summer storms. Frequent sand spikes and general high percent sand input into the lake during the ice free season also supported a stormy early Holocene at Dry Lake. Kirby et al. (2015) showed evidence of persistent perennial waters in Silver Lake, California during the early Holocene (11700 to 7500 cal yr BP). Percent clay based lake level analysis described high lake levels at Silver Lake for the

duration of the early Holocene which can only be caused by sustained regional precipitation. Nearer to Pear Lake, Tulare Lake, which is fed from snowmelt from the southern Sierra Nevada, showed two major high stands in the early Holocene (10700 to 7800 cal yr BP) (Negrini et al., 2006). The younger of the two high stands lasted over 1000 years and was the maximum shoreline elevation for the entire record. The high lake levels at Tulare Lake describe a wet early Holocene and high levels of precipitation in the southern and central Sierra Nevada. The Pear Lake record is in congruence with these records from across California. Repeated percent sand peaks and high overall percent sand for the majority of the early Holocene combined with a high frequency of all-sand modes to describe a storm-heavy, wet early Holocene with few short-lived arid periods intermixed.

Middle Holocene (7250 to 3000 cal yr BP)

The Pear Lake record describes an arid middle Holocene with centennial-scale extreme droughts. Sustained low sand percent with minimal sand peak incursions and frequent unimodal silt distributions infer low precipitation and few high-energy inputs into the lake. There are two pluvial deviations around 5500 and 4100 cal yr BP. The older pluvial is seen in other records in central California and the western Sierra Nevada, but not in some southern California records. The younger pluvial is congruent with many records on the west coast of North America with variable temporal bounds. After the pluvial periods that dominated the early Holocene, a transition into aridity has been noted in many regions throughout California and western North America. The exact temporal

scale is variable and most records have one or more unique deviations from dryness, but many records describe low precipitation levels and a drier climate. Kirby et al. (2015) identified an arid middle Holocene (7500 to 4000 cal yr BP) in Silver Lake. Lake level proxies and high densities of mud cracks in the sediment core lithology indicate repeated desiccation of the ephemeral lake. Barron et al. (2003) used sea surface temperature (SST) reconstructions from marine sediments off the coast of northern California and diatom assemblages to infer regional climate and discerned a drying trend during the middle Holocene (approximately 8500 to 3500 cal yr BP). The pollen record showed a steady transition into more drought-tolerant flora except for a deviation at ~6000 cal yr BP with the introduction of temperate redwood pollen. Pollen records from Pyramid Lake provide additional evidence of increased incidence of drought from 7530 to 6300 cal yr BP (Mensing et al., 2004). Pyramid Lake pollen, magnetic susceptibility lake level reconstructions, and $\delta^{18}O$ data all suggest dryness from approximately 7500 to 3400 cal yr BP. Within this interval, the authors describe two pluvial deviations from aridity (6300 to 5000, 4300 to 3900 cal yr BP) which are seen in other records along the west coast including the Pear Lake record described here. Additional climate reconstructions from Pyramid and Owens Lake showed increasing drought-like conditions from 8000 to 3800 cal yr BP (Benson et al., 2002). During this period Lake Tahoe was below spill level based on radiocarbon dating of submerged tree stumps (Lindström, 1990). Magnetic susceptibility, total inorganic carbon (TIC), and $\delta^{18}O$ data from Owens Lake described shallow lake levels leading to desiccation for the latter half of the middle Holocene. Fluctuating lake levels at Tulare Lake reconstructed from pollen and trench lithology

described fluctuating, but low lake levels throughout the middle Holocene (approximately 7000 to 3750 cal yr BP) (Negrini et al., 2006). Lowered lake levels and extended marshland at Tulare Lake argue a more arid climate in central California with exception of some short lived high stands.

Late Holocene (3000 cal yr BP to modern)

Pear Lake sediment records describe a variable first part of the late Holocene with local minima and maxima sand percent that lead into a heavily silt-weighted distributions and sustained low sand percent indicative of increasing aridity. The late Holocene is dominated by climatic extremes and shows a trend of drying toward the present with minimal excursions into positive standardized sand after 1500 cal yr BP (Figure 3-10). The late Holocene was (is) a more variable time than the earlier portions of the Holocene record. Many paleoclimate records in North America describe a mix of extended pluvials and droughts. Kirby et al. (2010) built a sand percent-based, lake level proxy for Lake Elsinore that shows a wet-dry-wet climate transition for the late Holocene (3400 to 150 cal yr BP). The authors grouped intervals of standardized sand to indicate positive and negative phases of the multi-decadal- to centennial-scale Pacific Decadal Oscillation (PDO) related climate signal. Reconstructions of lake level at Silver Lake suggests a climate that was wet enough to prevent persistent desiccation, but not so wet that the basin was permanently filled (Kirby et al., 2015). The authors note evidence of a few periods of multi-decadal lake persistence during the late Holocene (4000 cal yr BP to modern). Tulare Lake levels (Negrini et al., 2006) showed a similar pattern of low

amplitude lake level fluctuation. Pollen records and sediment trench lithology describe a series of local high stands at Tulare Lake during the late Holocene (3600 to 1000 cal yr BP). The regional climate of Pyramid Lake (Mensing et al., 2004) started the late Holocene (3500 to 200 cal yr BP) with a wet interval similar to Lake Elsinore. Pollen records argue a dry interval from 2500 to 2000 cal yr BP and a series of droughts leading into modern day (1500 to 1250, 800 to 725, 600 to 450 cal yr BP).

Regional Comparison

The Pear Lake record is congruent on a multi-decadal- to centennial-scale with many paleoclimate records from the west coast of North America with some temporal scale variability. Similar to the offsets seen in the San Joaquin Basin dendrohydrology reconstruction mentioned earlier, there are issues with perfect temporal matching based on differences in proxy, age models, and regional variability. That being said, the general climate trends observed at Pear Lake coincide with the millennial-scale climate trends in the literature and the major events present in the Pear Lake core are present in other records, as well. For this comparison, we will focus on Pyramid Lake about 200 miles to the northeast, Tulare Lake about 80 miles to the west, and Lake Elsinore about 180 miles to the south (Figure 3-13).

Pyramid Lake and Pear Lake show considerable synchrony of climate shifts. The positive (wet) and negative (dry) time periods are variable in duration between the two, but the records are mostly in phase with each other. Of note is the agreement of the short arid period around 8000 cal yr BP, the middle Holocene pluvial around 5500 cal yr BP

which is not seen in the southern California records, and the dry-wet-dry transitions between 5000 and 3500 cal yr BP. Tulare Lake high stands are in moderate agreement with pluvial periods in the Pear Lake climate reconstructions, particularly during the early Holocene. The relationship would be much more synchronized if the record was shifted slightly which could be a combined error from the two age models.

Although there are storms in the Lake Elsinore record during Pear Lake pluvials and the general millennial-scale climates are similar, there is much disagreement in the major pluvials between the two. Notably, the best correlations between Lake Elsinore and Pear Lake pluvials take place when the Pear Lake and Pyramid Lake reconstruction are out of phase. We argue that this may be evidence of a proposed climate dipole in California (Dettinger et al., 1998; Kirby et al., 2007). Regional precipitation measurements and dendrochronology in California and Oregon describe decadal scale precipitation variability seesawing near 40ºN. The authors propose that the precipitation fluctuations are related to teleconnections to tropical and subtropical conditions and pressure anomalies off the coast of California and Oregon. During times when Pear Lake and Lake Elsinore are in phase, and Pyramid Lake is out of phase, we conjecture that Pear Lake and Lake Elsinore are on the same side of the climate dipole. Conversely, when Pear Lake and Lake Elsinore are out of phase then the dipole may have dipped south and Pear Lake is on the same side of the dipole as Pyramid Lake.

Another component that could be affecting the connectivity of these climate records is the difference in how they receive precipitation. Pear Lake is a system that receives most of its precipitation as snow. Although the record is an aggregate of snowmelt, rain,

avalanches, rain-on-snow events, and summer thunderstorms, the majority of the sand peaks are likely sourced from the latter three occurrences, as stated previously in this chapter. Tulare Lake and Pyramid Lake, although not at high elevation, receive a large amount of water from aggregated snowmelt sourced from the Sierra Nevada and more direct precipitation as rain during the winter. Lake Elsinore lies at low elevation and precipitation in and around the lake as rain.

Productivity Proxies

On a fine temporal scale, %C and %N are not correlated to grain size proxies. When aggregated into 50-year bins, there is still no correlation from the principle component analysis (Figure 3-16d). If the temporal scale is further expanded and we look at the correlation over the early, middle, and late Holocene as described previously, some correlation is evident. In the early Holocene when Pear Lake was experiencing a wet period, %carbon and %nitrogen are low. As previously discussed in Chapter 2, %C and %N are proxies for organic matter and are diluted by inorganic inputs such as sand. The early Holocene has low levels of organic matter as evidenced by low standardized %C and %N and likely due to increased inorganic sediment deposition (Figure 3-5). The middle Holocene was described above as a period of increased aridity in the basin and sand levels were decreased. The increased %C and %N describe a period with increased organic matter in the sediments in congruence with the decreased inorganic inputs into the lake (Figure 3-5). The late Holocene was described as a time of increased variability of climate extremes. The %C and %N show conspicuous, repeated wet-dry-wet cycles

with a ~200 year interval from 3000 cal yr BP to present (Figure 3-5). On a decadal- to multi-decadal timescale, the %C and %N proxies are not connected to the hydrology of the lake, but on a centennial- to millennial-timescale the proxies show similar trends and support the Holocene climate periods proposed in the grain size analysis.

Starting at 1500 cal yr BP we observe a decline in $\delta^{15}N$. The late 20th century bin is the lowest value in the last 10000 years, but the $\delta^{15}N$ became consistently negative in the early 1800s. Holtgrieve et al. (2011) described a similar trend in remote watersheds across North America. The authors note that there is a significant decrease in sediment $\delta^{15}N$ in the last few decades resulting from elevated atmospheric N deposition caused by fertilizer production and fossil fuel combustion. Although the resolution of our record is lower, we see a similar influence of depleted anthropogenic atmospheric nitrogen deposition in Pear Lake. Concurrent with the decline in $\delta^{15}N$, our record also shows consistently low C:N ratios starting at about 1500 cal yr BP. The nitrogen enrichment prior to 1850 (start of the Anthropocene) may be connected to human activities such as widespread agriculture and increased fires.

In the beginning of the record we noticed an extended period of low $\delta^{15}N$ that was not matched anywhere in the record besides the very last bin in modern times. Other cores have shown similar shifts in $\delta^{15}N$ after glaciation that were attributed to large ecosystem shifts and development (Diefendorf et al., 2008; Wolfe et al., 2001). We hypothesize that the primary succession of the watershed continued until 9000-10000 cal yr BP. Although other proxies stabilize, $\delta^{15}N$ levels took another 2500 to 3500 years after

glaciation to reach relative steady state as the watershed fully reestablished soils and vegetation.

To account for the exceptionally low values of $\delta^{15}N$ in the beginning of the record, we ran PCA on each Holocene period separately with 50-year binned proxy data (Figure 3-16). The early Holocene showed different correlations than the middle and late Holocene. In the early Holocene, the $\delta^{13}C$ and C:N ratio were negatively correlated, whereas in the middle and late Holocene the two proxies were positively correlated. The middle and late Holocene also showed a positive correlation between $\delta^{15}N$ and $\delta^{13}C$, which is the opposite of the early Holocene and the correlations measured for the entire record. The differences in these correlations are likely due to the low $\delta^{15}N$ values at the beginning of the record and can be attributed to the primary succession of the watershed, as previously described (Diefendorf et al., 2008; Wolfe et al., 2001).

References

Amann, B., Mauchle, F., & Grosjean, M. (2014). Quantitative high-resolution warm season rainfall recorded in varved sediments of Lake Oeschinen, northern Swiss Alps: calibration and validation AD 1901-2008. *Journal of Paleolimnology, 51*(3), 375-391. doi:10.1007/s10933-013-9761-3

Ambers, R. K. R. (2001). Using the sediment record in a western Oregon flood-control reservoir to assess the influence of storm history and logging on sediment yield. *Journal of Hydrology, 244*(3-4), 181-200. doi:10.1016/s0022-1694(01)00331-6

Appleby, P., Nolan, P., Gifford, D., Godfrey, M., Oldfield, F., Anderson, N., & Battarbee, R. (1986). 210Pb dating by low background gamma counting. *Hydrobiologia, 143*(1), 21-27.

Appleby, P., & Oldfieldz, F. (1983). The assessment of 210Pb data from sites with varying sediment accumulation rates. *Hydrobiologia, 103*(1), 29-35.

Barron, J. A., Heusser, L., Herbert, T., & Lyle, M. (2003). High-resolution climatic evolution of coastal northern California during the past 16,000 years. *Paleoceanography, 18*(1). doi:10.1029/2002pa000768

Benson, L., Kashgarian, M., Rye, R., Lund, S., Paillet, F., Smoot, J., . . . Lindstrom, S. (2002). Holocene multidecadal and multicentennial droughts affecting Northern California and Nevada. *Quaternary Science Reviews, 21*(4-6), 659-682. doi:10.1016/s0277-3791(01)00048-8

Binford, M. W. (1990). Calculation and uncertainty analysis of 210 Pb dates for PIRLA project lake sediment cores. *Journal of Paleolimnology, 3*(3), 253-267.

Bird, B. W., & Kirby, M. E. (2006). An Alpine Lacustrine Record of Early Holocene North American Monsoon Dynamics from Dry Lake, Southern California (USA). *Journal of Paleolimnology, 35*(1), 179-192. doi:10.1007/s10933-005-8514-3

Blaauw M, A. C. J. (2011). Flexible Paleoclimate Age-Depth Models Using an Autoregressive Gamma Process. *Bayesian Analysis, 6*, 457-474.

Blott, S. J., & Pye, K. (2001). GRADISTAT: a grain size distribution and statistics package for the analysis of unconsolidated sediments. *Earth surface processes and Landforms, 26*(11), 1237-1248.

Brook, C. A. (1977). Stratigraphy and structure of the Saddlebag Lake roof pendant, Sierra Nevada, California. *Geological Society of America Bulletin, 88*(3), 321-334.

Brown, P., Kennett, J. P., & Ingram, B. L. (1999). Marine evidence for episodic Holocene megafloods in North America and the northern Gulf of Mexico. *Paleoceanography, 14*(4), 498-510. doi:10.1029/1999pa900017

Brown, S. L., Bierman, P. R., Lini, A., & Southon, J. (2000). 10 000 yr record of extreme hydrologic events. *Geology, 28*(4), 335-338. doi:10.1130/0091-7613(2000)028<0335:yroehe>2.3.co;2

Campbell, C. (1998). Late Holocene lake sedimentology and climate change in southern Alberta, Canada. *Quaternary Research, 49*(1), 96-101. doi:10.1006/qres.1997.1946

Cayan, D. R., Dettinger, M. D., Diaz, H. F., & Graham, N. E. (1998). Decadal variability of precipitation over western North America. *Journal of Climate, 11*(12), 3148-3166. doi:10.1175/1520-0442(1998)011<3148:dvopow>2.0.co;2

Cook, E. R., Woodhouse, C. A., Eakin, C. M., Meko, D. M., & Stahle, D. W. (2004). Long-term aridity changes in the western United States. *Science, 306*(5698), 1015-1018. doi:10.1126/science.1102586

Dettinger, M. D., Cayan, D. R., Diaz, H. F., & Meko, D. M. (1998). North-south precipitation patterns in western North America on interannual-to-decadal timescales. *Journal of Climate, 11*(12), 3095-3111. doi:10.1175/1520-0442(1998)011<3095:nsppiw>2.0.co;2

Diefendorf, A. F., Patterson, W. P., Holmden, C., & Mullins, H. T. (2008). Carbon isotopes of marl and lake sediment organic matter reflect terrestrial landscape change during the late Glacial and early Holocene (16,800 to 5,540 cal yr B.P.): a multiproxy study of lacustrine sediments at Lough Inchiquin, western Ireland. *Journal of Paleolimnology, 39*(1), 101-115. doi:10.1007/s10933-007-9099-9

Drake, D. E. (1999). Temporal and spatial variability of the sediment grain-size distribution on the Eel shelf: the flood layer of 1995. *Marine Geology, 154*(1-4), 169-182. doi:10.1016/s0025-3227(98)00111-x

Eden, D. N., & Page, M. J. (1998). Palaeoclimatic implications of a storm erosion record from late Holocene lake sediments, North Island, New Zealand. *Palaeogeography Palaeoclimatology Palaeoecology, 139*(1-2), 37-58. doi:10.1016/s0031-0182(97)00136-3

Enzel, Y., Brown, W. J., Anderson, R. Y., McFadden, L. D., & Wells, S. G. (1992). Short-duration Holocene Lakes in the Mojave River Drainage Basin, Southern California. *Quaternary Research, 38*(1), 60-73. doi:10.1016/0033-5894(92)90030-m

Folk, R. L., & Ward, W. C. (1957). Brazos River Bar: A Study in the Significance of Grain Size Parameters. *Journal of Sedimentary Petrology, 27*(1), 3-26.

Geotek. Magnetic Susceptibility. Retrieved from http://www.geotek.co.uk/products/magsusc/

Guan, B., Molotch, N. P., Waliser, D. E., Fetzer, E. J., & Neiman, P. J. (2013). The 2010/2011 snow season in California's Sierra Nevada: Role of atmospheric rivers and modes of large-scale variability. *Water Resources Research, 49*(10), 6731-6743. doi:10.1002/wrcr.20537

Holtgrieve, G. W., Schindler, D. E., Hobbs, W. O., Leavitt, P. R., Ward, E. J., Bunting, L., . . . Holmgren, S. (2011). A coherent signature of anthropogenic nitrogen deposition to remote watersheds of the northern hemisphere. *Science, 334*(6062), 1545-1548.

Kerrick, D., Crawford, K., & Randazzo, A. (1973). Metamorphism of calcareous rocks in three roof pendants in the Sierra Nevada, California. *Journal of Petrology, 14*(2), 303-325.

Kirby, M. E., Knell, E. J., Anderson, W. T., Lachniet, M. S., Palermo, J., Eeg, H., . . . Hiner, C. A. (2015). Evidence for insolation and Pacific forcing of late glacial through Holocene climate in the Central Mojave Desert (Silver Lake, CA). *Quaternary Research, 84*(2), 174-186. doi:10.1016/j.yqres.2015.07.003

Kirby, M. E., Lund, S. P., Anderson, M. A., & Bird, B. W. (2007). Insolation forcing of Holocene climate change in Southern California: a sediment study from Lake Elsinore. *Journal of Paleolimnology, 38*(3), 395-417. doi:10.1007/s10933-006-9085-7

Kirby, M. E., Lund, S. P., Patterson, W. P., Anderson, M. A., Bird, B. W., Ivanovici, L., . . . Nielsen, S. (2010). A Holocene record of Pacific Decadal Oscillation (PDO)-related hydrologic variability in Southern California (Lake Elsinore, CA). *Journal of Paleolimnology, 44*(3), 819-839. doi:10.1007/s10933-010-9454-0

Kirby, M. E., Zimmerman, S. R. H., Patterson, W. P., & Rivera, J. J. (2012). A 9170-year record of decadal-to-multi-centennial scale pluvial episodes from the coastal Southwest United States: a role for atmospheric rivers? *Quaternary Science Reviews, 46*, 57-65. doi:10.1016/j.quascirev.2012.05.008

Lamoureux, S. (2000). Five centuries of interannual sediment yield and rainfall-induced erosion in the Canadian High Arctic recorded in lacustrine varves. *Water Resources Research, 36*(1), 309-318. doi:10.1029/1999wr900271

Last, W. M., & Vance, R. E. (1997). Bedding characteristics of Holocene sediments from salt lakes of the northern Great Plains, Western Canada. *Journal of Paleolimnology, 17*(3), 297-318.

Lindström, S. (1990). Submerged tree stumps as indicators of mid-Holocene aridity in the Lake Tahoe Basin. *Journal of California and Great Basin Anthropology, 12*(2), 146-157.

Luckman, B. (1975). Drop stones resulting from snow-avalanche deposition on lake ice. *Journal of Glaciology, 14*(70), 186-188.

MacDonald, G. M., Moser, K. A., Bloom, A. M., Potito, A. P., Porinchu, D. F., Holmquist, J. R., . . . Kremenetski, K. V. (2016). Prolonged California aridity linked to climate warming and Pacific sea surface temperature. *Scientific Reports, 6*.

Mann, M. E., Zhang, Z. H., Hughes, M. K., Bradley, R. S., Miller, S. K., Rutherford, S., & Ni, F. B. (2008). Proxy-based reconstructions of hemispheric and global surface temperature variations over the past two millennia. *Proceedings of the National Academy of Sciences of the United States of America, 105*(36), 13252-13257. doi:10.1073/pnas.0805721105

Meko, D. M., Woodhouse, C. A., & Touchan, R. (2014). Klamath/San Joaquin/Sacramento hydroclimatic reconstructions from tree rings. *Draft Final Report to the California Department of Water Resources; University of Arizona: Tucson, AZ, USA*, 117.

Menking, K. M., & Anderson, R. Y. (2003). Contributions of La Nina and El Nino to middle holocene drought and late Holocene moisture in the American Southwest. *Geology, 31*(11), 937-940. doi:10.1130/g19807.1

Mensing, S. A., Benson, L. V., Kashgarian, M., & Lund, S. (2004). A Holocene pollen record of persistent droughts from Pyramid Lake, Nevada, USA. *Quaternary Research, 62*(1), 29-38. doi:10.1016/j.yqres.2004.04.002

Moore, J. J., Hughen, K. A., Miller, G. H., & Overpeck, J. T. (2001). Little Ice Age recorded in summer temperature reconstruction from vared sediments of Donard Lake, Baffin Island, Canada. *Journal of Paleolimnology, 25*(4), 503-517. doi:10.1023/a:1011181301514

Moy, C. M., Seltzer, G. O., Rodbell, D. T., & Anderson, D. M. (2002). Variability of El Nino/Southern Oscillation activity at millennial timescales during the Holocene epoch. *Nature, 420*(6912), 162-165. doi:10.1038/nature01194

Negrini, R. M., Wigand, P. E., Draucker, S., Gobalet, K., Gardner, J. K., Sutton, M. Q., & Yohe, R. M., II. (2006). The Rambla highstand shoreline and the Holocene lake-level history of Tulare Lake, California, USA. *Quaternary Science Reviews, 25*(13-14), 1599-1618. doi:10.1016/j.quascirev.2005.11.014

Nesje, A., Bakke, J., Dahl, S. O., Lie, Ø., & Bøe, A.-G. (2007). A continuous, high-resolution 8500-yr snow-avalanche record from western Norway. *The holocene, 17*(2), 269-277.

Nesje, A., Dahl, S. O., Matthews, J. A., & Berrisford, M. S. (2001). A similar to 4500 yr record of river floods obtained from a sediment core in Lake Atnsjoen, eastern Norway. *Journal of Paleolimnology, 25*(3), 329-342. doi:10.1023/a:1011197507174

Noren, A. J., Bierman, P. R., Steig, E. J., Lini, A., & Southon, J. (2002). Millennial-scale storminess variability in the northeastern United States during the Holocene epoch. *Nature, 419*(6909), 821-824. doi:10.1038/nature01132

Oldfield, F., & Appleby, P. (1984). Empirical testing of 210 Pb-dating models for lake sediments *Lake sediments and environmental history*.

Oliva, F., Viau, A. E., Bjornson, J., Desrochers, N., & Bonneau, M. A. (2016). A 1300 year reconstruction of paleofloods using oxbow lake sediments in temperate southwestern Quebec, Canada. *Canadian Journal of Earth Sciences, 53*(4), 378-386. doi:10.1139/cjes-2015-0191

Page, M. J., Trustrum, N. A., & DeRose, R. C. (1994). A high resolution record of storm-induced erosion from lake sediments, New Zealand. *Journal of Paleolimnology, 11*(3), 333-348. doi:10.1007/bf00677993

Parris, A. S., Bierman, P. R., Noren, A. J., Prins, M. A., & Lini, A. (2010). Holocene paleostorms identified by particle size signatures in lake sediments from the northeastern United States. *Journal of Paleolimnology, 43*(1), 29-49. doi:10.1007/s10933-009-9311-1

Power, M. J. (1998). *Paleoclimatic Interpretations of an Alpine Lake in South Central Sierra Nevada, California: Multiple Proxy Evidence.* (Master of Science), North Arizona University.

Rodbell, D. T., Seltzer, G. O., Anderson, D. M., Abbott, M. B., Enfield, D. B., & Newman, J. H. (1999). An similar to 15,000-year record of El Nino-driven

alluviation in southwestern Ecuador. *Science, 283*(5401), 516-520. doi:10.1126/science.283.5401.516

Rodionov, S. N. (2004). A sequential algorithm for testing climate regime shifts. *Geophysical Research Letters, 31*(9).

Schelske, C. L., Peplow, A., Brenner, M., & Spencer, C. N. (1994). Low-background gamma counting: applications for 210 Pb dating of sediments. *Journal of Paleolimnology, 10*(2), 115-128.

Seierstad, J., Nesje, A., Dahl, S. O., & Simonsen, J. R. (2002). Holocene glacier fluctuations of Grovabreen and Holocene snow-avalanche activity reconstructed from lake sediments in Grningstlsvatnet, western Norway. *The holocene, 12*(2), 211-222.

Stine, S. (1990). Late holocene fluctuations of Mono Lake, eastern California. *Palaeogeography, Palaeoclimatology, Palaeoecology, 78*(3-4), 333-381.

Stine, S. (1994). Extreme and persistent drought in California and Patagonia during mediaeval time. *Nature, 369*(6481), 546-549.

Stuiver, M., & Polach, H. A. (1977). Discussion reporting of 14 C data. *Radiocarbon, 19*(3), 355-363.

Thorndycraft, V., Hu, Y., Oldfield, F., Crooks, P. R. J., & Appleby, P. G. (1998). Individual flood events detected in the recent sediments of the Petit Lac d'Annecy, eastern France. *Holocene, 8*(6), 741-746. doi:10.1191/095968398668590504

Vasskog, K., Nesje, A., Støren, E. N., Waldmann, N., Chapron, E., & Ariztegui, D. (2011). A Holocene record of snow-avalanche and flood activity reconstructed from a lacustrine sedimentary sequence in Oldevatnet, western Norway. *The holocene, 21*(4), 597-614.

Wolfe, A. P., Baron, J. S., & Cornett, R. J. (2001). Anthropogenic nitrogen deposition induces rapid ecological changes in alpine lakes of the Colorado Front Range (USA). *Journal of Paleolimnology, 25*(1), 1-7. doi:10.1023/a:1008129509322

Chapter 4: Conclusions and Future Work

Pear Lake is an ideal subject for sediment analysis due to its complex morphology, particularly the single deep depression that allows for increased sedimentation rates. The lake sediments archived conditions for the duration of the Holocene. Although the sediment archive was complete, conditions at Pear Lake were dissimilar to other lakes used for paleo reconstruction in that productivity proxies (e.g. $\delta^{15}N$, $\delta^{13}C$, C:N ratio) were not able to unequivocally definitively identify sources of organic matter or clearly indicate times of increased productivity in the lake system. The low levels of organic matter and lack of significant vegetation in the watershed likely explain the inability to utilize the productivity proxies in Pear Lake. Other proxies, such as magnetic susceptibility, were also ineffective at investigating the hydrologic conditions through the Holocene and connections between the hydrology and productivity were not present. The lake morphology and steep sides of the basin are a likely cause for the ineffectiveness of the magnetic susceptibility proxy for hydrologic conditions. Snowmelt inter-annual dynamics are another major contributing factor to the lack of correlation between hydrology and productivity in Pear Lake.

Grain size analysis of the Pear Lake sediment core showed that Pear Lake sediments record precipitation at a multi-decadal time scale. Using a grain size proxy and modal analysis, thresholds were set to identify multi-decadal scale periods of increased wetness (including the possible presence of extreme events such as rain-on-snow events, atmospheric rivers, or avalanches) and aridity (including possible droughts). Three

intense centennial scale droughts were identified (7500 – 6900, 5000 - 4750, and 700 - 350 cal yr BP) during the record. The data were then binned and aggregated using a climate phase criteria to categorize centennial to millennial scale periods of increased precipitation (pluvials) and increased aridity. The Holocene was split up into three periods with different overall climate regimes. The early Holocene (11250 to 7250 cal yr BP) was a time of increased precipitation and storminess, the middle Holocene (7250 to 3000 cal yr BP) was a time of increased aridity that experienced two significant pluvial excursions, and the late Holocene (3000 cal yr BP to present) was a time of highly variable climate beginning with intense pluvials and ending with a significant drying trend towards present. The trends seen in Pear Lake were congruent with other records in western North America. Deviations from other climate records to the north and south could be evidence of the proposed California climate dipole.

The Pear Lake productivity proxy analysis would benefit from a more thorough investigation of the current isotope values of aquatic and terrestrial organic matter in the basin as well as the examination of elemental and isotope values in modern sediments on a finer time scale. Connecting the modern isotope and elemental analysis with the paleo record would allow for more refined discussion of the sources of organic matter in the lake sediment and allow for more conclusions to be drawn about Holocene lake productivity.

Diatom community structure analysis and pollen analysis of the sediment core would be useful to understand the aquatic and terrestrial ecosystem and their relative shifts through the Holocene. In particular, detailed analysis of diatoms and pollen at sub-

centimeter intervals of the core should be conducted at the regime transitions identified in Figure 3-13. These analyses could confirm and refine the presence of arid and pluvial periods in the climate reconstruction of Pear Lake and help tie climate variability to terrestrial and lake ecology. Diatom community structure can also indicate changes in temperature and lake chemistry which could be connected to the climate trends presented for Pear Lake.

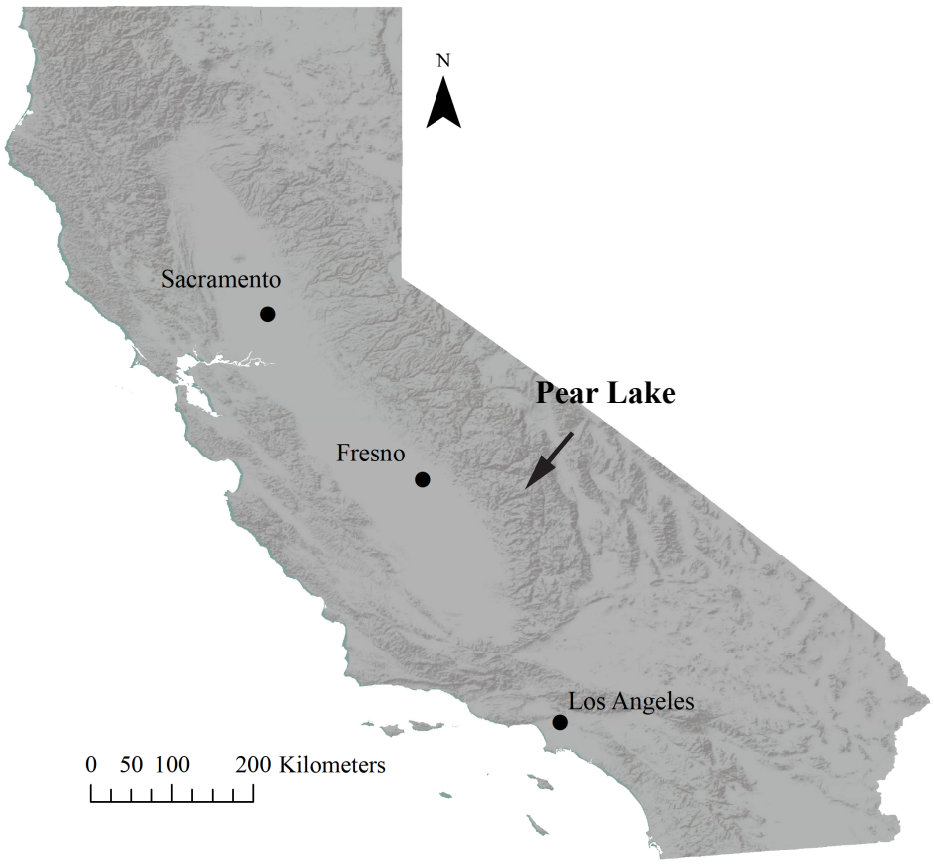

Figure 1-1. Map of California showing Pear Lake in the Sierra Nevada.

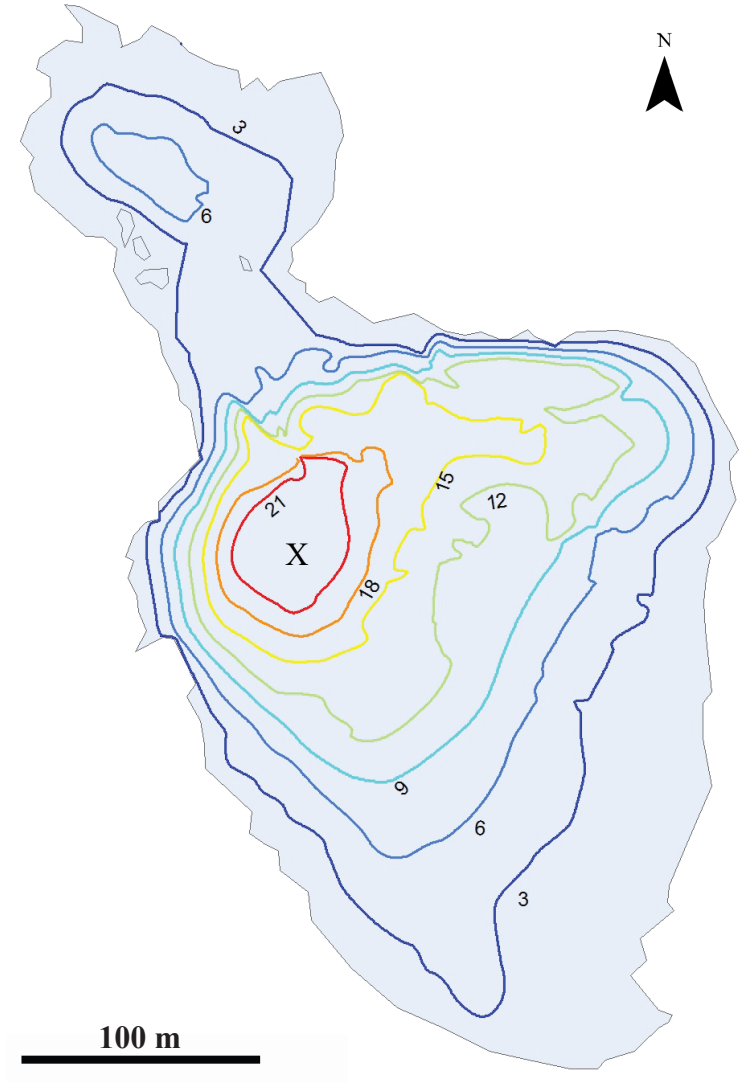

Figure 1-2. Bathymetric map of Pear Lake. Contours are depicted in meters. "X"marks core location. Surface elevation = 2904 m.

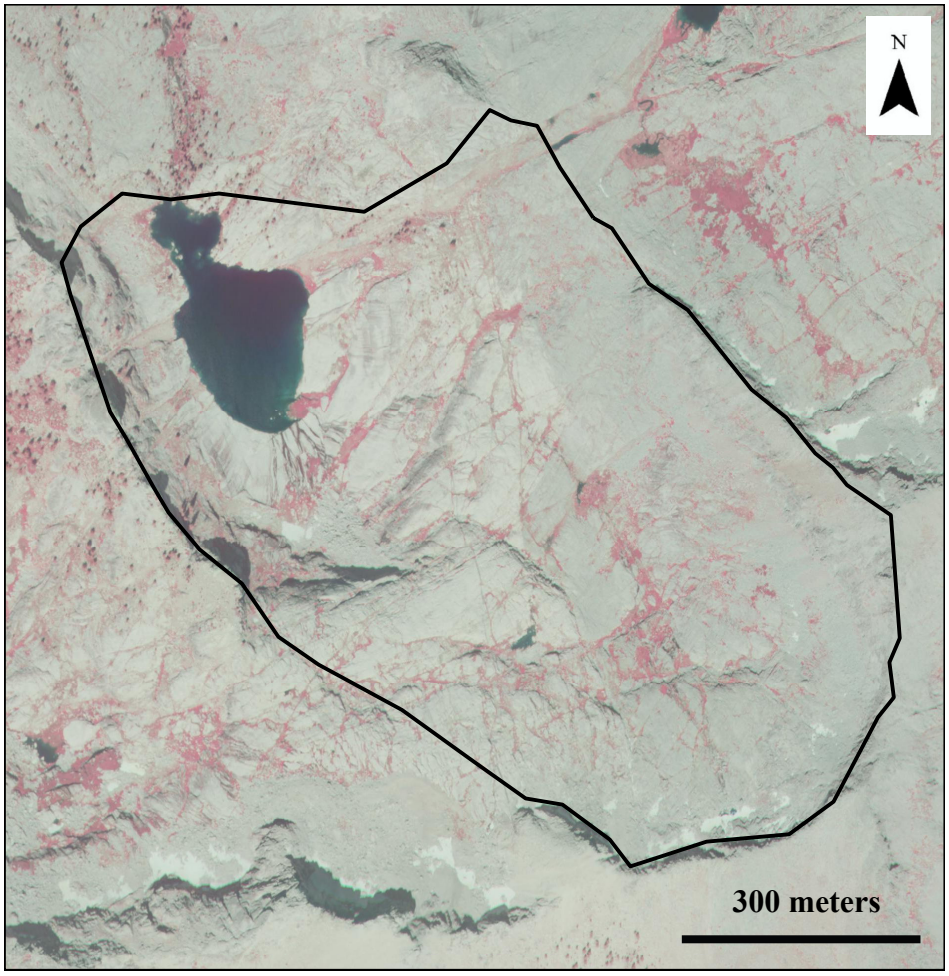

Figure 1-3. Infrared image of Pear Lake depicting the limited vegetation coverage (red shading). Black line delineates the watershed area.

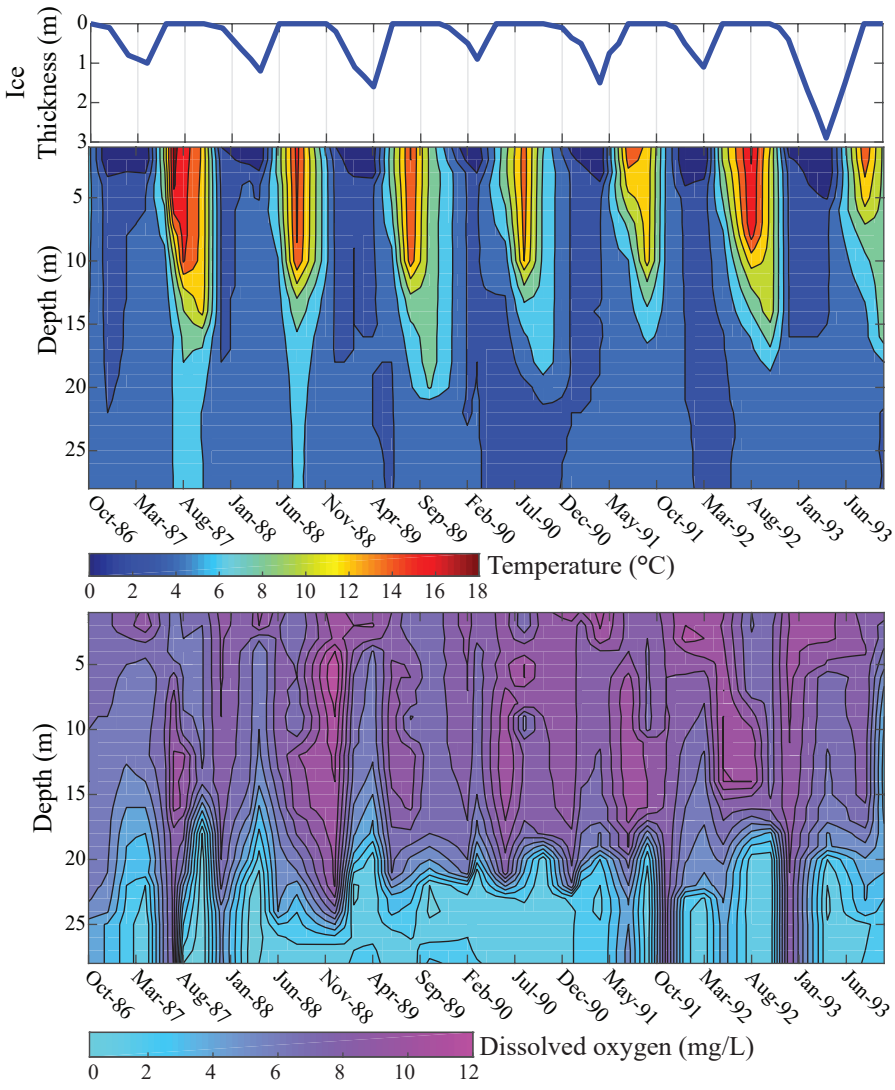

Figure 1-4. Time-depth plots of temperature (middle) and dissolved oxygen (bottom) in Pear Lake. Top: Ice thickness on top of Pear Lake.

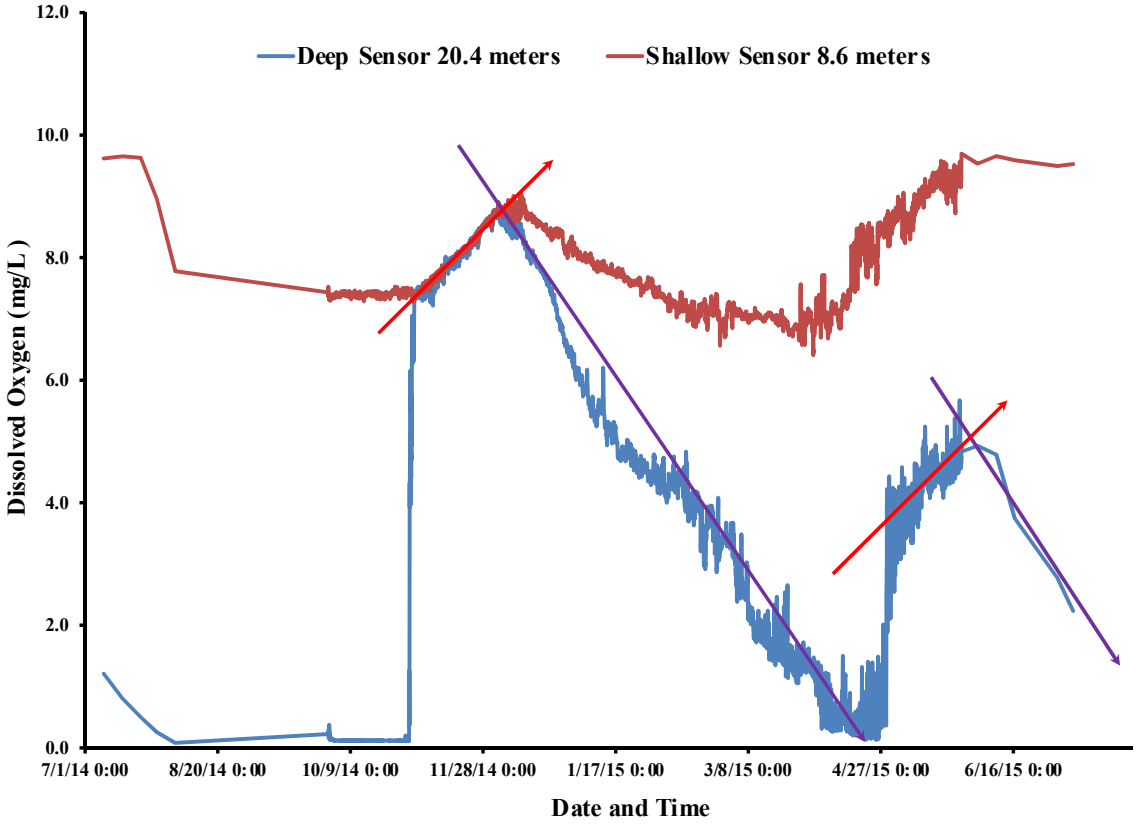

Figure 1-5. Dissolve oxygen versus time depicting seasonal shifts in Pear Lake for 2014-2015.

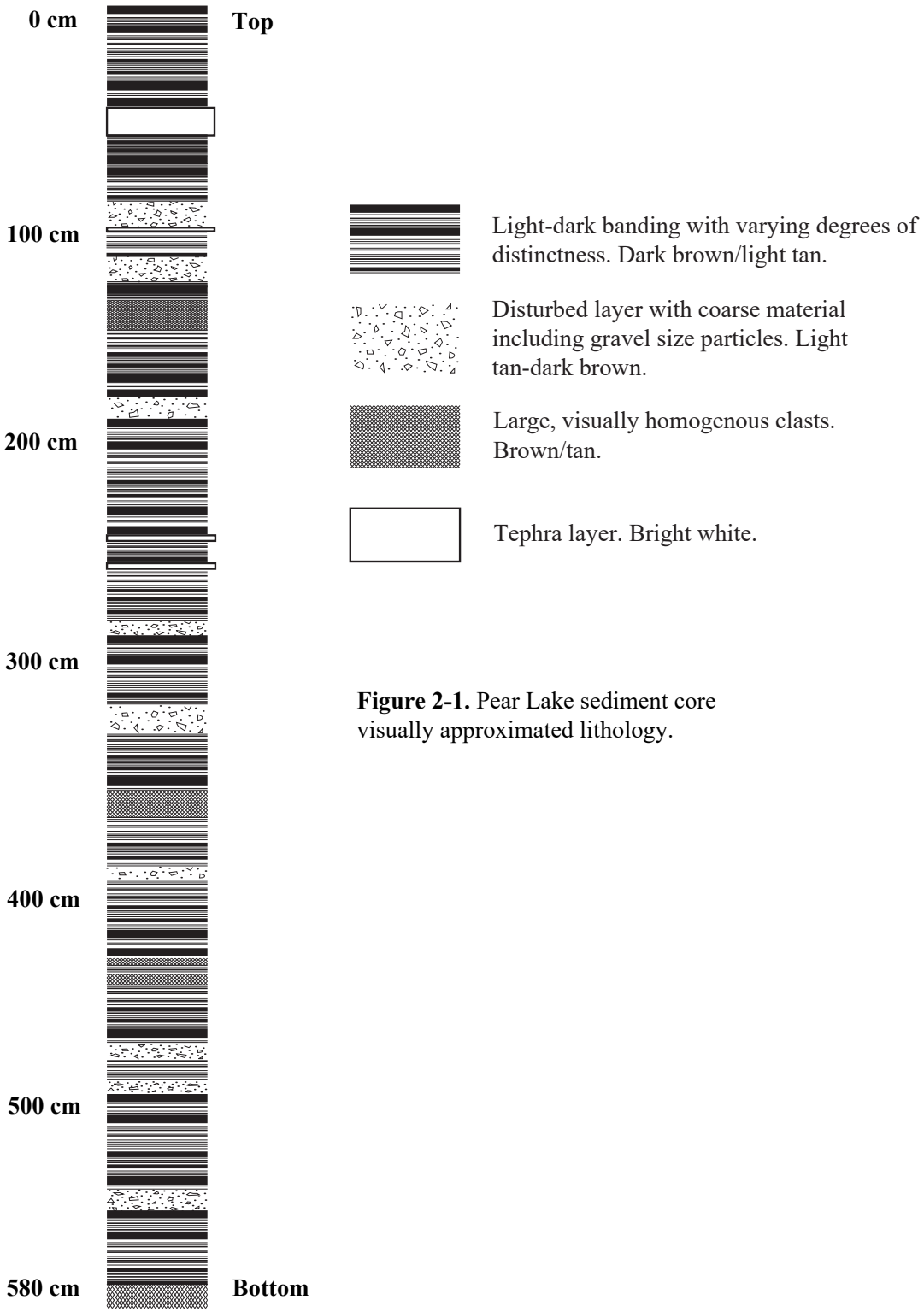

Figure 2-1. Pear Lake sediment core visually approximated lithology.

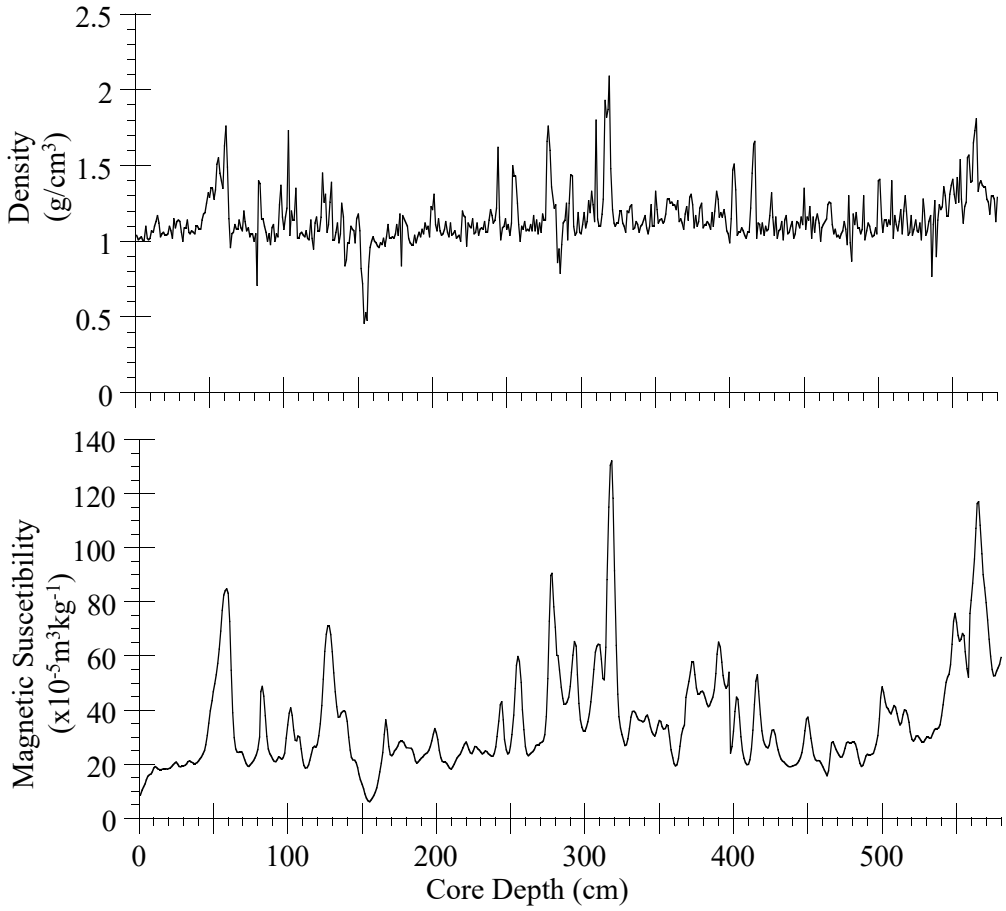

Figure 2-2. Density and magnetic susceptibility versus core depth.

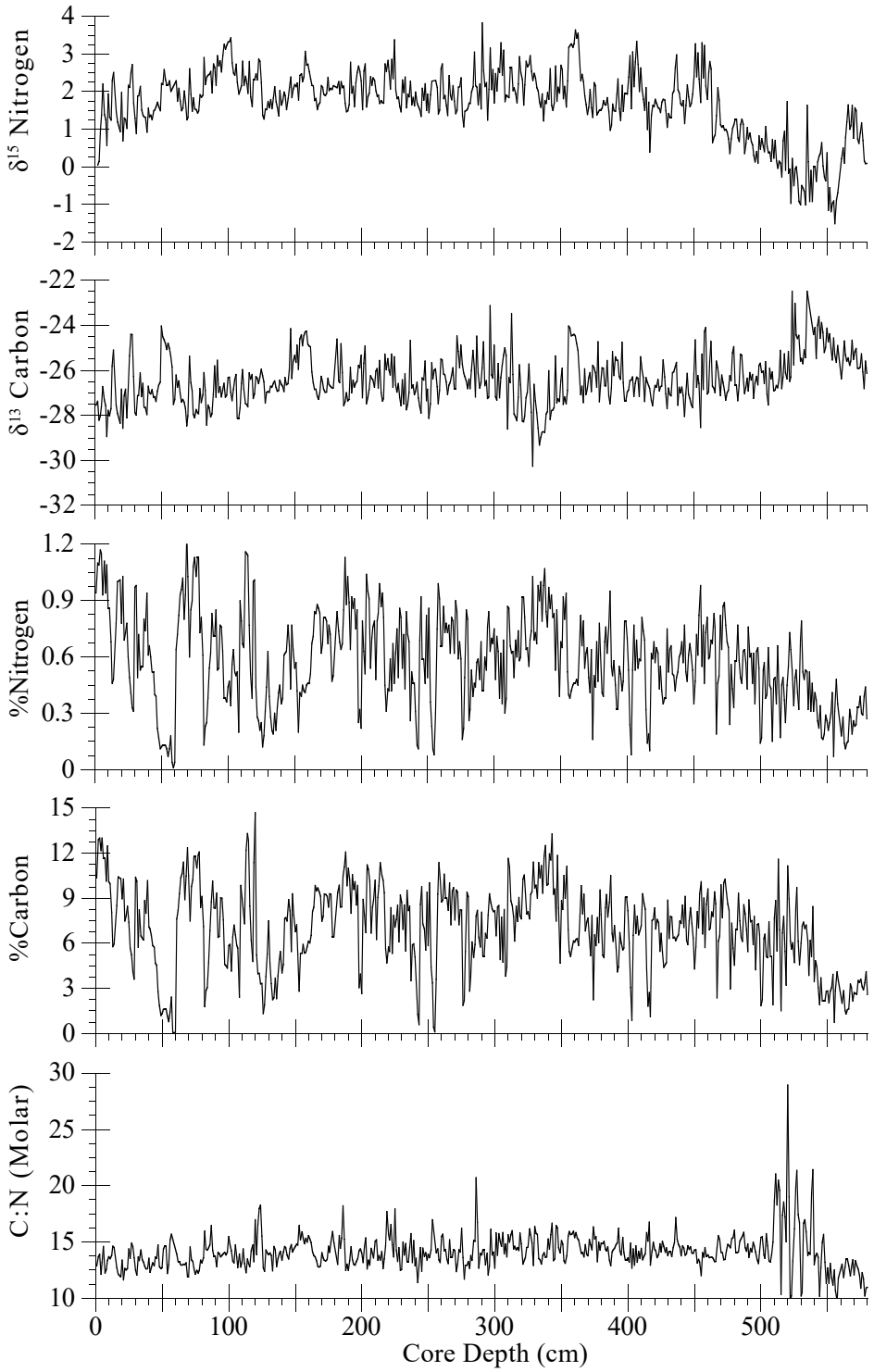

Figure 2-3. Elemental and stable isotope analysis data versus core depth.

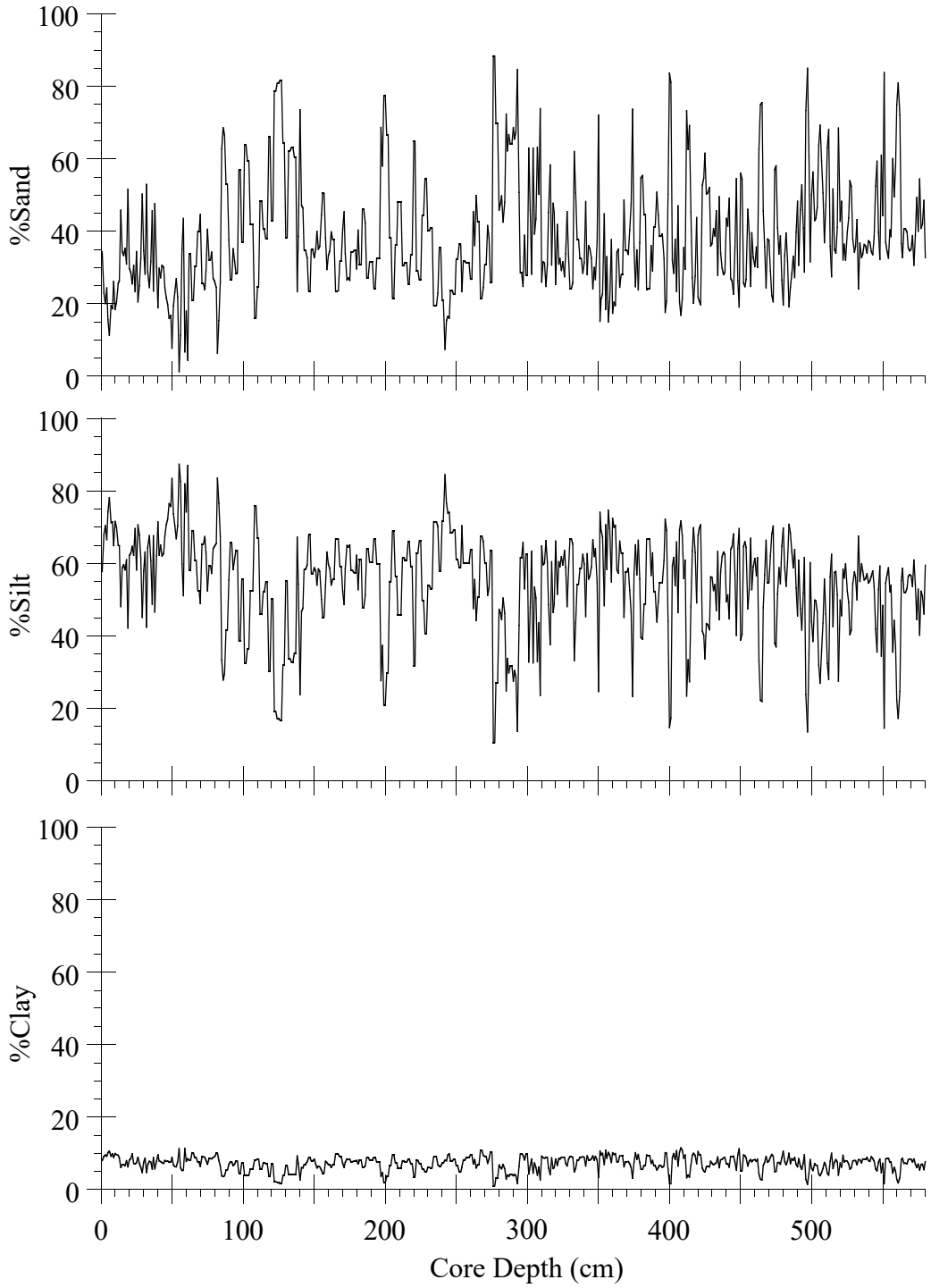

Figure 2-4. Percent sand, silt, and clay by weight versus core depth.

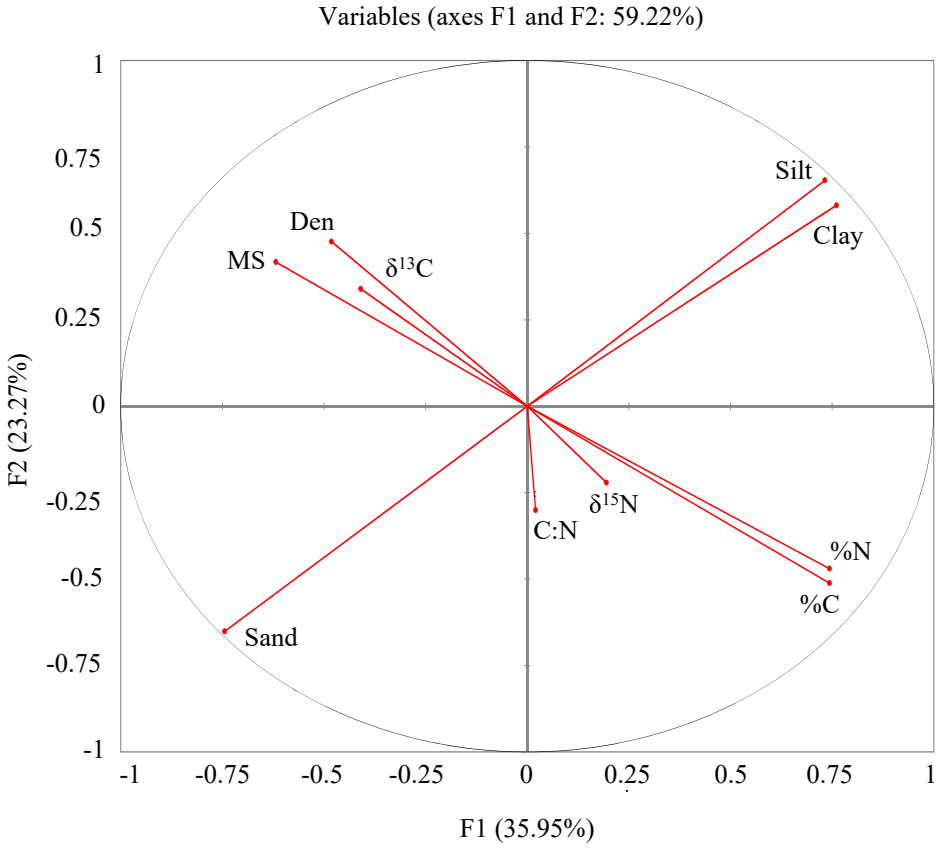

Figure 2-5. PCA of all proxies from Pear Lake.

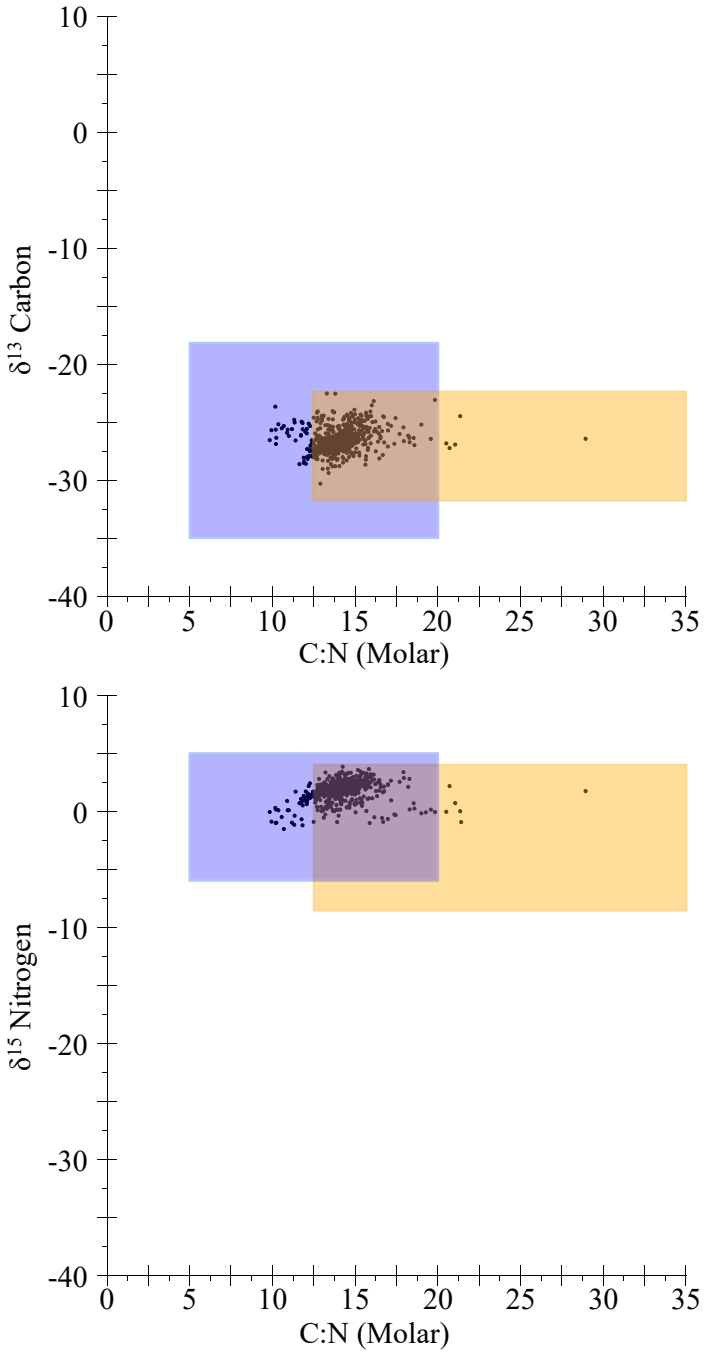

Figure 2-6. Stable isotope measurements (Top: $\delta^{13}C$, Bottom: $\delta^{15}N$) of all samples versus molar C:N ratios. Orange box is terrestrial organic matter range; blue box is aquatic organic matter range (Sadro, unpublished; Lamb, 2006; Meyers, 1993).

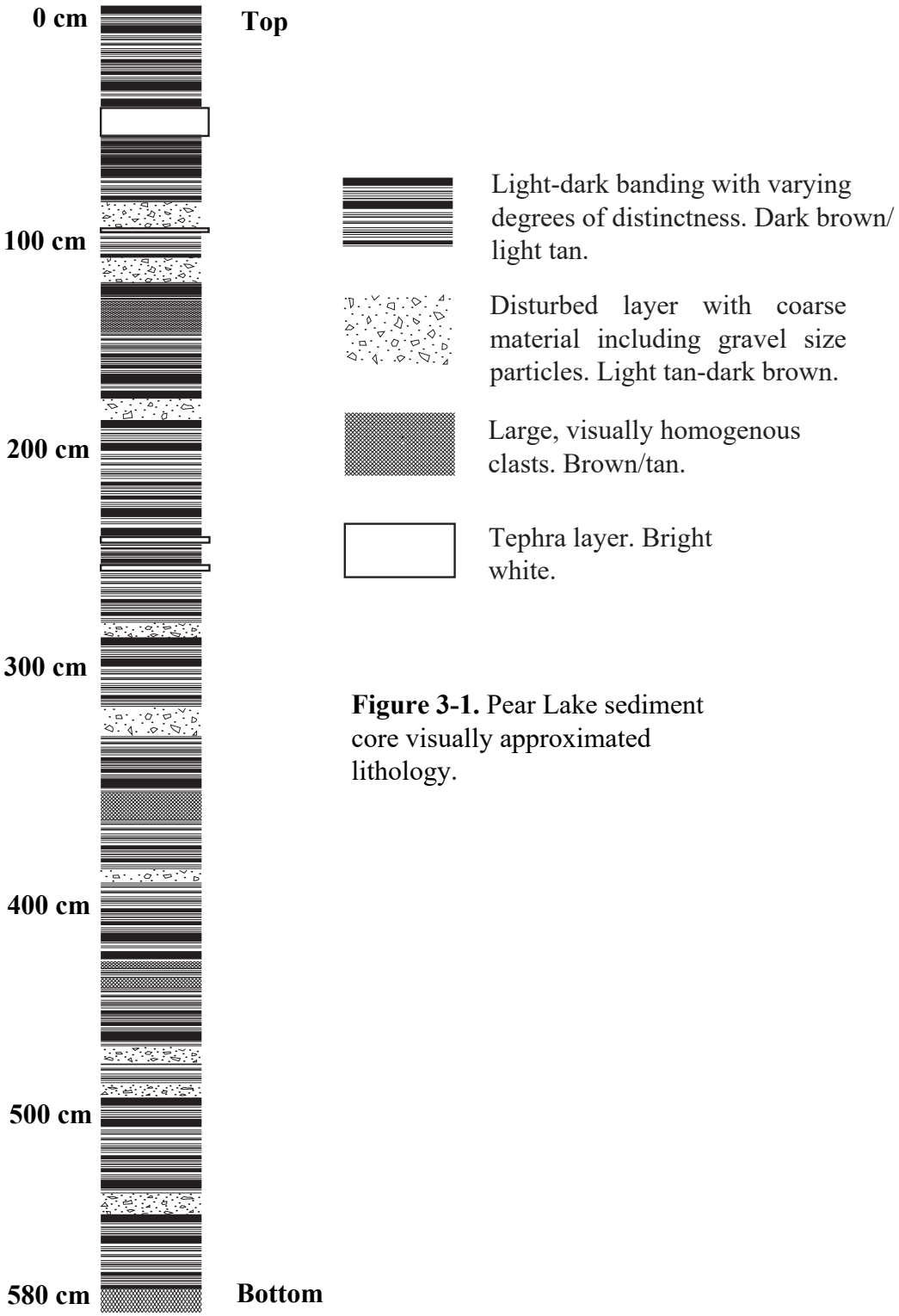

Figure 3-1. Pear Lake sediment core visually approximated lithology.

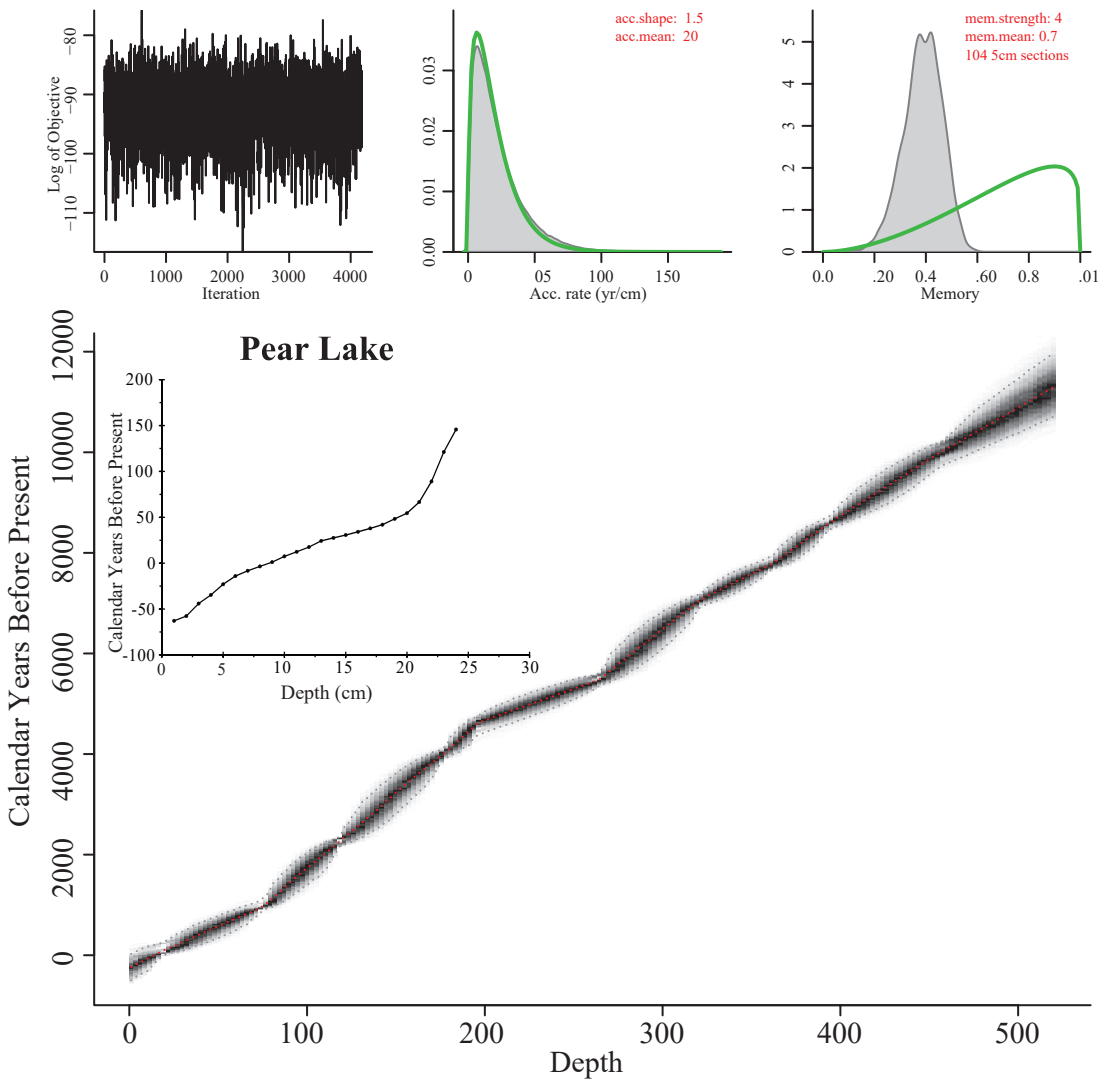

Figure 3-2. Age model produced with the software program BACON (see text for details). Inlay: ^{210}Pb chronology for the first 24 cm of the sediment core.

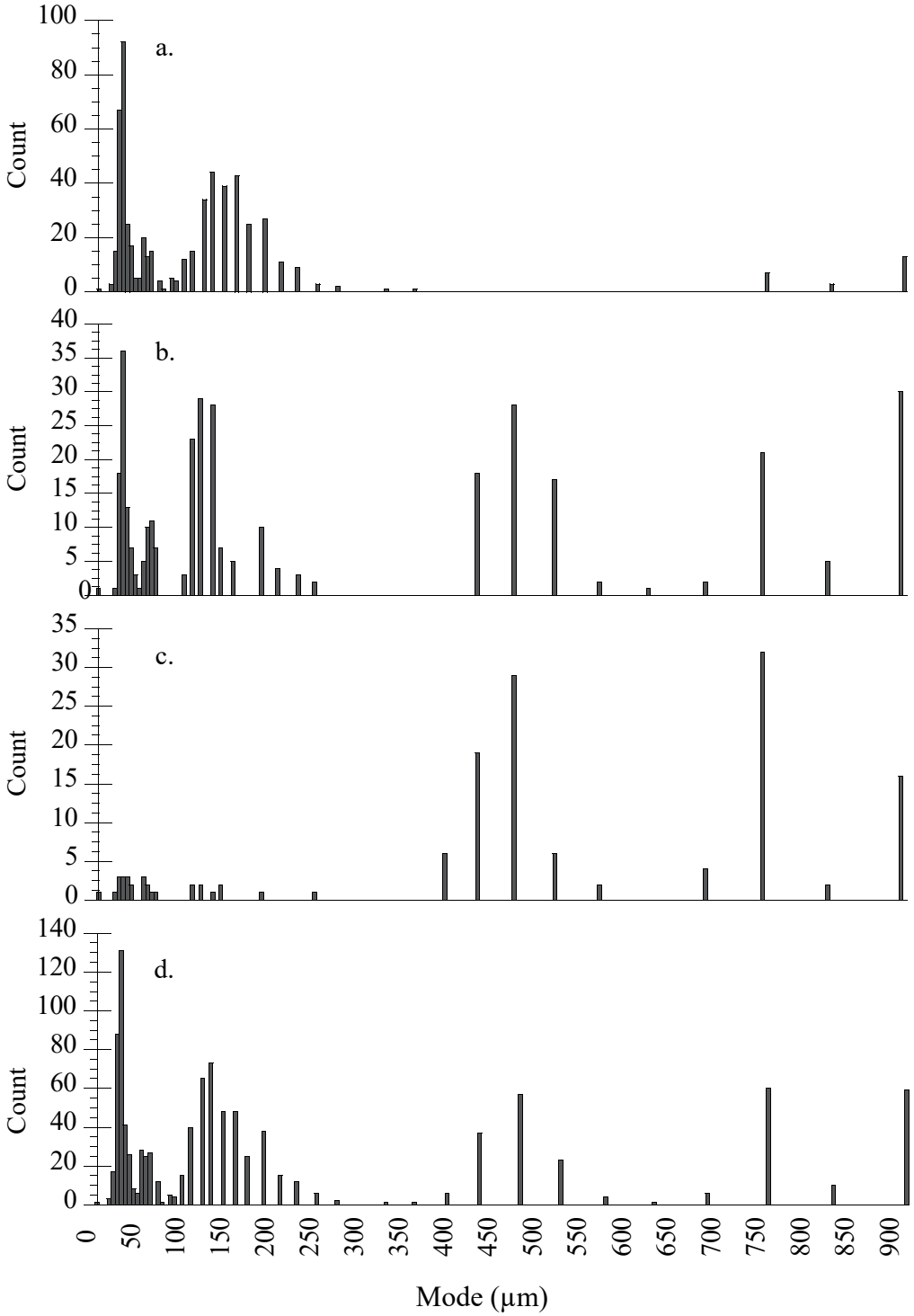

Figure 3-3. Mode distribution histograms for grain size analysis: a) primary mode distribution b) secondary mode distribution c) tertiary mode distribution d) all modes composite histogram.

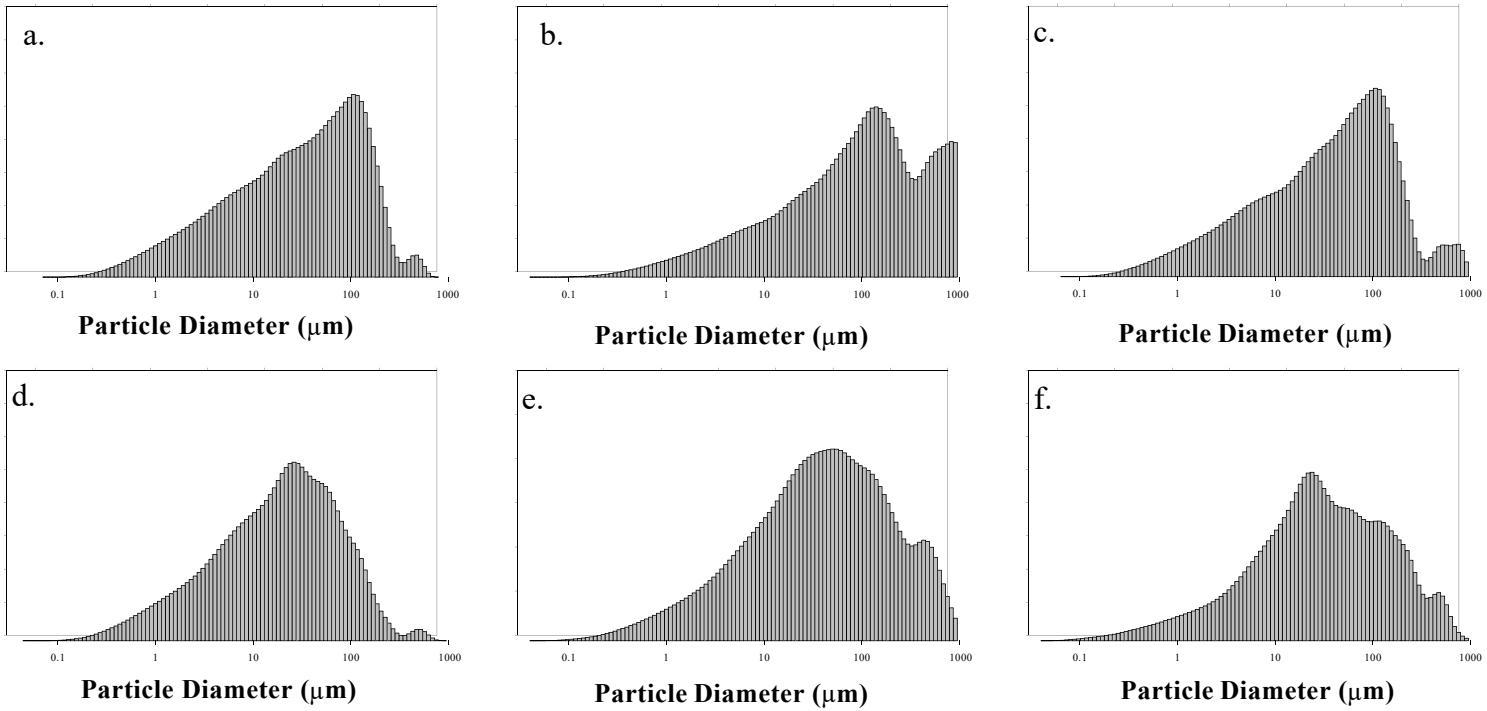

Figure 3-4. GRADISTAT output histogram of grain size analysis: a) unimodal sand distribution b) bimodal sand distribution c) trimodal sand distribution d) unimodal silt distribution e) bimodal silt distribution f) trimodal silt distribution

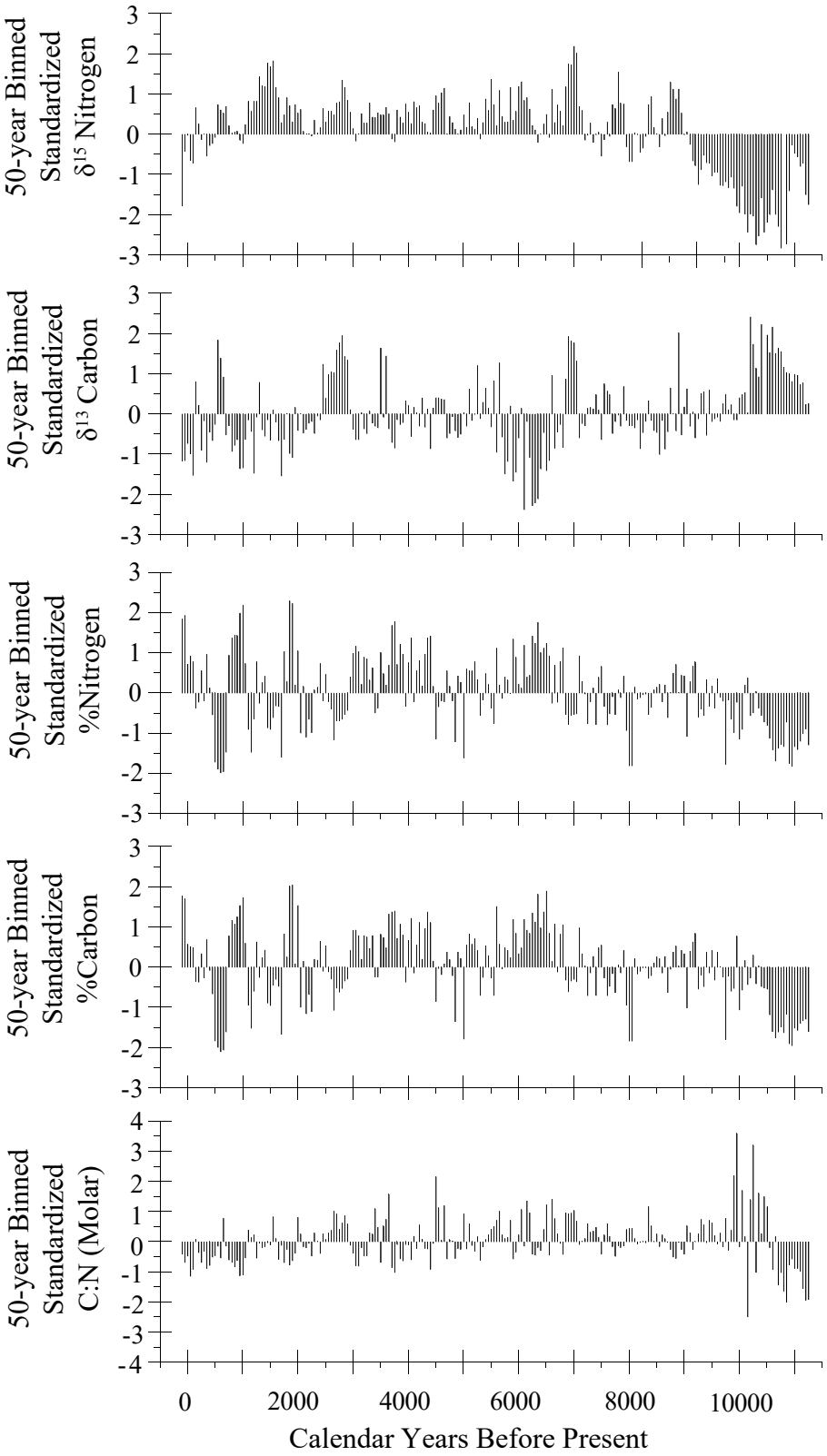

Figure 3-5. 50-year binned, standardized (by mean) sediment stable isotope and elemental analysis data versus calibrated years before present.

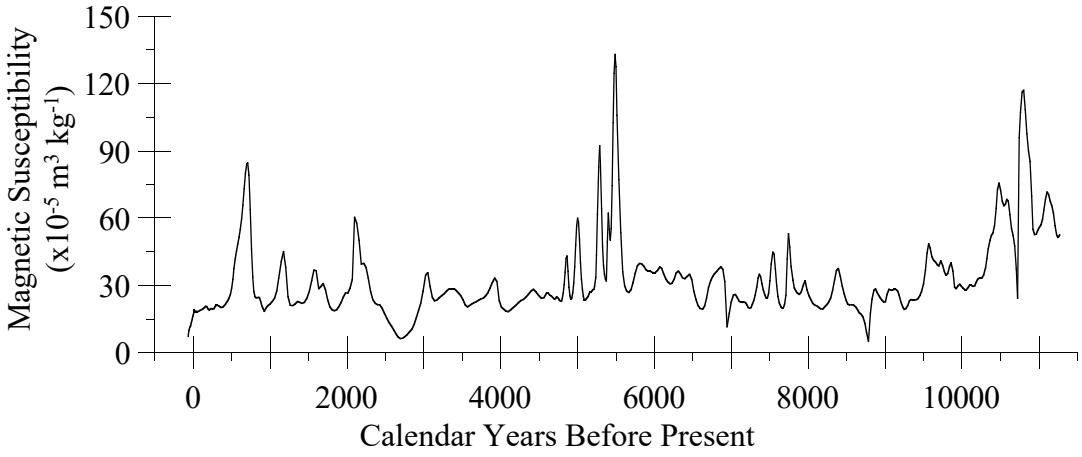

Figure 3-6. Magnetic susceptibility versus calibrated years before present.

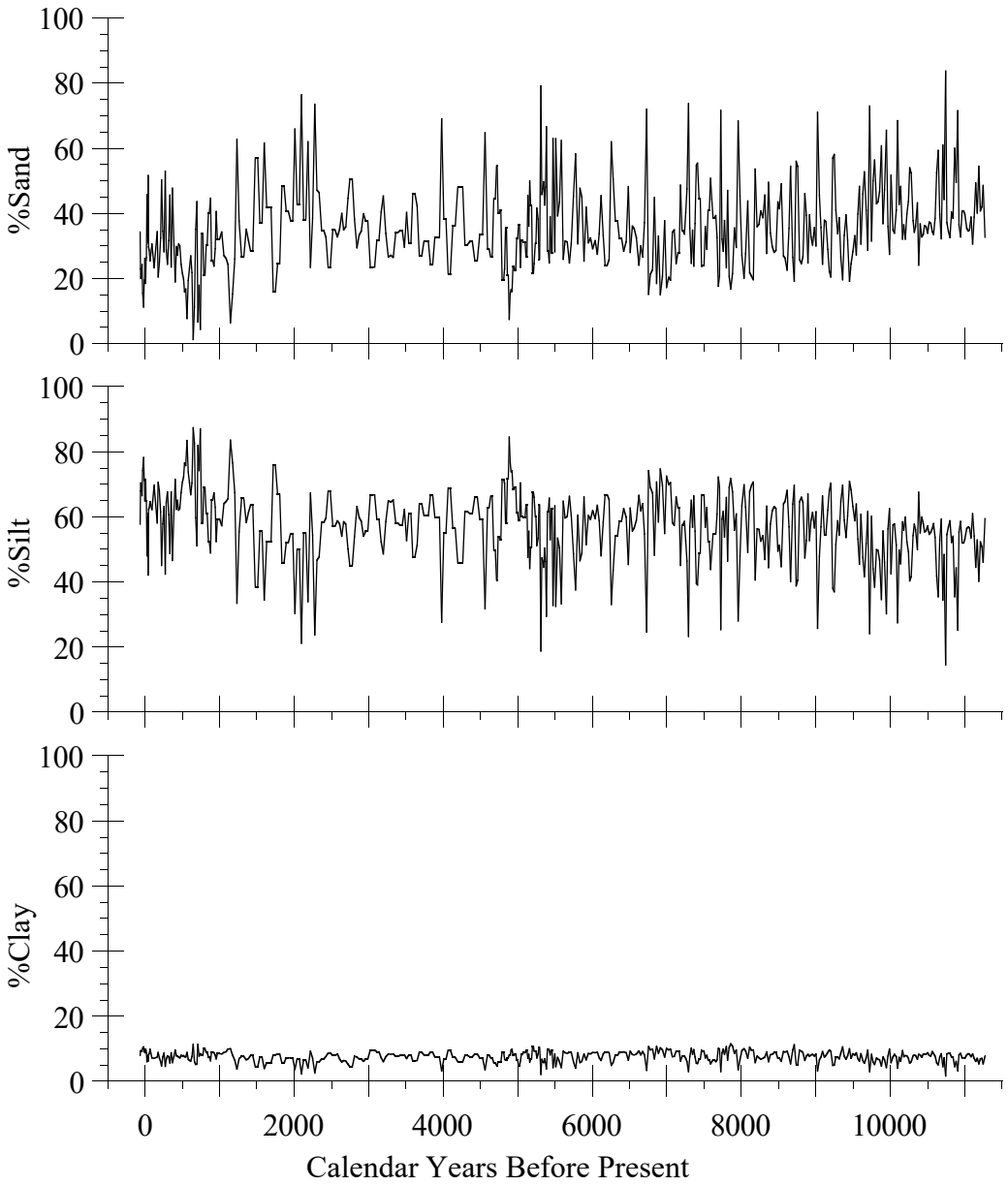

Figure 3-7. Percent sand, silt, and clay by volume versus calibrated years before present.

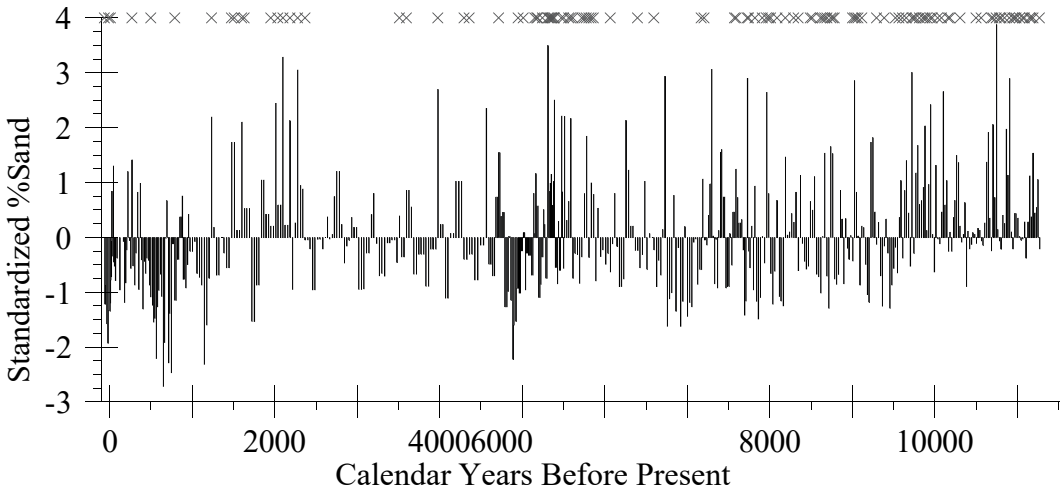

Figure 3-8. Standardized (by mean) percent sand versus calibrated years before present. "X" markers depict occurences of gravel larger than 2 mm in diameter.

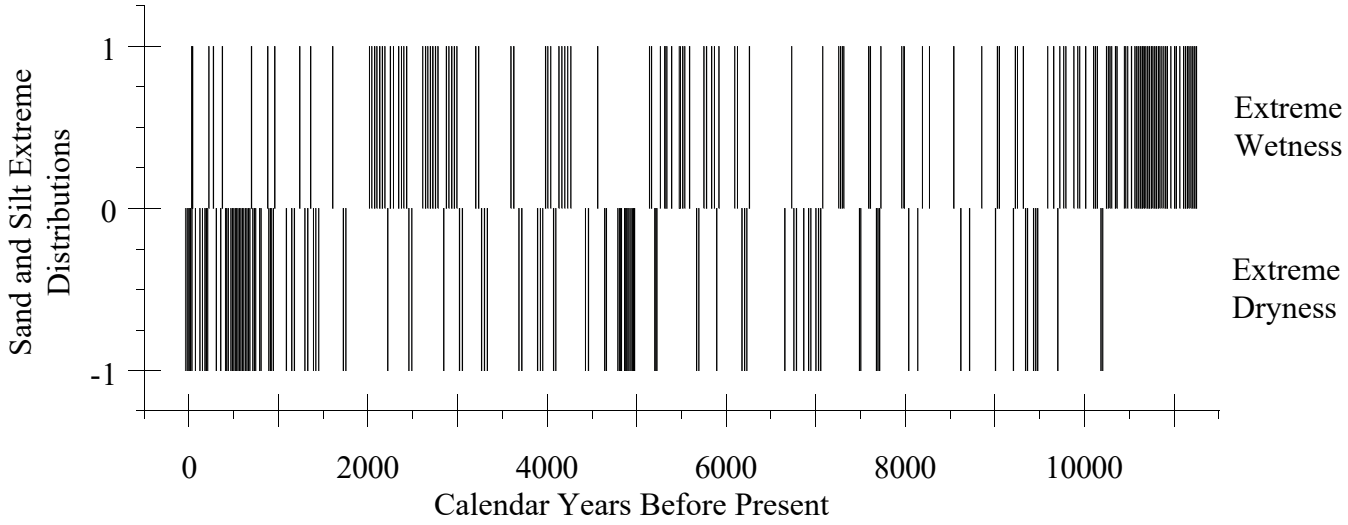

Figure 3-9. Extreme sand and silt distribution depicted by all sand mode distributions (above zero) and unimodal silt distributions (below zero).

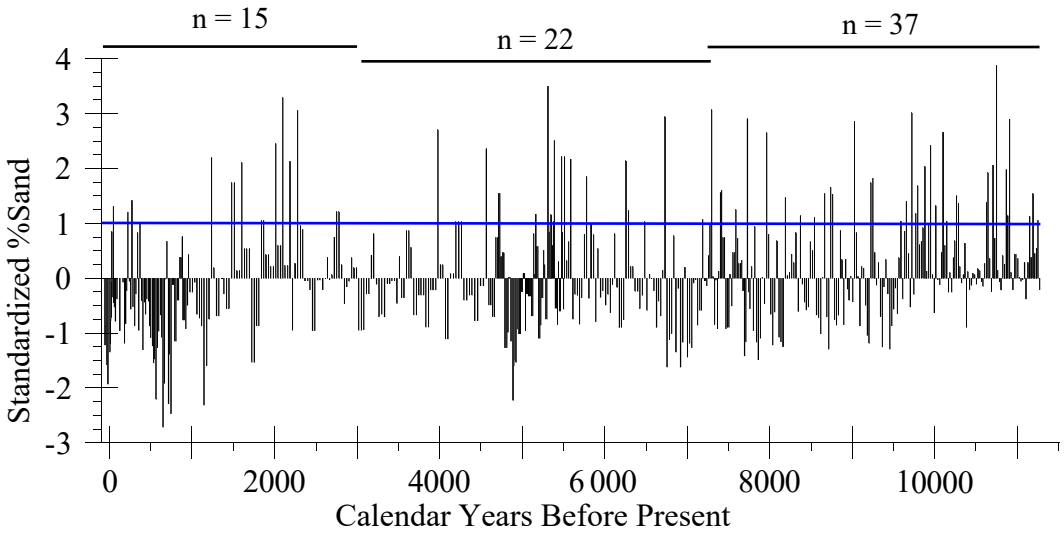

Figure 3-10. Standardized (by mean) percent sand versus calibrated years before present. Blue line: event threshold at approximately 1 standard deviation (50% sand) above the mean.

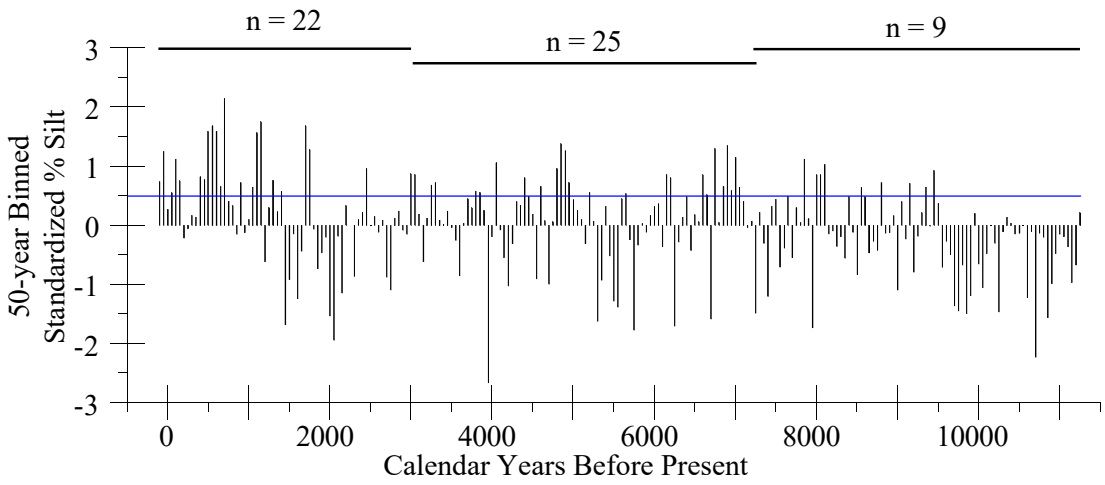

Figure 3-11. 50-year binned standardized (by mean) percent silt. Blue line: drought threshold at approximately 0.49 standard deviation (63% silt) above the mean.

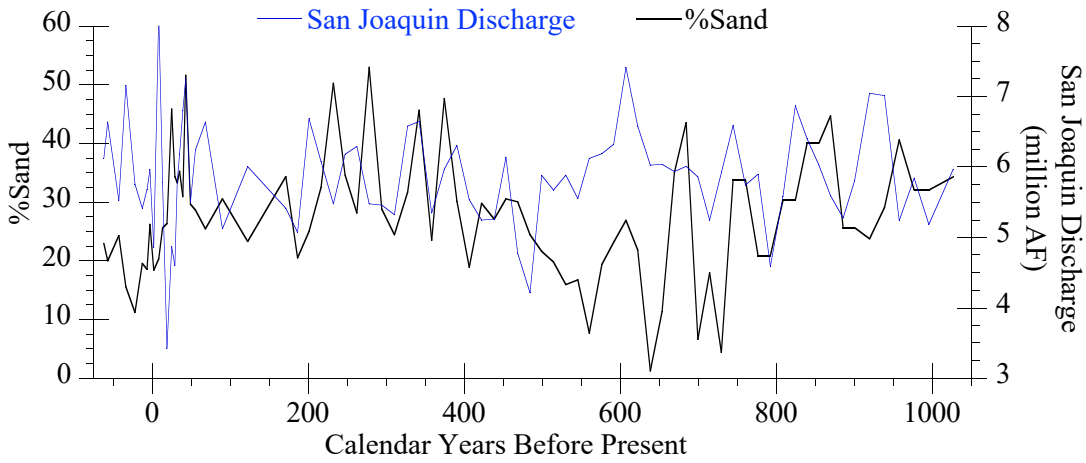

Figure 3-12. San Joaquin Basin discharge (blue) reconstruction (Meko et al., 2014) temporally aggregated to match Pear Lake percent sand (black) data time steps.

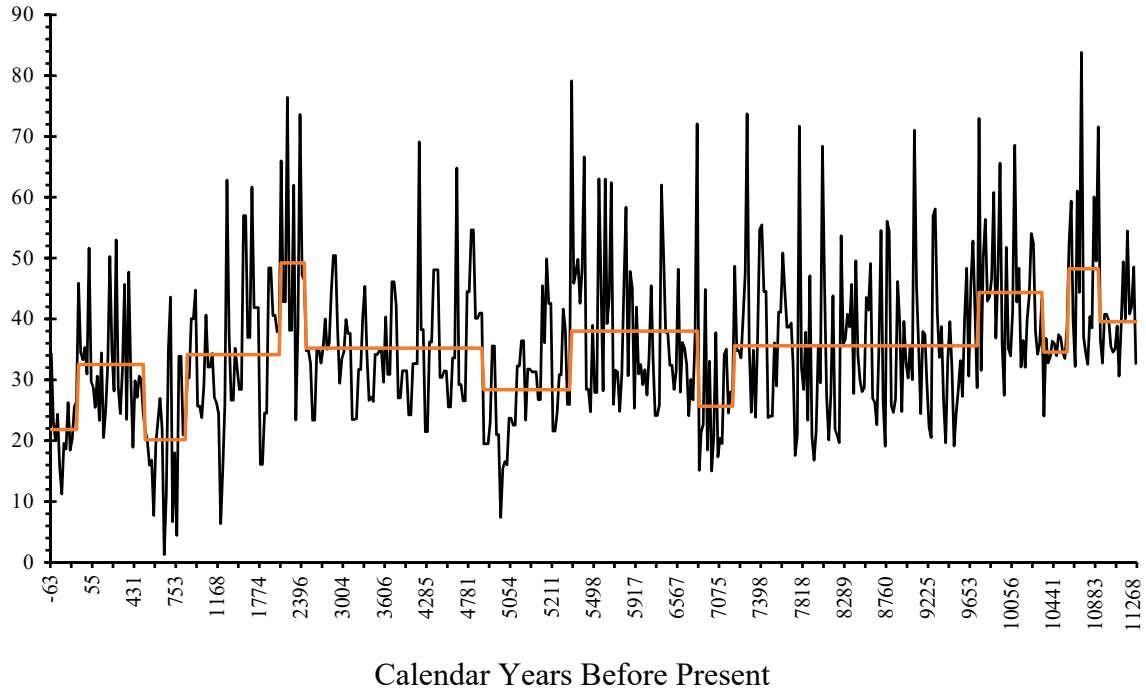

Figure 3-13. Regime shift analysis of percent sand. Target p = 0.05, cutoff length = 12, tuning constant = 2.

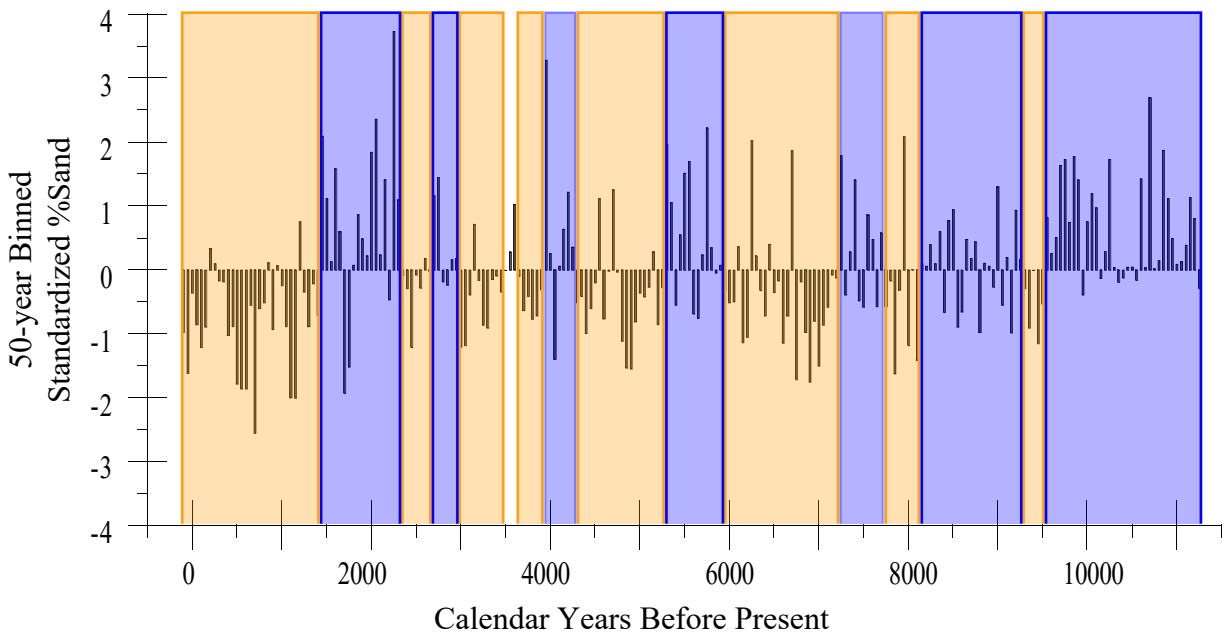

Figure 3-14. 50-year binned standardized percent sand. Blue boxes highlight pluvial (wet) periods and orange boxes highligh arid (dry) periods.

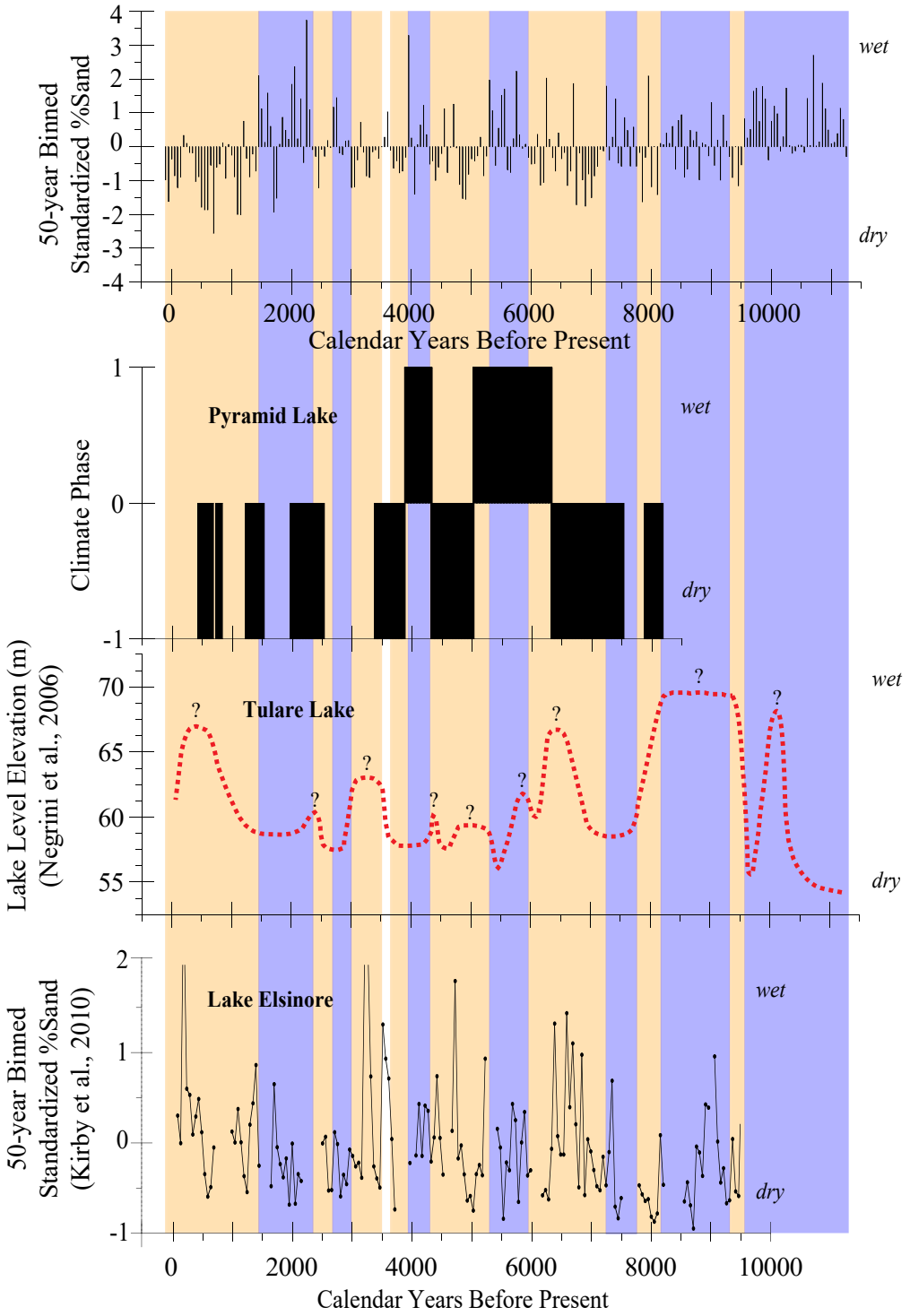

Figure 3-15. Regional comparison for Pear Lake sediment record. Pear Lake climate regimes highlighted over all four lake records. Question marks in Tulare Lake reconstruction depict uncertainty in exact lake level.

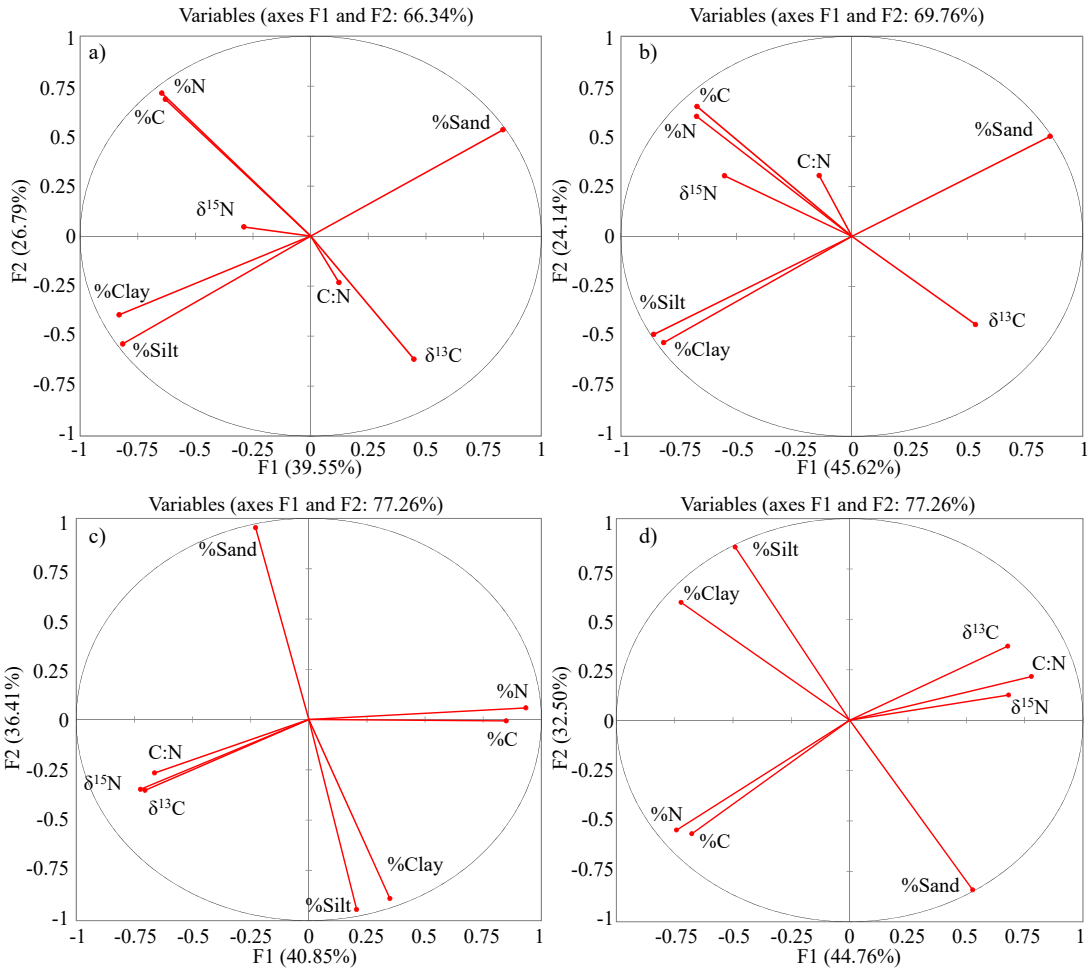

Figure 3-16. PCA of chosen proxies for a) entire Holocene record, b) early Holocene, c) middle Holocene, d)late Holocene.

Table 2-1. Correlation table showing r values for sediment proxies in Lake Pear Sediment. With n = 568, bold values are different from zero with a significance level of alpha = 0.05.

	Sand	Silt	Clay	$\delta^{13}C$	$\delta^{15}N$	%C	%N	C:N	Density	MS
Sand	**1**									
Silt	**-0.998**	**1**								
Clay	**-0.922**	**0.898**	**1**							
$\delta^{13}C$	0.058	-0.055	-0.077	**1**						
$\delta^{15}N$	-0.061	0.070	-0.004	-0.003	**1**					
%C	**-0.193**	**0.177**	**0.291**	**-0.505**	**0.171**	**1**				
%N	**-0.204**	**0.188**	**0.294**	**-0.555**	**0.113**	**0.966**	**1**			
C:N	**0.105**	**-0.109**	-0.066	**0.184**	**0.284**	**0.163**	-0.050	**1**		
Density	0.079	-0.076	**-0.088**	**0.085**	**-0.124**	**-0.385**	**-0.359**	**-0.190**	**1**	
MS	**0.214**	**-0.213**	**-0.198**	**0.155**	**-0.217**	**-0.465**	**-0.447**	**-0.171**	**0.730**	**1**

Table 3-1. Details from ^{210}Pb chronology of Pear Lake.

Sample	Section	Interval	Type	^{210}Pb activity	Age at Given Depth	Calendar Years	Correlated Age
		cm		(dpm/g)	yr	BP	1s Error
Pear	1A-1P-1	1	bulk	125.2	1.1	-61.9	0.6
Pear	1A-1P-1	2	bulk	143.7	6.3	-56.7	0.7
Pear	1A-1P-1	3	bulk	131.0	20.0	-43.0	0.9
Pear	1A-1P-1	4	bulk	99.5	29.3	-33.7	1.2
Pear	1A-1P-1	5	bulk	94.0	40.9	-22.1	1.5
Pear	1A-1P-1	6	bulk	58.0	49.9	-13.1	2.0
Pear	1A-1P-1	7	bulk	25.6	55.7	-7.3	2.4
Pear	1A-1P-1	8	bulk	29.0	60.5	-2.5	2.7
Pear	1A-1P-1	9	bulk	21.7	65.1	2.1	3.2
Pear	1A-1P-1	10	bulk	16.2	71.4	8.4	3.8
Pear	1A-1P-1	11	bulk	12.5	76.4	13.4	4.2
Pear	1A-1P-1	12	bulk	11.4	81.6	18.6	4.3
Pear	1A-1P-1	13	bulk	11.3	88.3	25.3	4.9
Pear	1A-1P-1	14	bulk	8.6	91.6	28.6	5.3
Pear	1A-1P-1	15	bulk	7.3	94.7	31.7	5.7
Pear	1A-1P-1	16	bulk	8.2	98.2	35.2	6.2
Pear	1A-1P-1	17	bulk	7.3	101.9	38.9	6.9
Pear	1A-1P-1	18	bulk	6.3	106.0	43.0	7.4
Pear	1A-1P-1	19	bulk	6.9	112.3	49.3	8.9
Pear	1A-1P-1	20	bulk	9.4	118.4	55.4	9.6
Pear	1A-1P-1	21	bulk	9.3	130.6	67.6	12.2
Pear	1A-1P-1	22	bulk	8.3	153.1	90.1	11.1
Pear	1A-1P-1	23	bulk	7.9	185.1	122.1	17.3
Pear	1A-1P-1	24	bulk	6.2	209.7	146.7	30.8

Table 3-2. Details from radiocarbon chronology of Pear Lake.

Sample	Section	Interval	Type	$\delta^{13}C$	Radiocarbon Age	1s Error	Calendar Years	+/-
		cm		per mil	BP		BP	
Pear	1A-1P-1	30.5-31	fossil	-36.2	53	23	54	22
Pear	1A-1P-1	85	fossil	-28.10	1020	24	944	28
Pear	1A-2B-1	56.8	fossil	-16.10	2263	23	2326	23
Pear	1A-3B-1	17-21	fossil	-28.70	3671	27	4003	86
Pear	1A-3B-1	40	fossil	-29.80	4196	34	4694	74
Pear	1A-4B-1	20	fossil/bulk	-35.50	4659	32	5393	78
Pear	1A-4B-1	80	bulk	-24.90	6189	35	7081	101
Pear	1A-5L-1	30	bulk	-32.60	6892	40	7747	85
Pear	1A-5L-1	70	bulk	-28.70	7802	36	8580	68
Pear	1A-6L-1	50	bulk	-33.60	8933	51	10065	158

Table 3-3. Climate distinction of mode categories.

Primary Mode	Unimodal	Bimodal (secondary mode)	Trimodal (secondary, tertiary modes)
Sand	Wet	(sand) Extremely Wet	(sand, sand) Extremely Wet
		(silt) Moderately Wet	(sand, silt) Moderately Wet
Silt	Dry	(sand) Moderate	(sand, silt) Moderate

Table 3-4. Elemental and Stable Isotope statistics.

	Maximum	**Minimum**	**Mean**	**Standard Deviation**	**Slope**
Total Carbon (%C)	14.7%	0.02%	7.1%	2.8%	-2.07×10^{-4}% yr^{-1} ($p < 0.0001$)
Total Nitrogen **(%N)**	1.2%	0.01%	0.59%	0.25%	-2.2×10^{-5}% yr^{-1} ($p < 0.0001$)
$\delta^{13}C$	-22.5‰	-30.2‰	-26.4‰	1.1‰	9.9×10^{-5}‰ yr^{-1} ($p < 0.0001$)
$\delta^{15}N$	3.6‰	-1.5‰	1.7‰	0.90‰	-1.2×10^{-4}‰ yr^{-1} ($p < 0.0001$)
C:N	28.9	9.8	14.1	1.6	7.3×10^{-5} yr^{-1} ($p < 0.0001$)

Table 3-5. Climate conditions by proxy.

Proxy		Dry	Moderate	Wet	Extremely Wet
Unimodal Sand				X	
Bimodal	Sand/Sand				X
	Sand/Silt		X		
Trimodal	Sand/Sand/Sand				X
	Sand/Sand/Silt		X		
Unimodal Silt		X			
Above %Sand Threshold				X	
Above Binned %Silt Threshold		X			
Gravel Presence					X